Techniques and Unique and Characteristic Signatures to Identify Hydrino are Predicted from Exact Closed-Form Solutions of Atoms and Molecules

Over 100 peer reviewed publications:
https://brilliantlightpower.com/publications/

Hydrino States of Hydrogen (Review article:
https://brilliantlightpower.com/pdf/Hydrino_States_of_Hydrogen_Paper.pdf)

August 18, 2025

Catalytic Reaction of Atomic Hydrogen to Hydrino®

1. Atomic hydrogen reacts with an energy acceptor called a catalyst wherein energy is transferred from atomic hydrogen to the catalyst which forms an ion due to accepting the energy
2. Then, the negative electron drops to a lower shell closer to the positive proton to form a smaller hydrogen atom called a "hydrino" releasing energy that ultimately is in the form of heat
3. The catalyst ion regains its lost electrons to reform the catalyst for another cycle with the release of the initial energy accepted from hydrogen. With the imposition of an arc current condition, the limiting space charge of the ionized electrons is eliminated and the rate becomes massively high.

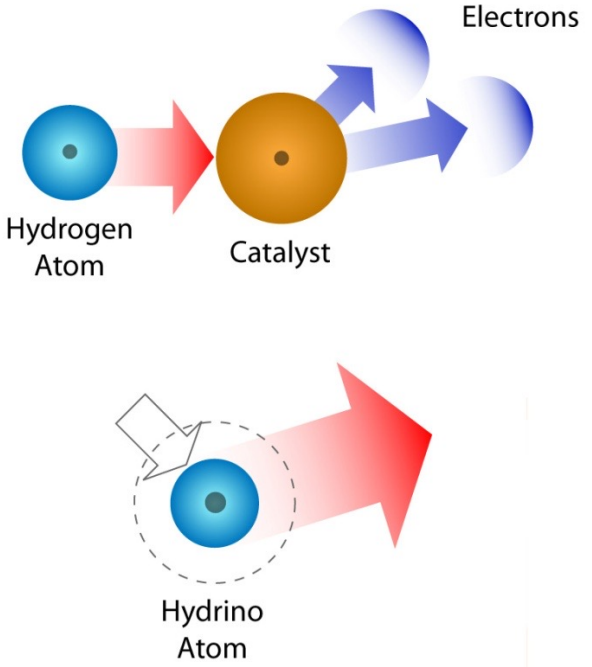

Hydrino transition EUV continuum results offer resolution to many otherwise inexplicable celestial observations with

(a) the energy and radiation from the hydrino transitions being the cause of sunspots and other solar activity, why the Sun emits X-rays, the missing energy balance, the source of extraordinary temperatures and power regarding the solar corona problem wherein the highly ionized ions are from EUV continuum radiation rather than thermal ionization,

(b) the transition of H to H(1/4) being the source of the 10.1 nm cutoff EUV continuum radiation observed from interstellar medium,

(c) the hydrino continuum radiation being the source of the diffuse ubiquitous EUV and soft X-ray cosmic background, the radiation source behind the observation that diffuse Ha emission is ubiquitous throughout the Galaxy and widespread sources of flux shortward of 912 Å are required, and the source of ionization of the interstellar medium (ISM) wherein a large component of the baryonic matter of the universe is in the form of WHIM (warm-hot ionized media) in the absence of a conventional ionizing energy source,

Hydrino® power source in the Sun's corona

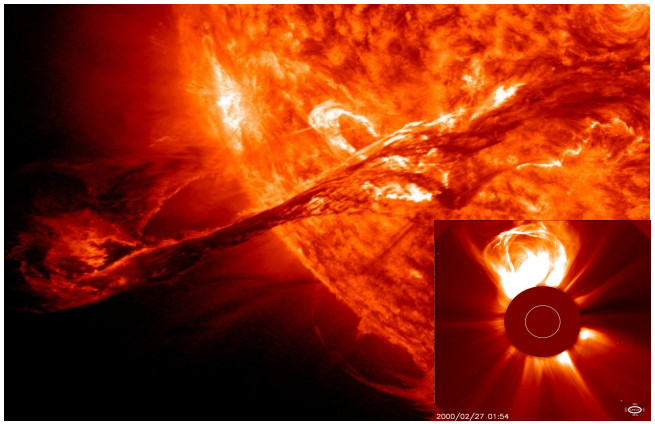

Hydrino® >912 Å continuum in the Sun's corona

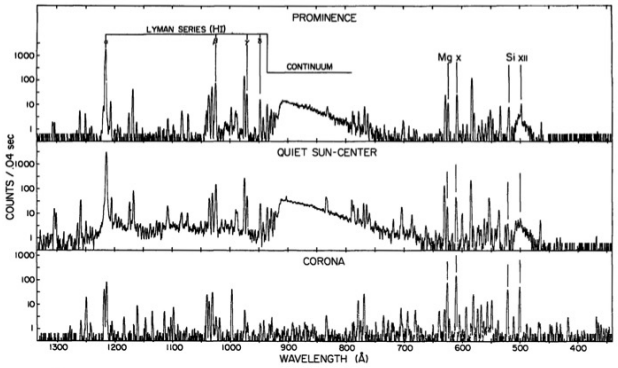

SunCell® EUV continuum emission

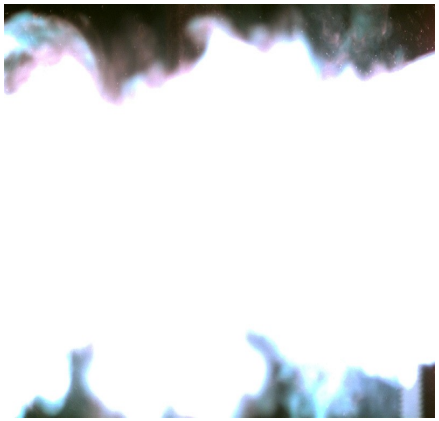

Hydrino transition EUV continuum results offer resolution to many otherwise inexplicable celestial observations with

(d) the transitions of H to H(1/2), H(1/3), and H(1/4) being the source of the continua bands in the EUV spectra of white dwarfs,

(e) the hydrino transition H to H(1/17) catalyzed by H(1/4) being the source of the 3.48 keV emission assigned to dark matter, (f) the energy release from H to H(1/4) being the source of the temperature of galactic halo gas is in the range of 86 eV to 215 eV,

(f) molecular hydrino rotational transitions with spin-orbital and fluxon linkage spitting such as those observed Raman spectroscopy and electron beam emission spectroscopy match the Diffuse Interstellar Medium (DIBs) lines and further match lines observed by electron paramagnetic resonance (EPR) spectroscopy at a 10^{-6} lower energy scale.

Hydrino® EUV plasma source

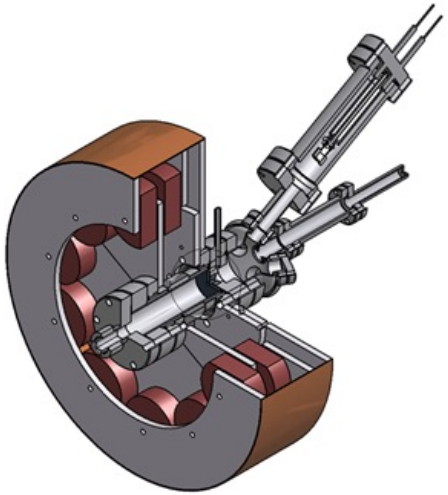

Hydrino® EUV continuum emission

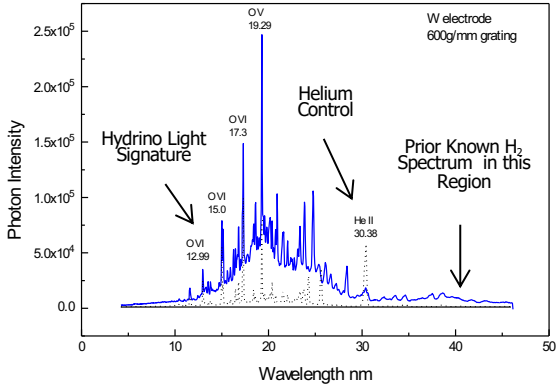

EUV spectra of white dwarfs

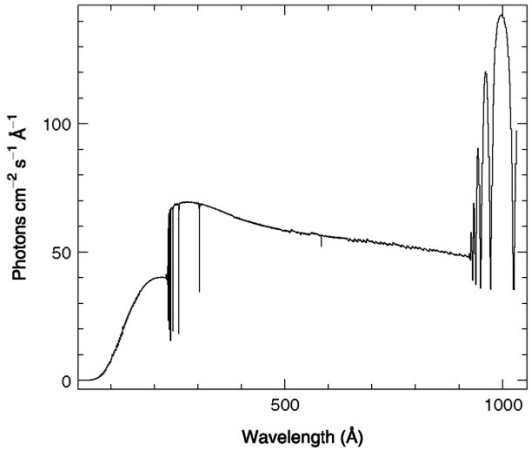

Hydrino transition EUV continuum results offer resolution to many otherwise inexplicable celestial observations with

g) the identity of dark matter being hydrinos.

R. Mills, "Hydrino States of Hydrogen", https://brilliantlightpower.com/pdf/Hydrino_States_of_Hydrogen_Paper.pdf.
R. Mills, J. Lotoski, Y. Lu, "Mechanism of soft X-ray continuum radiation from low-energy pinch discharges of hydrogen and ultra-low field ignition of solid fuels", Plasma Science and Technology, Vol. 19, (2017), pp. 1-28.
R. L. Mills, Y. Lu, "Hydrino continuum transitions with cutoffs at 22.8 nm and 10.1 nm," Int. J. Hydrogen Energy, 35 (2010), pp. 8446-8456, doi: 10.1016/j.ijhydene.2010.05.098.
R. L. Mills, Y. Lu, K. Akhtar, "Spectroscopic observation of helium-ion- and hydrogen-catalyzed hydrino transitions," Cent. Eur. J. Phys., 8 (2010), pp. 318-339, doi: 10.2478/s11534-009-0106-9.
R. L. Mills, Y. Lu, "Time-resolved hydrino continuum transitions with cutoffs at 22.8 nm and 10.1 nm," Eur. Phys. J. D, Vol. 64, (2011), pp. 65, DOI: 10.1140/epjd/e2011-20246-5.
R. L. Mills, R. Booker, Y. Lu, "Soft X-ray Continuum Radiation from Low-Energy Pinch Discharges of Hydrogen," J. Plasma Physics, Vol. 79, (2013), pp 489-507; doi: 10.1017/S0022377812001109.
A. Bykanov, "Validation of the observation of soft X-ray continuum radiation from low energy pinch discharges in the presence of molecular hydrogen," http://www.blacklightpower.com/wp-content/uploads/pdf/GEN3_Harvard.pdf.

Distribution of visible (L) and dark (R) matter

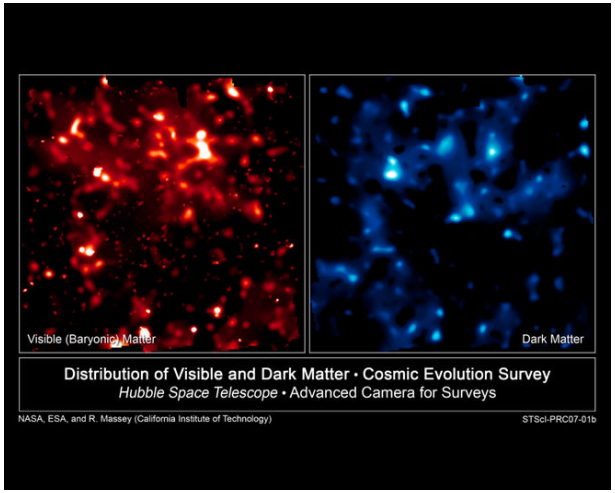

Distribution of dark matter in the universe

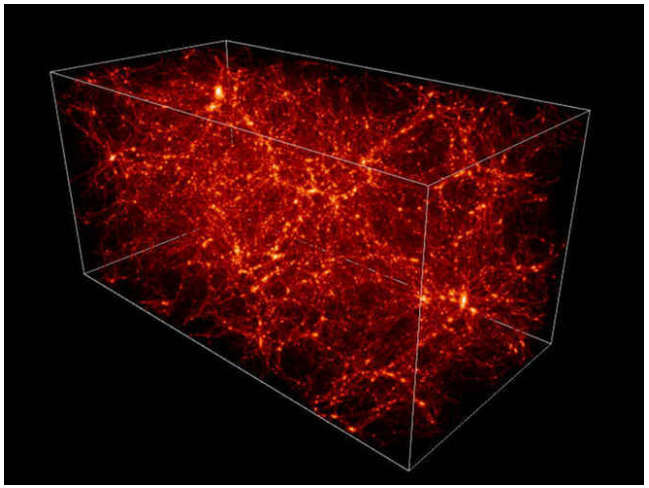

Dark matter ring in galaxy cluster

Optical Power Measurement Using NIST Standards Over 10-800 nm Region: Spectral Emission in the High Energy Region Only

Validated Hydrino Reaction's Extraordinary High-Energy Continuum Light and Optical Power at over 1,000,000W Levels

The continuum radiation with the predicted 10.1 nm cutoff confirms the production of H(1/4).

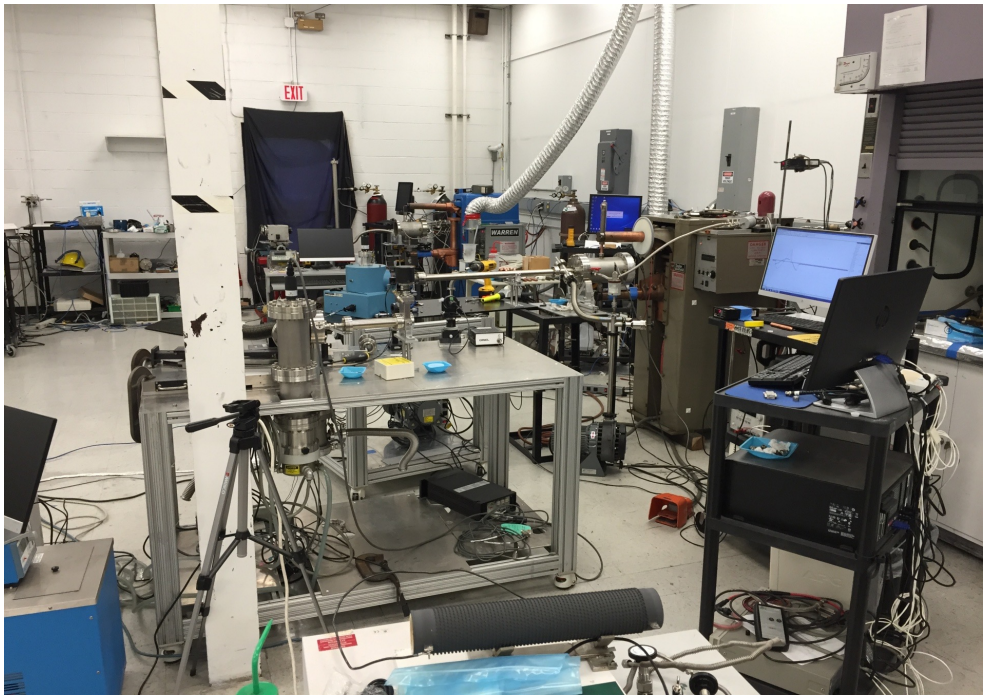

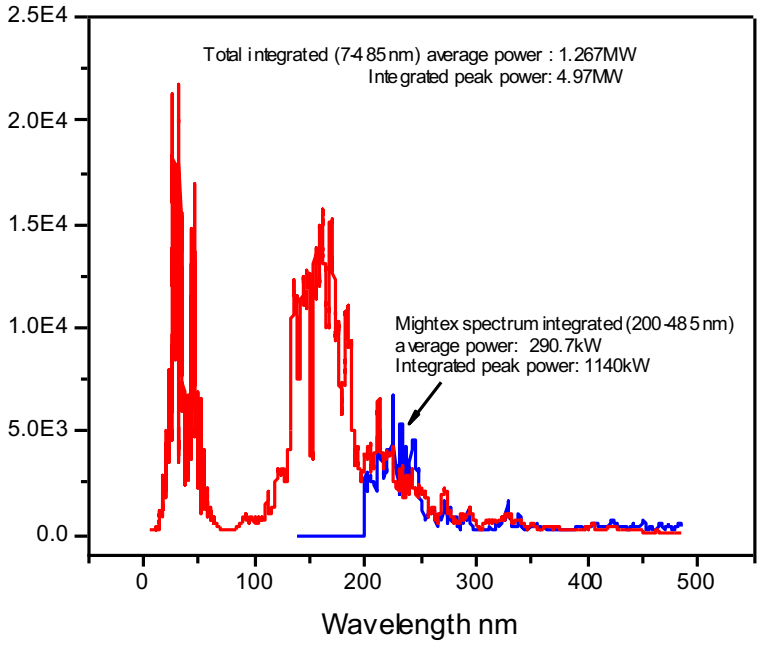

4.6 MW Characteristic H to H(1/4) Transition EUV Continuum Radiation with a Predicted 10.1 nm Cutoff

- Hydrated silver shots comprising a source of H and HOH catalyst were ignited by passing a low voltage, high current through the shot to produce explosive plasma that emitted brilliant light predominantly in the short-wavelength 10 to 300 nm region.

- The peak power of 20 MW and time-average power of 4.6 MW was measured using absolute spectroscopy over the 22.8-647 nm region wherein the optical emission energy was 250 times the applied energy.

- The wavelength calibrated and absolute intensity calibrated spectrum (10-45 nm) of the emission of hydrated silver shots recorded on the GIS with a Zr filter showed the EUV continuum cutoff at *10.1 nm that matches dark matter emission*.

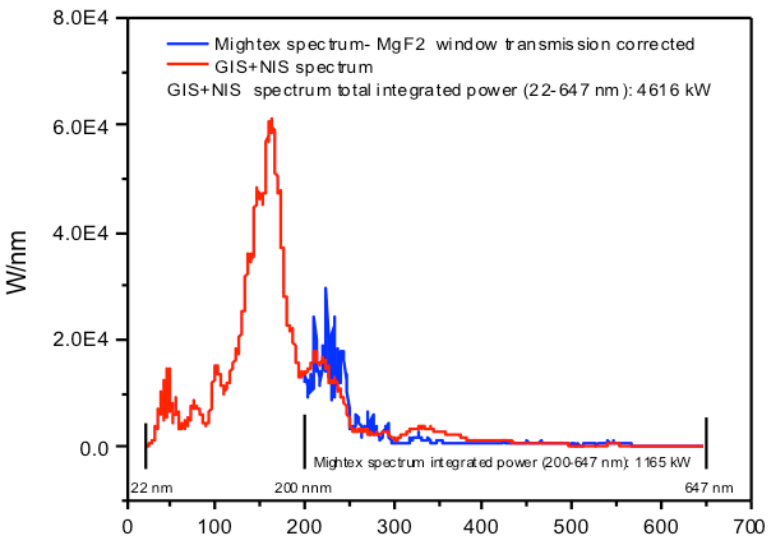

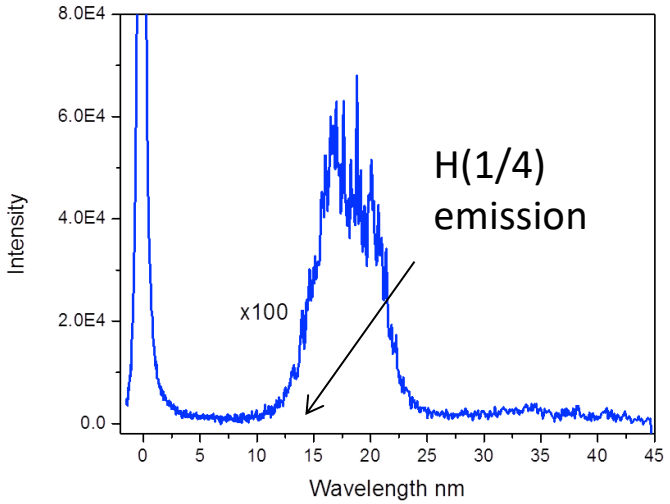

R. Mills, Y. Lu, R. Frazer, "Power Determination and Hydrino Product Characterization of Ultra-low Field Ignition of Hydrated Silver Shots", Chinese Journal of Physics, Vol. 56, (2018), pp. 1667-1717.

Massive Ionization Determined by Stark Broadening at High Pressure

- Stark broadening of the H alpha line of 1~1.3 nm corresponds to an electron density of 2.4-3.5X10^{23}/m^3.
- The SunCell® gas density was calculated to be 2.5X10^{25} atoms/m^3 based on an argon-H_2 pressure of 800 Torr and temperature of 3000K.
- The corresponding ionization fraction was about 10%.
- Given that argon and H_2 have ionization energies of about 15.5 eV and a recombination lifetime of less than 100 us at high pressure, the power density to sustain the ionization is

$$P = \left(\frac{3.5X10^{23}\,electrons}{m^3}\right)(15.5\,eV)\left(\frac{1.6X10^{-19}\,J}{eV}\right)\left(\frac{1}{10^{-4}s}\right) = \frac{8.7X10^{9}W}{m^3}$$

R. Mills, Y. Lu, R. Frazer, "Power Determination and Hydrino Product Characterization of Ultra-low Field Ignition of Hydrated Silver Shots", Chinese Journal of Physics, Vol. 56, (2018), pp. 1667-1717.

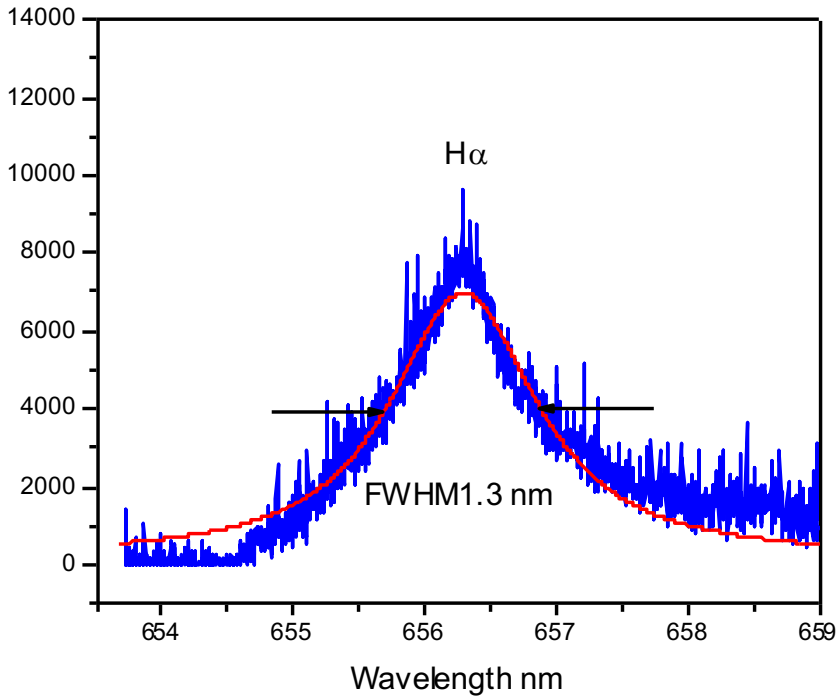

Energetic Signatures

In addition to hydrogen line broadening, other signatures of the energetics of the hydrino reaction are chemically generated or so called resonance transfer (RT) plasmas, plasma afterglow, high optical output power, and an inverted hydrogen population.

Hydrino Reaction with Explosive Power

- 70 mg hydrated silver shot comprising a source of H and HOH catalyst were ignited by passing a low voltage, high current through the shot.
-
- Extraordinary effects consisting of EUV emissions, explosively formed plasma fields, EMP effects and blast effects which cannot be explained through conventional chemistry and physics.
-
- Based on the shockwave propagation velocity and the corresponding pressure, the high-current ignition of water in a silver matrix was measured to produce a shock wave that was equivalent to about 10 times more moles of gunpowder.

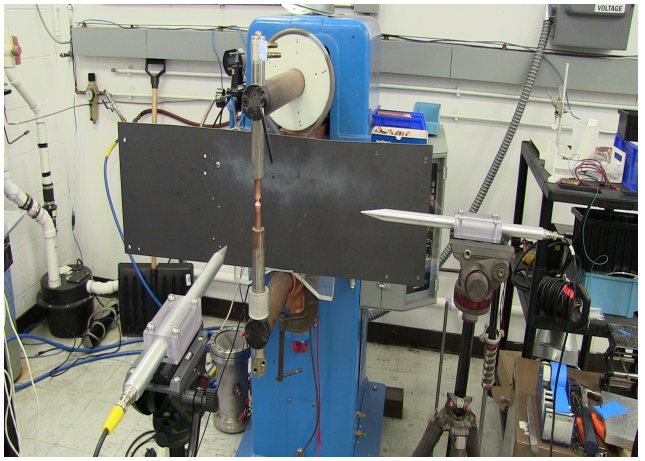

R. Mills, Y. Lu, R. Frazer, “Power Determination and Hydrino Product Characterization of Ultra-low Field Ignition of Hydrated Silver Shots”, Chinese Journal of Physics, Vol. 56, (2018), pp. 1667-1717.

Dr. J. Renick, Free-Air Blast Analysis, April 24, 2018, https://www.brilliantlightpower.com/wp-content/uploads/pdf/Free-Air-TNT-Analysis.pdf.

Chemically-Generated RT Plasma

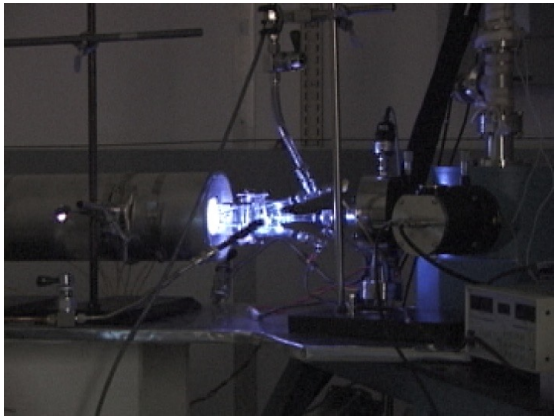

- Hydrogen Plasmas Formed with Incandescently Heating of Hydrogen Gas in the Presence of Trace Amounts of Potassium Carbonate.

H. Conrads, R. Mills, Th. Wrubel, "Emission in the Deep Vacuum Ultraviolet from a Plasma Formed by Incandescently Heating Hydrogen Gas with Trace Amounts of Potassium Carbonate," Plasma Sources Science and Technology, Vol. 12, (2003), pp. 389-395.

Experimental Set-up for Chemically-Generated RT Plasma

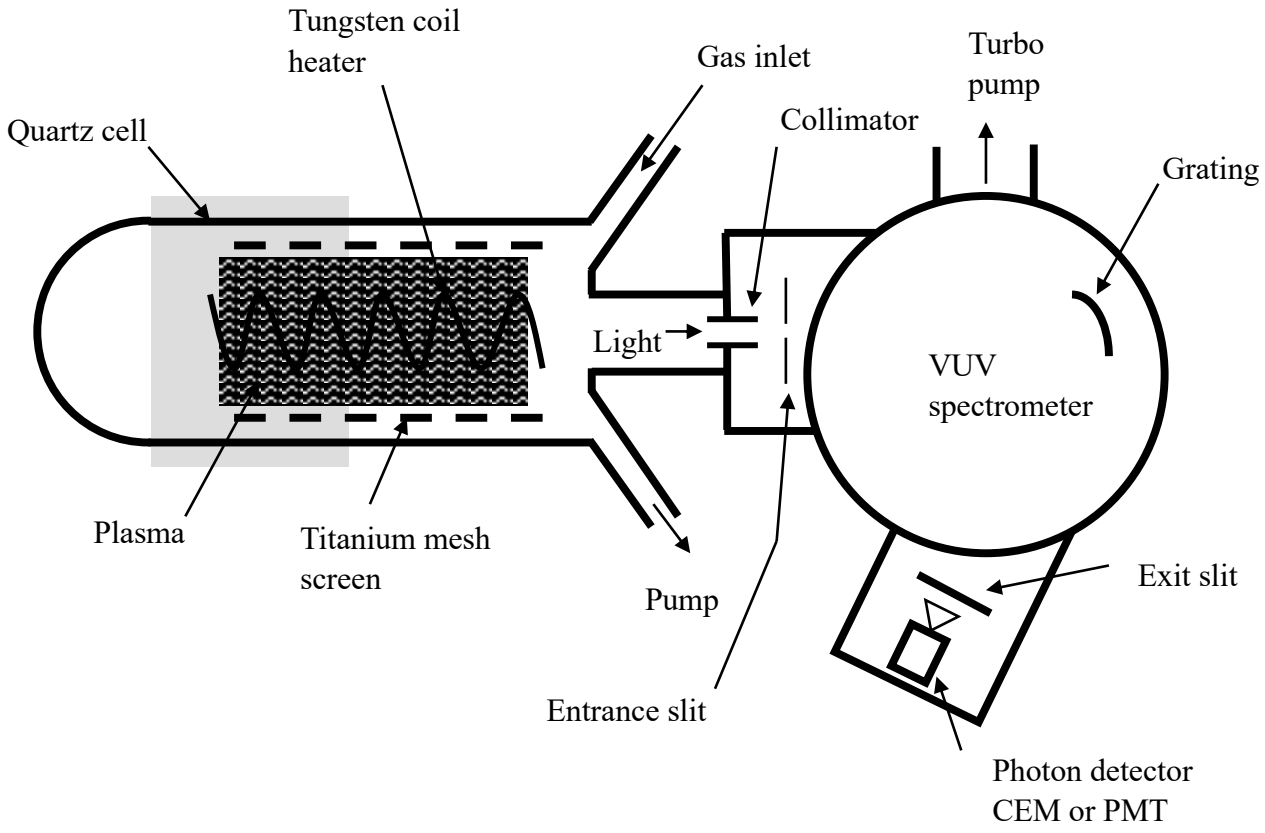

Inverted Hydrogen Population

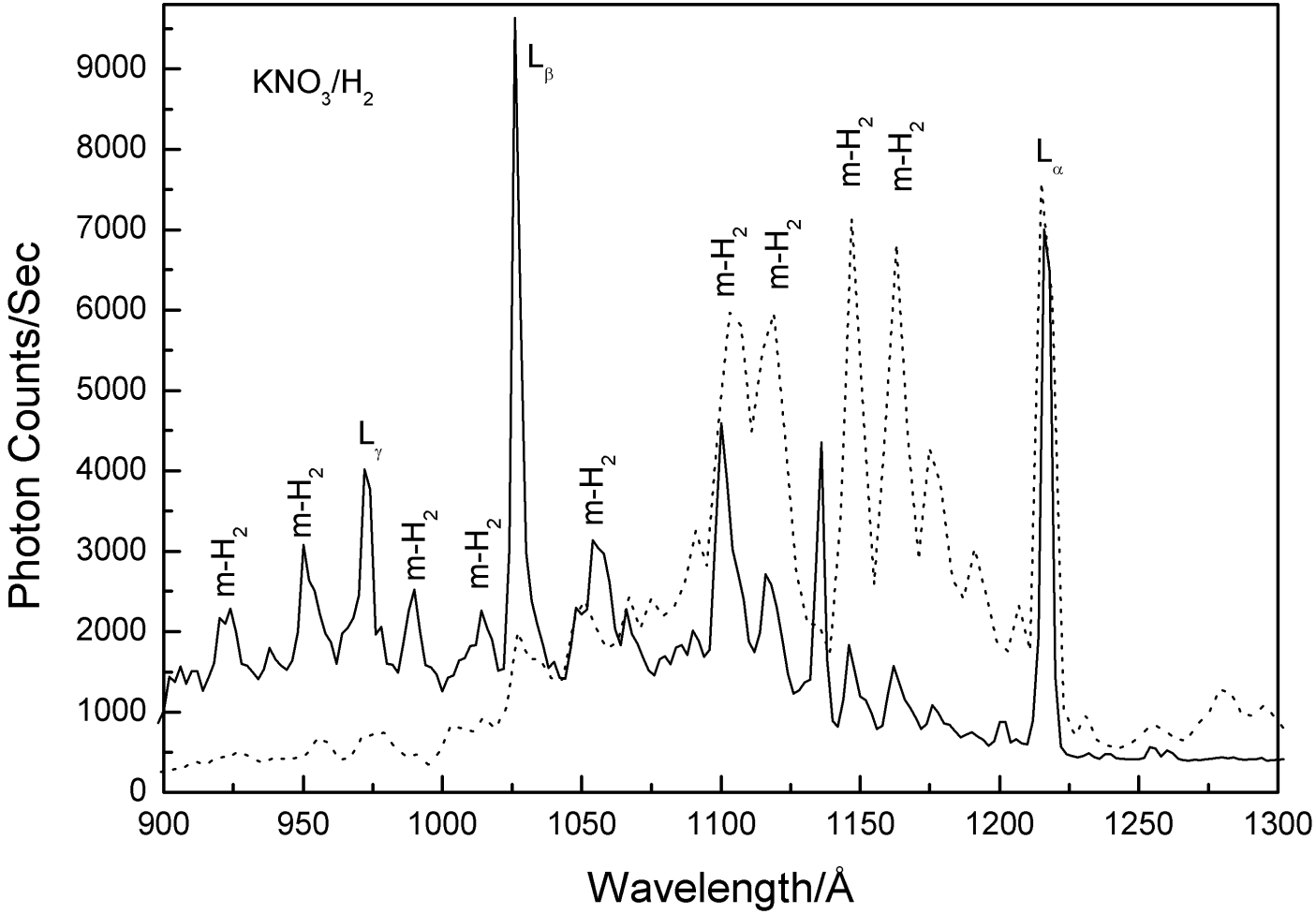

The VUV spectra (900–1300 Å) of the cell emission from hydrogen microwave plasma (dotted line) and the KNO_3–H_2 rt-plasma (solid line) with an inverted Lyman population.

R. L. Mills, P. Ray, "Stationary Inverted Lyman Population Formed from Incandescently Heated Hydrogen Gas with Certain Catalysts," J. Phys. D, Applied Physics, Vol. 36, (2003), pp. 1504–1509.

Plasma Afterglow

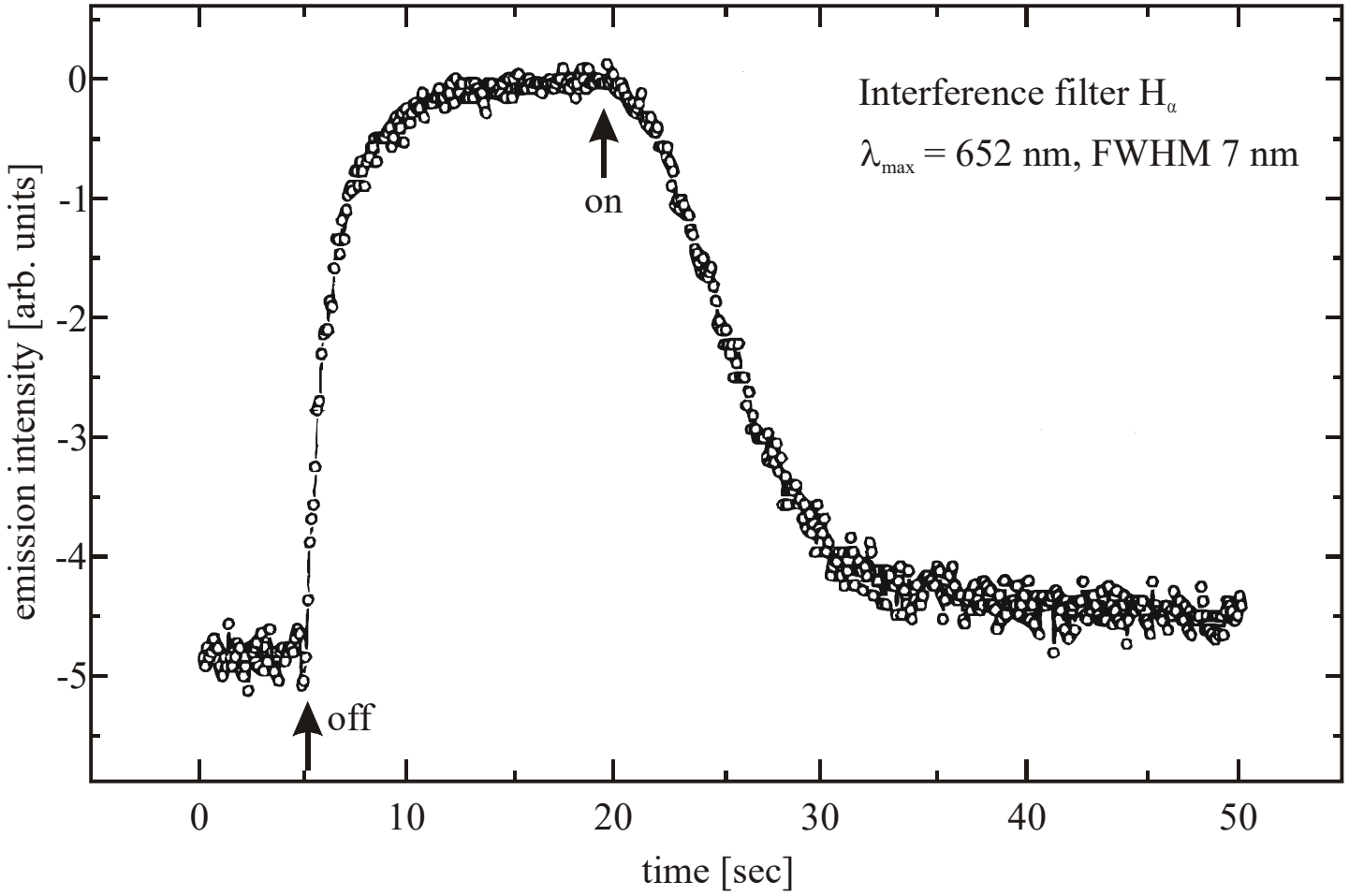

Emission of the cell as a function of time while the filament current was turned off and on. The plasma decay with no electric field present followed the decay of atomic hydrogen from the filament dissociator. Upon restoration of the filament temperature, dissociation and the plasmas resumed.

J. Conrads, R. Mills, Th. Wrübel, Plasma Sources Sci. Technol. **12**, 389 (2003).

Extraordinary Doppler Broadening of the Balmer α Line at Low Pressure Due to the Hydrino Reaction

- From the width of the emitted Balmer lines, it was found that low-pressure capacitively coupled radio frequency (rf) water-vapor plasmas showed the presence of both slow and fast excited hydrogen atoms.
- The typical slow component was independent of time.
- A new phenomenon, an extraordinary fast Doppler broadened component (130–150 eV) that increases to a significant portion of the Balmer emission with time, was also observed.
- These studies demonstrate excessive line broadening in the absence of an observable effect attributable to a strong electric field since the xenon–hydrogen plasma emission showed no broadening.
- To conserve energy during the resonant energy transfer of 81.6 eV (3 X 27.2 eV) from H to HOH catalyst to form H(1/4), the resulting protons gain high kinetic energy and result in fast H emission with proton-electron recombination.

The Balmer α line width profile recorded on water-vapor and Xe/H_2 (90/10%) rf plasmas at matched conditions of no-flow, 100 mTorr, 200 W, and 4-h plasma duration.

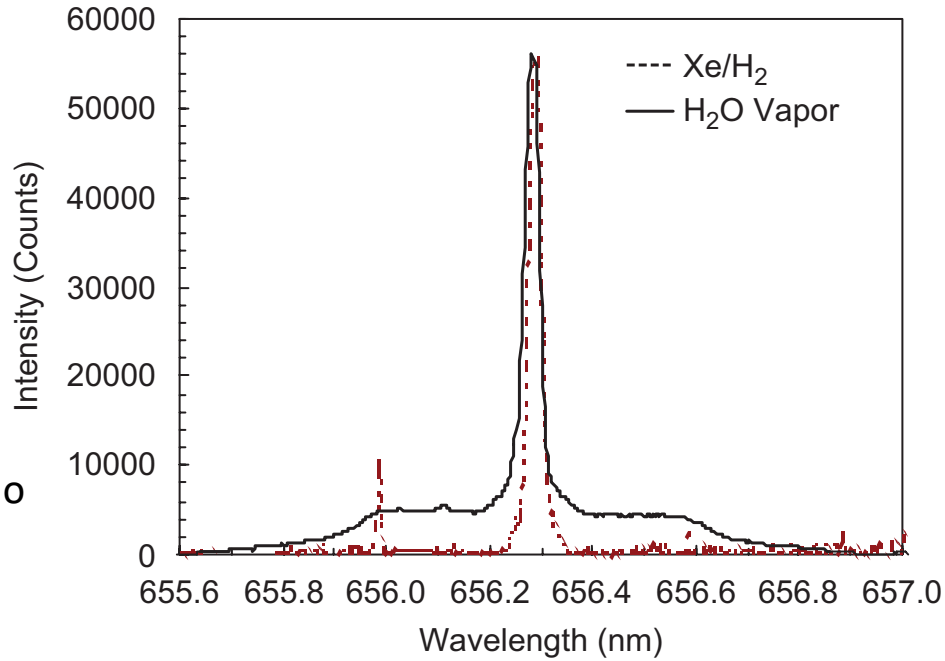

R. L. Mills, B. Dhandapani, K. Akhtar, "Excessive Balmer α Line Broadening of Water-Vapor Capacitively-Coupled RF Discharge Plasmas," Int. J. Hydrogen Energy, Vol. 33, (2008), 802–815.

Fast H Continued: Excessive Doppler hydrogen line broadening in low pressure H_2 discharge corresponding to fast H atom with energies of 100 eV wherein H atoms serve as a catalyst and a reactant to form hydrinos.

The 656.3 nm Balmer α line width recorded with the Jobin Yvon Horiba 1250 M spectrometer parallel to the electric field. Even though hydrogen ions were accelerated away from the detector, a symmetrical emission profile was observed indicating that the broadening was not dependent on the electric field. The line profile recorded on a 200 mTorr H_2 pinch plasma showed a trimodal distribution wherein 18% and 33% of the hydrogen in the excited n = 3 state was fast with an average hydrogen atom energy of 98 eV and 8.8 eV, respectively, compared to 1.3 eV for the slow population.

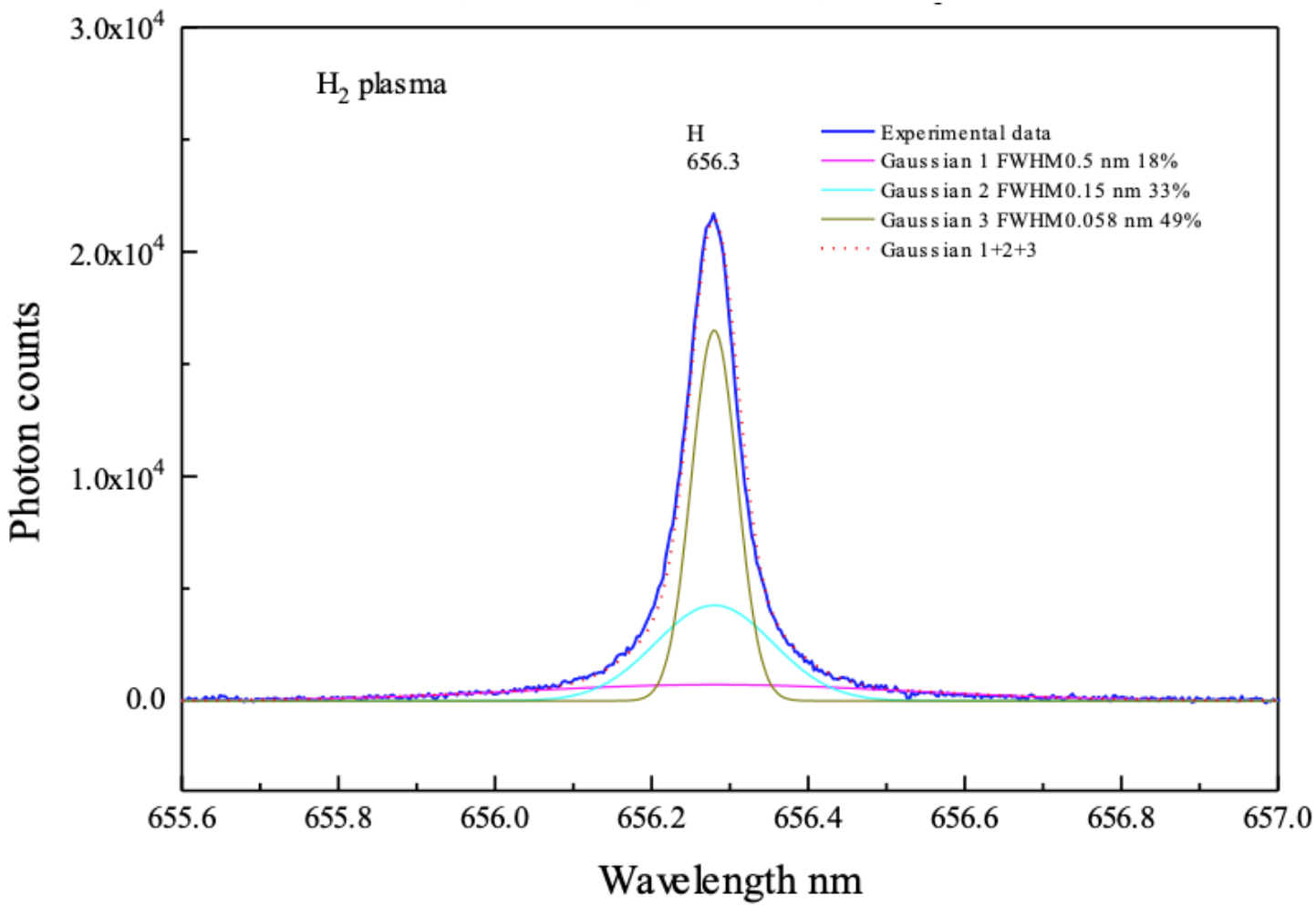

R. Mills, X Yu, Y. Lu, G Chu, J. He, J. Lotoski, "Catalyst induced hydrino transition (CIHT) electrochemical cell," (2012), Int. J. Energy Res., (2013), DOI: 10.1002/er.3142.

K. Akhtar, J. Scharer, R. L. Mills, "Substantial Doppler Broadening of Atomic Hydrogen Lines in DC and Capactively Coupled RF Plasmas," J. Phys. D: Appl. Phys., Vol. 42, Issue 13 (2009), 135207 (12pp).

R. L. Mills, K. Akhtar, "Tests of Features of Field-Acceleration Models for the Extraordinary Selective H Balmer α Broadening in Certain Hydrogen Mixed Plasmas," Int. J. Hydrogen Energy, Vol. 34, (2009), 6465–6477.

R. L. Mills, R. Booker, Y. Lu, "Soft X-ray Continuum Radiation from Low-Energy Pinch Discharges of Hydrogen," J. Plasma Physics, doi: 10.1017/S0022377812001109, Published online: January 3, 2013, 19 pages.

Fast H Continued

Doppler Balmer alpha line broadening is observed with hydrogen addition to argon plasma due the presence of oxygen in argon. The oxygen is present since it co-condenses with liquid argon during purification from the atmosphere. Hydrogen reacts with trace oxygen to form HOH that serves as the hydrino catalyst for atomic H of the argon-H_2 plasma.

Axial scan of the 656.3 nm Balmer α line width recorded on a 1 Torr *Ar* /H2 (95/5%) DC plasma discharge with needle-like electrodes at 400 V and 20 mA showing 80% of the hydrogen in excited n=3 state was fast with an average hydrogen atom energy of 40 eV, compared to < 0.5 eV for the slow population.

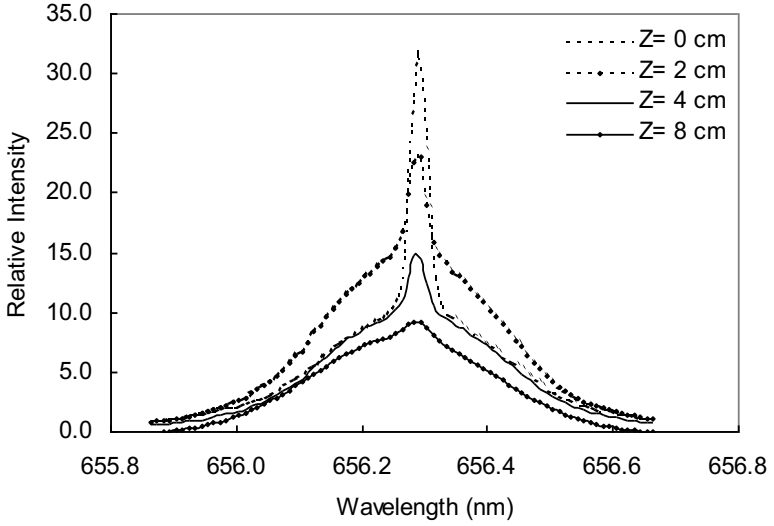

The 656.3 nm Balmer α line width recorded end-on (parallel to the electric field) on a 1 Torr *Ar* /H2 (95/5%) DC plasma discharge with needle-like electrodes at 400 V and 20 mA. Both views looking towards the cathode as well as the anode show a symmetrical emission profile. Fast hydrogen atoms have energies in the range of 38-40 eV.

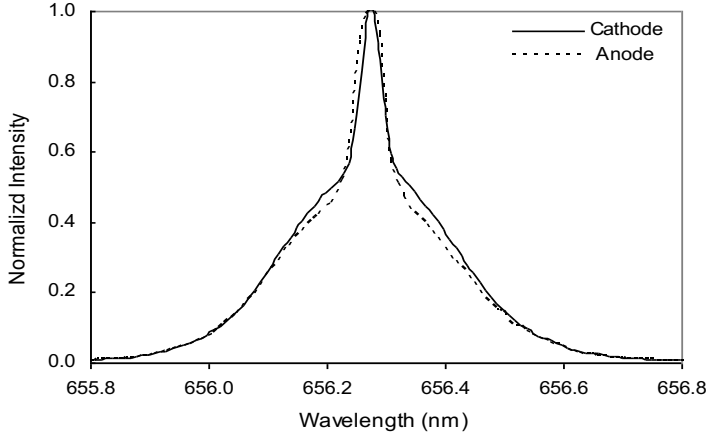

K. Akhtar, J. Scharer, R. L. Mills, "Substantial Doppler Broadening of Atomic Hydrogen Lines in DC and Capactively Coupled RF Plasmas," J. Phys. D: Appl. Phys., Vol. 42, Issue 13 (2009), 135207 (12pp).

Commercial Differential Scanning Calorimeter Power Measurement on Hydrino Reaction Solid Fuels

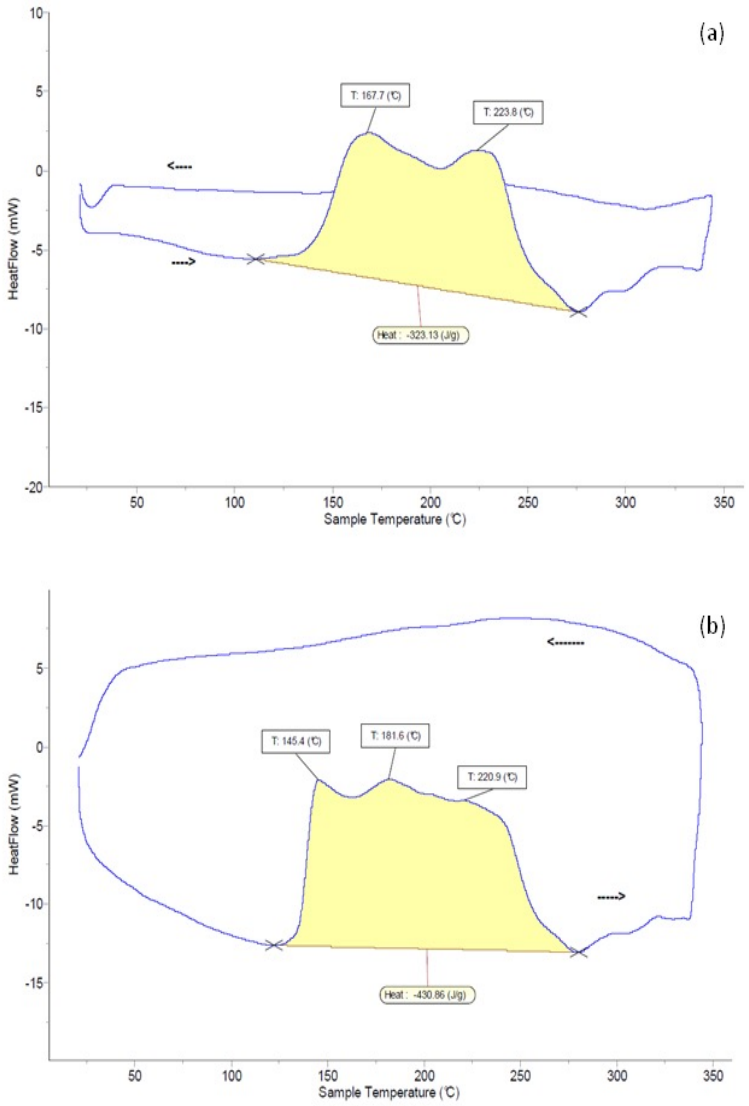

Exchange reactions of the anions between an alkali hydroxide and halide (e.g. $Cu(OH)_2 + FeBr_2$) as well as dehydration reactions of metal oxyhydroxides (e.g. FeOOH) create HOH catalyst and H as transient species that react to form hydrinos.

These hydrino solid fuels release thermal energy in significant excess than possible according to enthalpy balance due to conventional known chemical reactions.

Independently validated by scientists at Perkin Elmer, Setaram, University of Illinois, Norte Dane, and Auburn University. (https://brilliantlightpower.com/validation-reports/)

Hydrino products are observed by multiple analytical techniques.

Figure – (a) DSC (Setaram DSC131) performed on $Cu(OH)_2 + CuBr_2$ by Setaram. The theoretical energy was -39.8 J/g based on the limiting reagent such that the DSC exothermic energy of -323.1 J/g corresponded to an energy gain of 8.1 times the maximum theoretical from conventional chemistry; (b) Duplicate DSC performed on $Cu(OH)_2 + CuBr_2$ by Setaram. The theoretical energy was -39.8 J/g based on the limiting reagent such that the DSC exothermic energy of -430.9 J/g corresponded to an energy gain of 10.8 times the maximum theoretical from conventional chemistry.

R. Mills, J. Lotoski, W. Good, J. He, "Solid Fuels that Form HOH Catalyst," Int'l J. Hydrogen Energy, Vol. 39 (2014), pp. 11930–11944 DOI: 10.1016/j.ijhydene.2014.05.170.

Hydrino Reaction Used to Directly Produce Electrical Power in BrLP's CIHT® Electrochemical Cell

- CIHT cells, such as one comprising a MoCu hydrogen permeable membrane anode, NiO cathode, a LiOH-LiBr eutectic mixture as the electrolyte, and MgO matrix exploit hydrino formation as a half-cell reaction to serve as a new electrical energy source wherein HOH catalyst formed by an oxidation reaction of OH^- at a hydrogen anode.
- The cells were operated under intermittent H_2O electrolysis to generate H at the anode and then discharged to form hydrinos wherein H_2O vapor as well as some O_2 was supplied from the atmosphere in open cells.
- Net electrical production over the electrolysis input and hydrogen supplied to the anode measured using an Arbin BT 2000 was multiples of the electrical input that in most cases exceed the input by a factor of about 2 at about 10 mW/cm^2 anode area over months of continuous operation.
- The predicted molecular hydrino $H_2(1/4)$ was spectroscopically identified as a product of CIHT cells.

R. Mills, J. Lotoski, J. Kong, G. Chu, J. He, J. Trevey, "High-Power-Density Catalyst Induced Hydrino Transition (CIHT) Electrochemical Cell." Int. J. Hydrogen Energy, 39 (2014), pp. 14512–14530 DOI: 10.1016/j.ijhydene.2014.06.153.

R. Mills, X Yu, Y. Lu, G Chu, J. He, J. Lotoski, "Catalyst induced hydrino transition (CIHT) electrochemical cell," (2012), Int. J. Energy Res., (2013), DOI: 10.1002/er.3142.

Validations by leading academic and industry experts: https://brilliantlightpower.com/validation-reports/

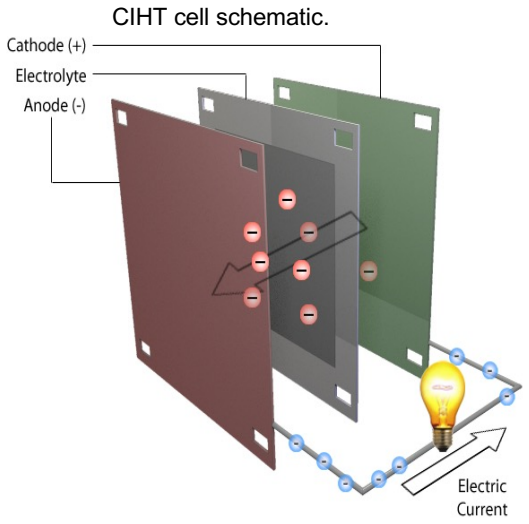

Charge and discharge voltage and current waveform of the CIHT cell [MoCu/LiOH-LiBr/NiO].

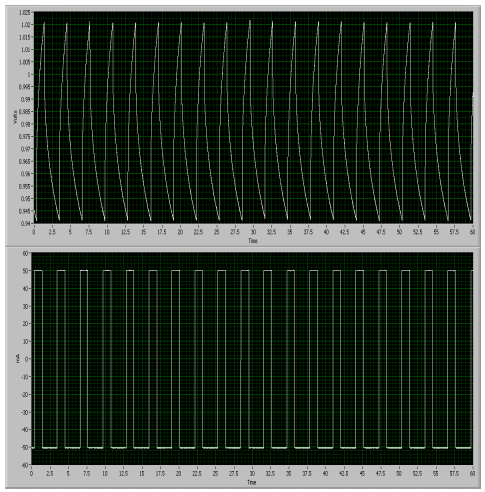

The charge and discharge voltages, and accumulated electrical charge and discharge energies over time of the CIHT cell [MoCu/LiOH-LiBr/NiO].

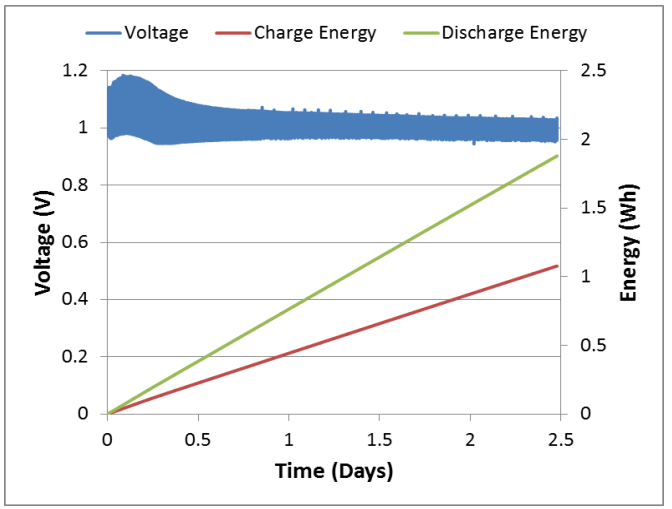

Commercial Parr Water Bath Calorimetry on Hydrated Silver Shot Detonation: Validated Hydrino Reaction Power at over 100,000 W Levels

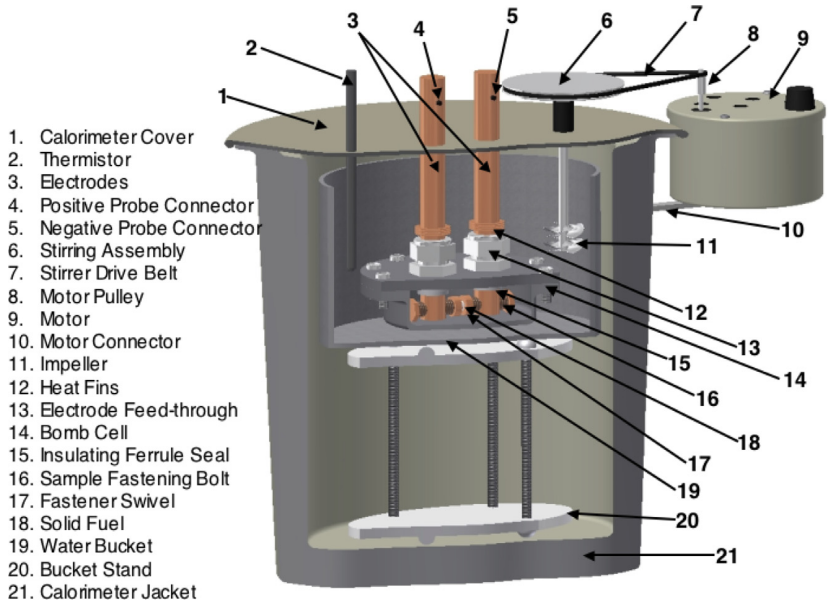

Fig. 1 – The setup of the Parr 1341 calorimeter used for the energy balance determination.

Parr Analysis	
Total Temp Rise (oC)	0.056
60% Temp Rise	0.0336
Temp of 60% T Rise, tb	21.1236
Time of 60% T Rise, b	7.016666667
Firing Temp, Ta	21.09
Firing Time, a	5.116666667
Heat End Temp, Tc	21.146
Heat End Time, c	16.58333333
r1	-0.000511272
r2	-1.17582E-06
dT=Tc - Ta - r1*(b-a)-r2*(c-b)	0.056982665
Cp	12300
Eout =Cp*dT (J)	700.89
Ein (J)	189.00
dE (J)	511.89
Excess (X)	3.71

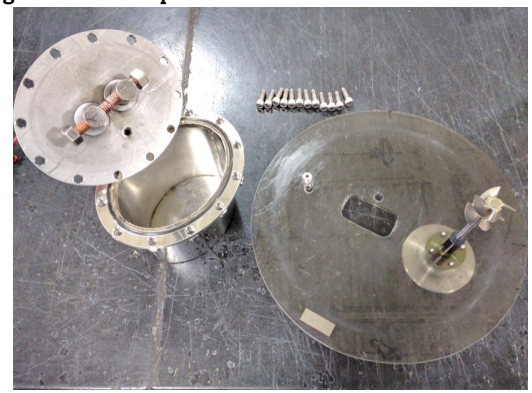

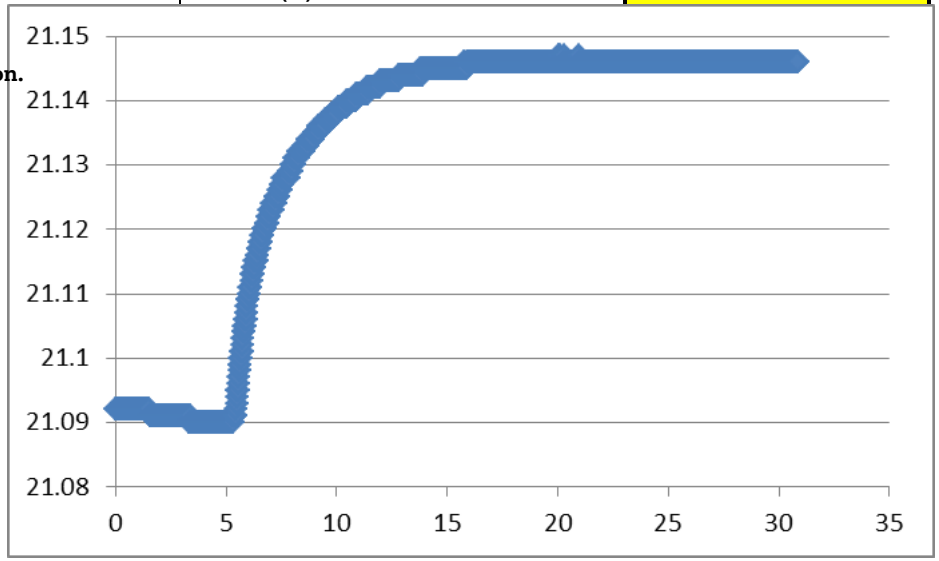

R. Mills, Y. Lu, R. Frazer, "Power Determination and Hydrino Product Characterization of Ultra-low Field Ignition of Hydrated Silver Shots", Chinese Journal of Physics, Vol. 56, (2018), pp. 1667-1717.

Validation: Molten Metal Bath Calorimetry Measured 200 kW of Hydrino Power Production

Heat transfer expert Dr. Mark Nansteel validated 200 kW of power produced by BrLP's proprietary hydrino plasma reaction maintained in its SunCell® using molten metal bath calorimetry.

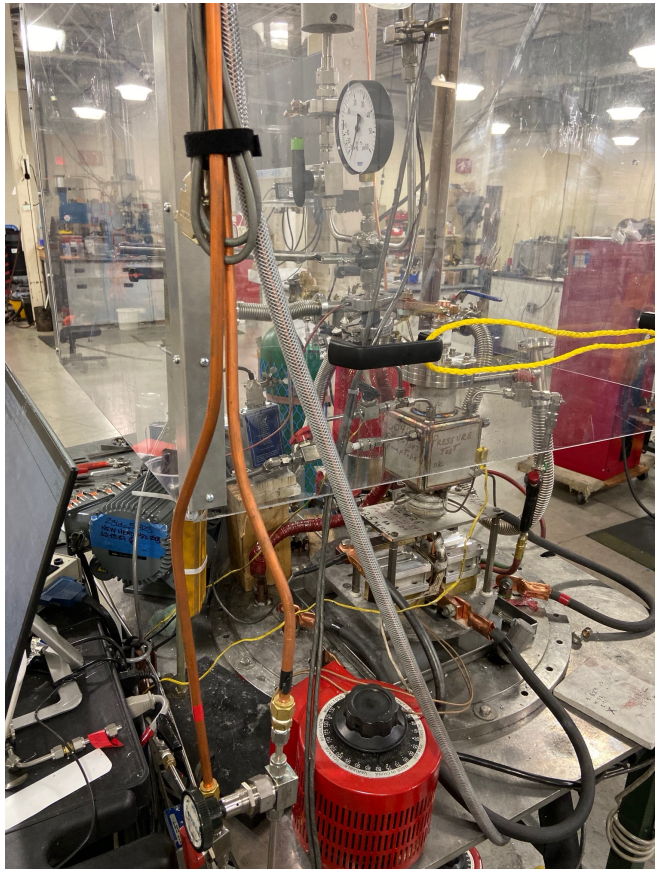

Duration (s)	Input Energy (kJ)	Output Energy (kJ)	Input Power (kW)	Output Power (kW)	Power Gain	Net Excess Power (kW)
1.27	212.9	485.8	167.6	382.5	2.28	272.9

(brilliantlightpower.com/pdf/Mark_Nansteel_Report.pdf)

Validation: Molten Metal Bath Calorimetry Measured 200 kW of Hydrino Power Production

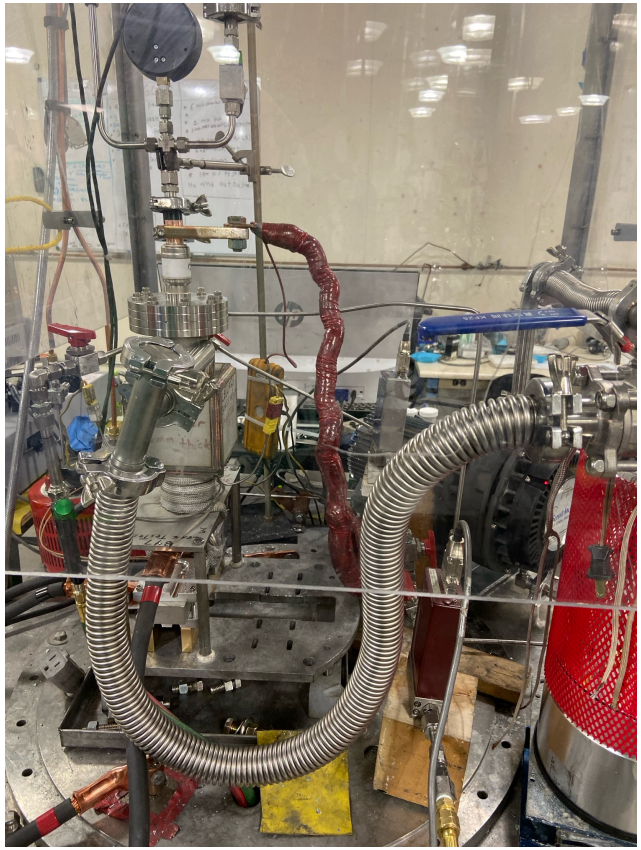

Dr. Randy Booker, Physics Chairman, University of North Carolina-Ashville validated 200 kW of power produced by BrLP's proprietary hydrino plasma reaction maintained in its SunCell® using molten metal bath calorimetry.

Duration (s)	Input Energy (kJ)	Output Energy (kJ)	Input Power (kW)	Output Power (kW)	Gain	Excess Power (kW)
5.055	554.7	1535.3	109.7	303.7	2.77	194.0

Duration (s)	Input Energy (kJ)	Output Energy (kJ)	Input Power (kW)	Output Power (kW)	Gain	Excess Power (kW)
2.917	422.1	1058.1	144.7	362.8	2.50	218.1

(brilliantlightpower.com/pdf/Randy_Booker_Report.pdf)

Validation: Water Bath Calorimetry Measured 300 kW of Hydrino Power Production

Dr. Randy Booker, Physics Chairman, University of North Carolina-Ashville 300 kW of power produced by BrLP's proprietary hydrino plasma reaction maintained in its SunCell® using water bath calorimetry. (brilliantlightpower.com/pdf/Randy_Booker_Report.pdf)

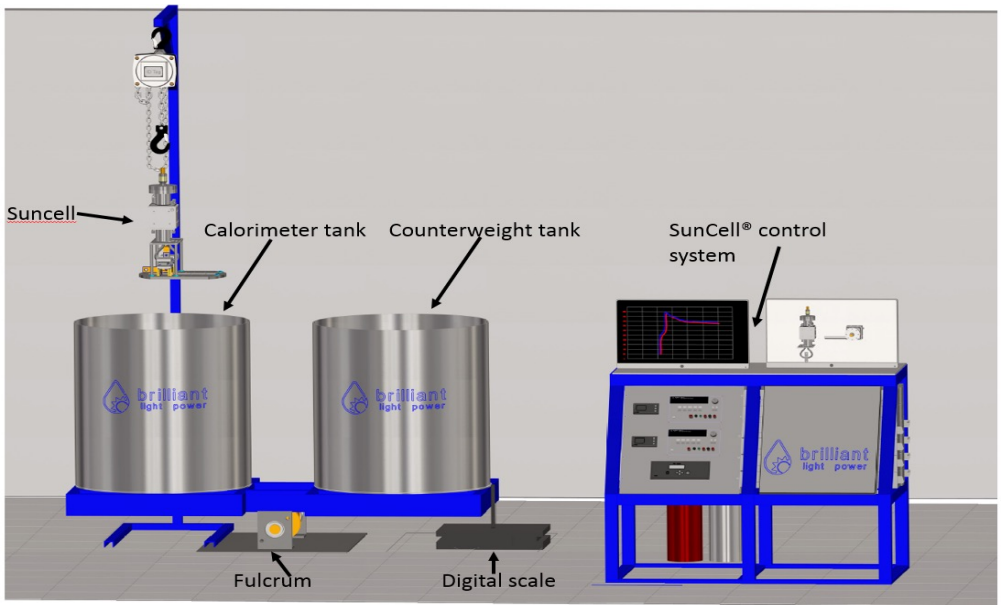

Duration (s)	Input Energy (kJ)	Output Energy (kJ)	Input Power (kW)	Output Power (kW)	Power Gain	Net Excess Power (kW)
2.115	192.95	818.38	91.23	386.94	4.24	295.71

Validation: Water Bath Calorimetry Measured 340 kW of Hydrino Power Production and Molten Metal Calorimeter Measured 220 kW

Stephen Tse, Ph.D. Department of Mechanical and Aerospace Engineering, Rutgers University validated up to 340 kW of power produced by BrLP's proprietary hydrino plasma reaction maintained in its SunCell® using molten metal bath and water bath calorimetry. (https://brilliantlightpower.com/pdf/Tse-Validation-Report-Brilliant-Light-Power.pdf)

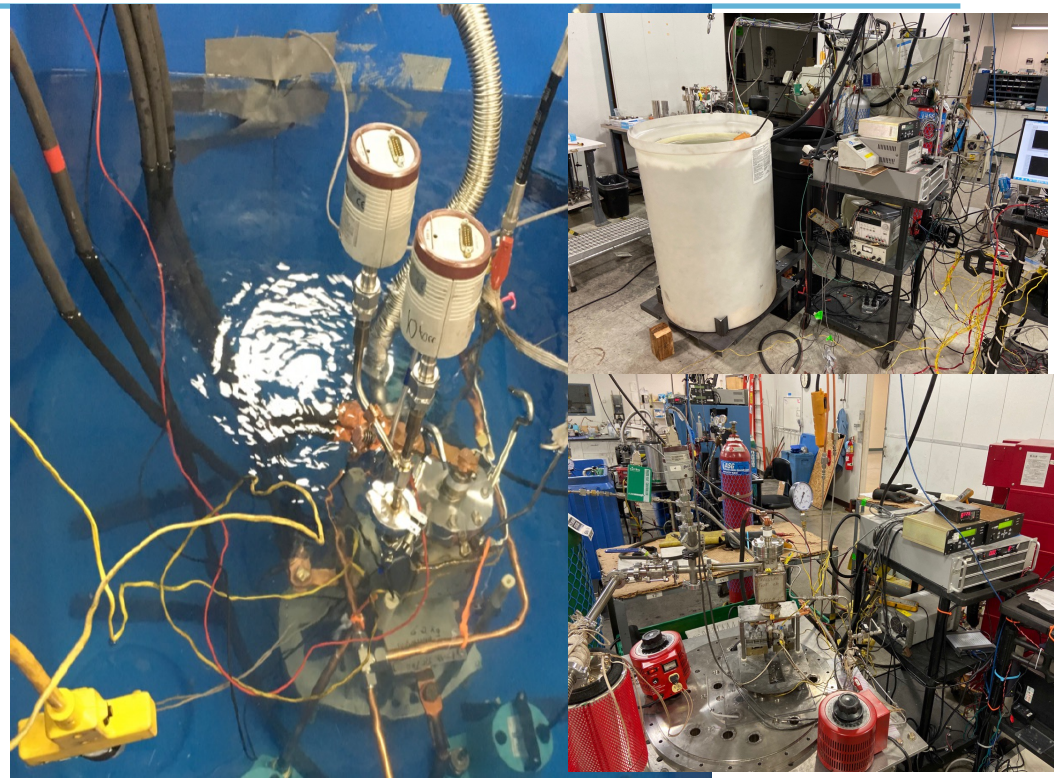

Calorimeter	Duration (s)	Input Energy (kJ)	Output Energy (kJ)	Input Power (kW)	Output Power (kW)	Power Gain	Net Excess Power (kW)
Molten Metal Bath	2.917	422.1	1058.1	144.7	362.7	2.51	218
Molten Metal Bath	5.055	554.7	1548.1	109.7	306.25	2.79	196.5
Water Bath	2.115	192.95	915.35	91.2	432.8	4.74	341.6

Validation: Water Bath Calorimetry Measured 273 kW of Hydrino Power Production in 50 cm^3 Corresponding to 5 MW/liter Power Density

Dr. Mark Nansteel, Ph.D. University of California, Berkeley and heat transfer expert validated up to 273 kW of power produced by BrLP's proprietary hydrino plasma reaction maintained in its advanced tube-type SunCell® using water bath calorimetry. The power density was a remarkable 5 MW/liter. (https://brilliantlightpower.com/pdf/Waterbath_Calorimetry_Data_and_Analysis_031120.pdf)

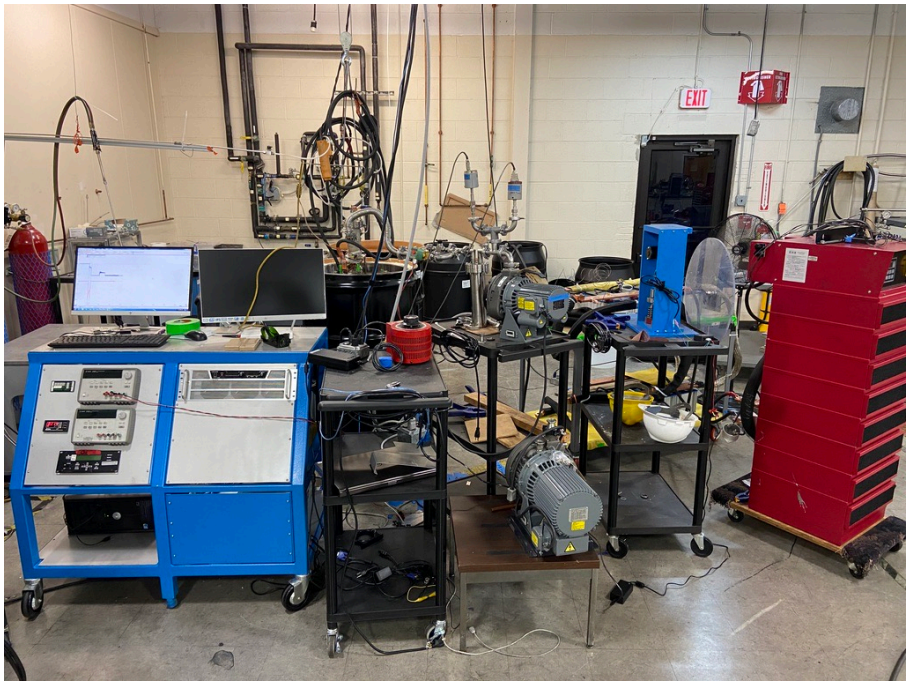

Duration (s)	Input Energy (kJ)	Output Energy (kJ)	Input Power (kW)	Output Power (kW)	Power Gain	Net Excess Power (kW)
2.95	274.9	1080.2	93.2	366.2	3.93	273.0

Validation: Steam Loss Calorimetry Measured 210 kW of Continuous Steam Production by the Hydrino Reaction Maintained in a SunCell® Operated as a Boiler

Dr. Mark Nansteel, Ph.D. University of California, Berkeley and heat transfer expert validated 210 kW of excess power produced by a hydrino plasma reaction maintained in a SunCell® using mass balance in the production of steam. The hydrino reaction was shown to be dependent on operating temperature and activation of the gas reactants by a glow discharge plasma.
https://brilliantlightpower.com/pdf/Report_on_Water_Bath_Calorimetry_12.04.20.pdf
https://brilliantlightpower.com/pdf/Report_on_Water_Bath_Calorimetry_(031621)_rev.pdf

Steam production was maintained over a 100-hour duration in an internal field trial.

Discharge	Gallium Temperature (°C)	Duration (s)	Input Energy (kJ)	Output Energy (kJ)	Input power (kW)	Output Power (kW)	Power Gain	Net Excess Power (kW)
Yes	196	302	10,346	16,480	34.26	54.57	1.59	20.3
Yes	177	296	9341	18,708	31.56	63.2	2	31.7
No	458	167	6951	16,264	41.62	97.39	2.34	55.8
Yes	425	200	7800	26,392	39	131.96	3.38	93
Yes	716	50	3232	10,480	65	274.2	4.22	210

Novel Hydrino Compounds

Web-like compounds self-aggregate from dispersed particles in air. Particle aggregation by molecular hydrino can also be observed in aqueous solution and by electron microscopy.

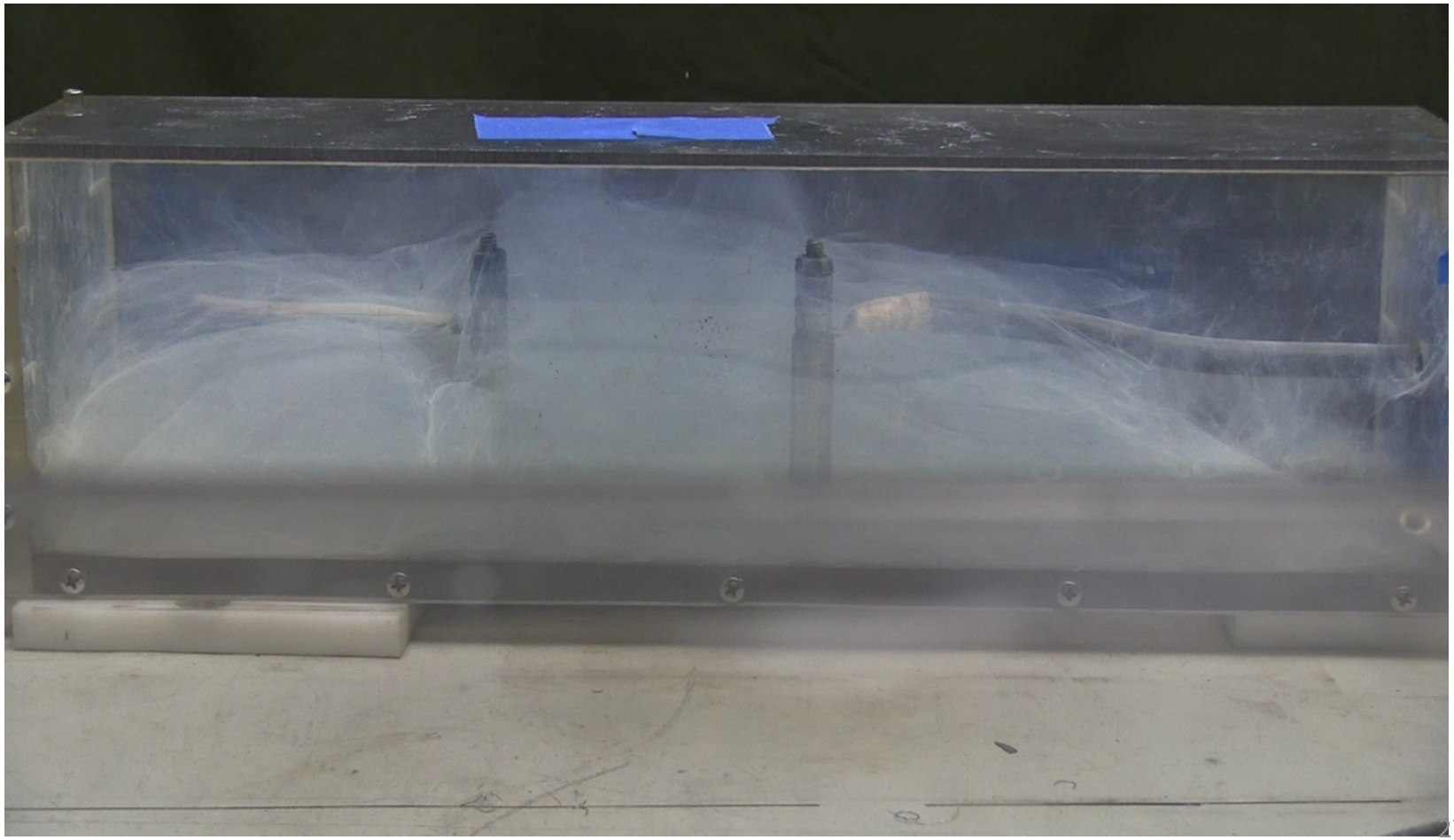

Methods for measuring Hydrino® product

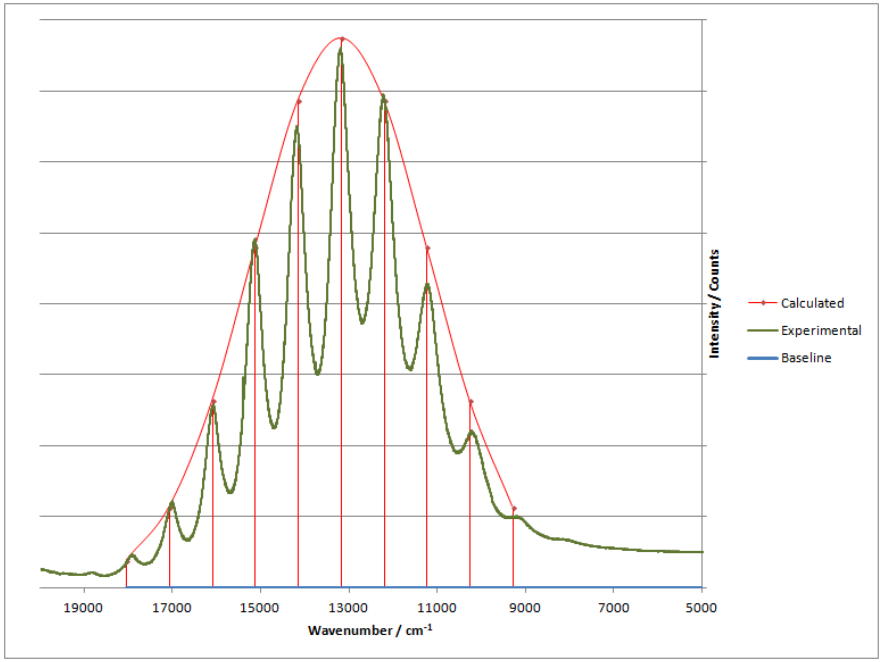

- GUT
- Molecular modeling
- H(1/2) and H(1/4) hydrino transitions observed by continuum radiation
- Astronomy data verifying hydrinos such as H(1/2), H(1/3), and H(1/4) hydrino transitions
- H (1/4) spin-nuclear hyperfine transition
- Hydrino trapped on witness plates and in alkali halide-hydride crystals
- Polymeric molecular hydrino compounds
- H_2 (1/4) 1000 times gas chromatographic concentration

- H_2 (1/4) ro-vib spectrum in crystals by e-beam excitation emission spectroscopy
- H_2 (1/4) X-ray photoelectron spectroscopy (XPS) binding energy
- H_2 (1/4) Fourier Transform Infrared (FTIR)
- H_2 (1/4) Inverse Raman effect (IRE)
- H_2 (1/4) Raman spectroscopy
- H_2 (1/4) Photoluminescence spectroscopy
- Electron paramagnetic resonance spectroscopy (EPR)
- Time of flight secondary ion mass spectroscopy (ToF-SIMs) and electrospray ionization time of flight (ESI-ToF) identification of hydrino compounds
- MAS H NMR
- Thermogravimetric analysis (TGA)
- Gas chromatography
- Liquid chromatography-mass spectroscopy
- Fast H in plasmas including microwave and rt-plasmas
- Rt-plasma with filament and discharge
- Plasma afterglow
- Highly pumped states
- H inversion
- Commercial differential scanning calorimetric (DSC) and water flow calorimetry with multiple solid fuels chemistries
- Arbin-Instrument measured electricity gain over theoretical in CIHT cells
- 20 MW extreme ultraviolet NIST-calibrated optically measured power in shot blasts
- Commercial bomb calorimetry of energetic shots
- Shock wave 10X TNT
- SunCell® fully ionized energetic plasma and electromagnetic pulse
- SunCell® water bath and molten metal bath calorimetry at over 100 kW excess power
- Continuous power engineering

Identification of Molecular Hydrino by the Gold Standard: Rotational Energies that Match the Predicted p^2 Energies of H_2 Using Exact Closed-Form Solutions of H_2^+ and H_2

The Laplacian in ellipsoidal coordinates is solved with the constraint of nonradiation

$$(\eta-\zeta)R_\xi\frac{\partial}{\partial\xi}(R_\xi\frac{\partial\varphi}{\partial\xi})+(\zeta-\xi)R_\eta\frac{\partial}{\partial\eta}(R_\eta\frac{\partial\varphi}{\partial\eta})+(\xi-\eta)R_\zeta\frac{\partial}{\partial\zeta}(R_\zeta\frac{\partial\varphi}{\partial\zeta})=0$$

The total energy of the hydrogen molecular ion having a central field of $+pe$ at each focus of the prolate spheroid molecular orbital

$$E_T=-p^2\left\{\frac{e^2}{8\pi\varepsilon_o a_{\mathrm{H}}}(4\ln 3-1-2\ln 3)\left[1+\sqrt{\frac{2\hbar\sqrt{\frac{2e^2}{4\pi\varepsilon_o\left(2a_{\mathrm{H}}\right)^3}}{m_e}}{m_e c^2}}\right]-\frac{1}{2}\hbar\sqrt{\frac{k}{\mu}}\right\}=-p^2 16.13392\ eV-p^3 0.118755\ eV$$

The total energy of the hydrogen molecule having a central field of $+pe$ at each focus of the prolate spheroid molecular orbital

$$E_T=-p^2\left\{\frac{e^2}{8\pi\varepsilon_o a_0}\left[\left(2\sqrt{2}-\sqrt{2}+\frac{\sqrt{2}}{2}\right)\ln\frac{\sqrt{2}+1}{\sqrt{2}-1}-\sqrt{2}\right]\left[1+p\sqrt{\frac{2\hbar\sqrt{\frac{e^2}{4\pi\varepsilon_o a_0^3}}{m_e}}{m_e c^2}}\right]-\frac{1}{2}\hbar\sqrt{\frac{k}{\mu}}\right\}=-p^2 31.351\ eV-p^3 0.326469\ eV$$

The Nature of the Chemical Bond of Hydrogen cont'd

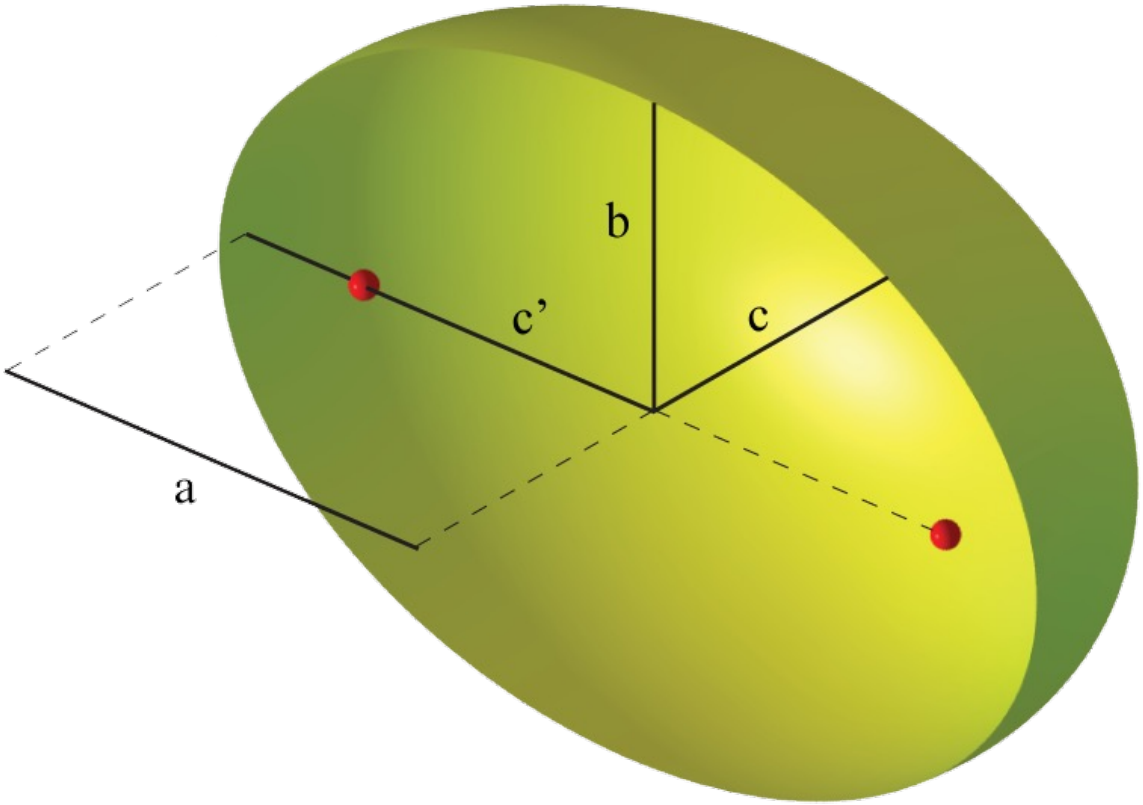

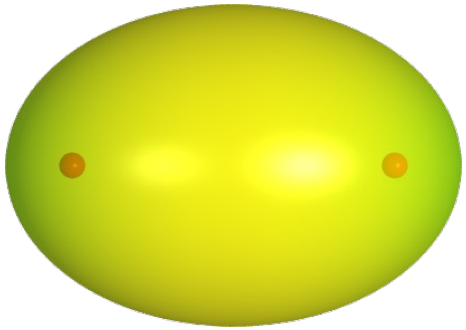

Front view

The Internuclear Distance, $2c'$, which is the distance between the foci is $2c' = \sqrt{2}a_o$.

The experimental internuclear distance is $\sqrt{2}a_o$.

The Semiminor Axis, *b*, is $b = \frac{1}{\sqrt{2}}a_o$ The Eccentricity, *e*, is $e = \frac{1}{\sqrt{2}}$

Charge-Density Function

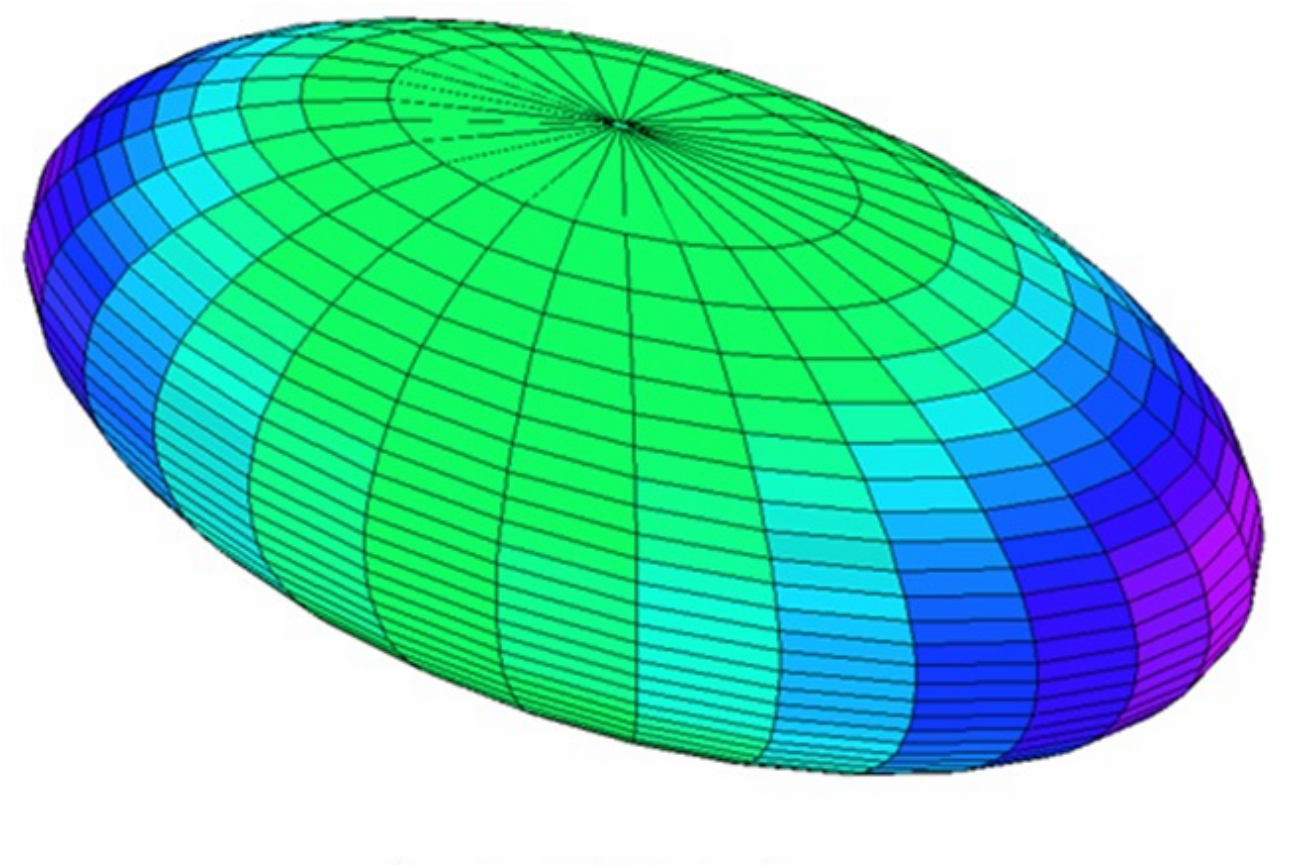

Molecular Orbital Current Corresponding to Electron Spin s=1/2

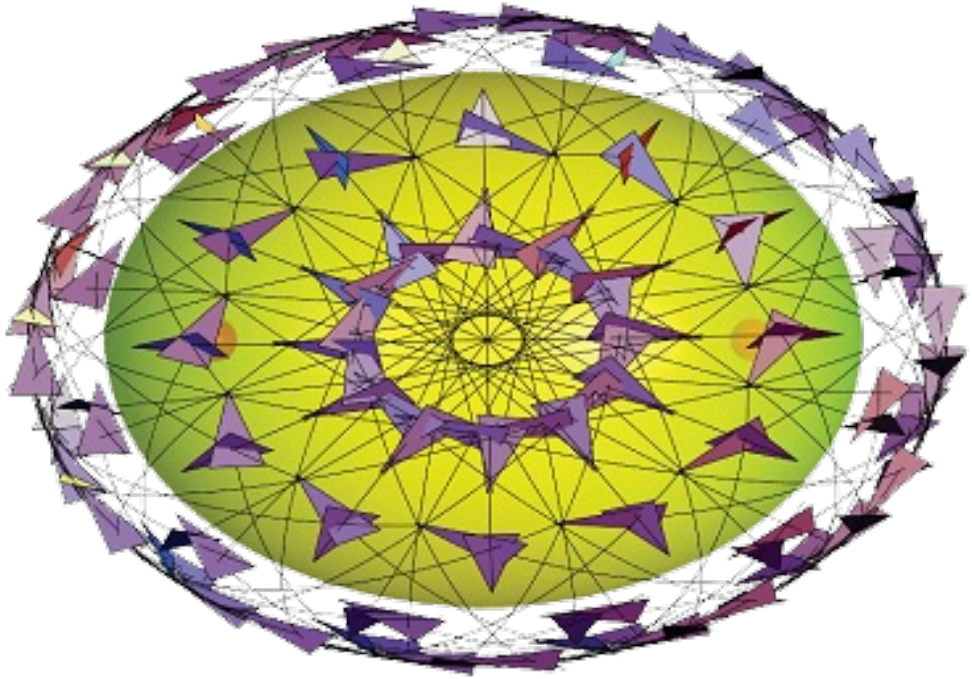

A representation of the z-axis view of the continuous charge-density and supercurrent-density distributions of the MO with 144 vectors overlaid giving the direction of the currents (nuclei not to scale).

The calculated and experimental parameters of H_2, H_2^+, D_2, D_2^+

Parameter	Calculated	Experimental	Eqs.	Ref. for Exp.
H_2 Bond Energy	4.478 eV	4.478 eV	11.300	24
D_2 Bond Energy	4.556 eV	4.556 eV	11.302	24
H_2^+ Bond Energy	2.654 eV	2.651 eV	11.269	24
D_2^+ Bond Energy	2.696 eV	2.691 eV	11.271	25
H_2 Total Energy	31.677 eV	31.675 eV	11.296	24, 30, 19[a]
D_2 Total Energy	31.760 eV	31.760 eV	11.297	20, 25[b]
H_2 Ionization Energy	15.425 eV	15.426 eV	11.298	30
D_2 Ionization Energy	15.463 eV	15.466 eV	11.299	25
H_2^+ Ionization Energy	16.253 eV	16.250 eV	11.267	24, 19[c]
D_2^+ Ionization Energy	16.299 eV	16.294 eV	11.268	20, 25[d]
H_2^+ Spin Magnetic Moment	$0.5\mu_B$	$0.5\mu_B$	12.24	31
Absolute H_2 Gas-Phase NMR Shift	-28.0 ppm	-28.0 ppm	11.416	32-33
H_2 Quadrupole Moment	0.4764 X 10^{-16} cm^2	0.38 0.15 X 10^{-16} cm^2	11.430-11.431	46
H_2 Internuclear Distance	0.7411 Å	0.741 Å	12.75	34
D_2 Internuclear Distance	0.7411 Å	0.741 Å	12.75	34
H_2^+ Internuclear Distance	1.0577 Å	1.06 Å	12.81	24
D_2^+ Internuclear Distance	1.0577 Å	1.0559 Å	12.81	25
H_2 Vibrational Energy	0.517 eV	0.516 eV	11.308	27, 28
D_2 Vibrational Energy	0.371 eV	0.371 eV	11.313	14, 20
H_2 $\omega_e x_e$	120.4 cm^{-1}	121.33 cm^{-1}	11.310	25
D_2 $\omega_e x_e$	60.93 cm^{-1}	61.82 cm^{-1}	11.314	20
H_2^+ Vibrational Energy	0.270 eV	0.271 eV	11.277	14, 20
D_2^+ Vibrational Energy	0.193 eV	0.196 eV	11.281	20
H_2 J=1 to J=0 Rotational Energy	0.01511 eV	0.01509 eV	12.77	24
D_2 J=1 to J=0 Rotational Energy	0.007557 eV	0.00755 eV	12.78	24
H_2^+ J=1 to J=0 Rotational Energy	0.00742 eV	0.00739 eV	12.83	24
D_2^+ J=1 to J=0 Rotational Energy	0.0037095 eV	0.003723 eV	12.84	25

E-beam Emission Hydrino $H_2(1/4)$ Gas Ro-vibrational P Branch

Of the noble gases, argon uniquely contains trace hydrino gas due to contamination during purification. Argon and oxygen co-condense during cryo-distillation of air and the oxygen is removed by reaction with hydrogen on a recombination catalyst such as platinum whereby hydrino is formed during the recombination reaction due to the subsequent reaction of HOH catalyst with H. The known peaks are H I, O I, O_2 bands. The unknown peaks match molecule hydrino ($H_2(1/4)$ P branch) with no other unassigned peaks present in the spectrum.

The small satellite lines match the rotational spin-orbital splitting energies that were also observed by Raman spectroscopy. The spin-orbital splitting energies due to rotation of m528 cm^{-1}, m = 1, 1.5 wherein 1.5 involves the m = 0.5 and m = 1 splittings. It is extraordinary that the EPR, Raman, and electron-beam excitation spectra give the same information about the structure of molecular hydrino in energy ranges that differ by reciprocal of the $H_2(1/4)$ diamagnetic susceptibility coefficient: $1/7X10^{-7}$ = $1.4X10^{6}$ wherein the induced diamagnetic orbital magnetic moment active during EPR was replaced by the orbital molecular rotational magnetic moment active during Raman and electron-beam excitation of rotational transitions.

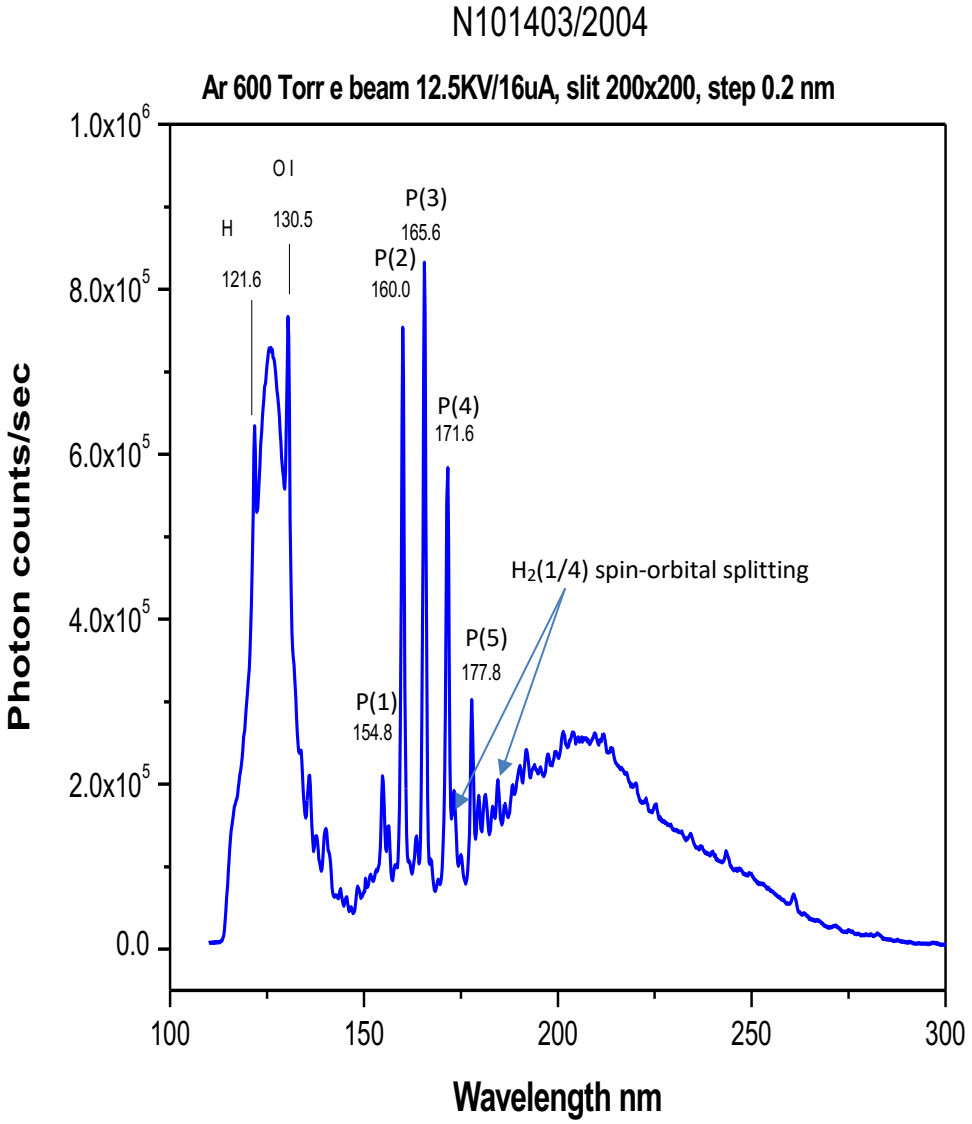

E-beam Emission Hydrino $H_2(1/4)$ Gas Ro-vibrational P Branch

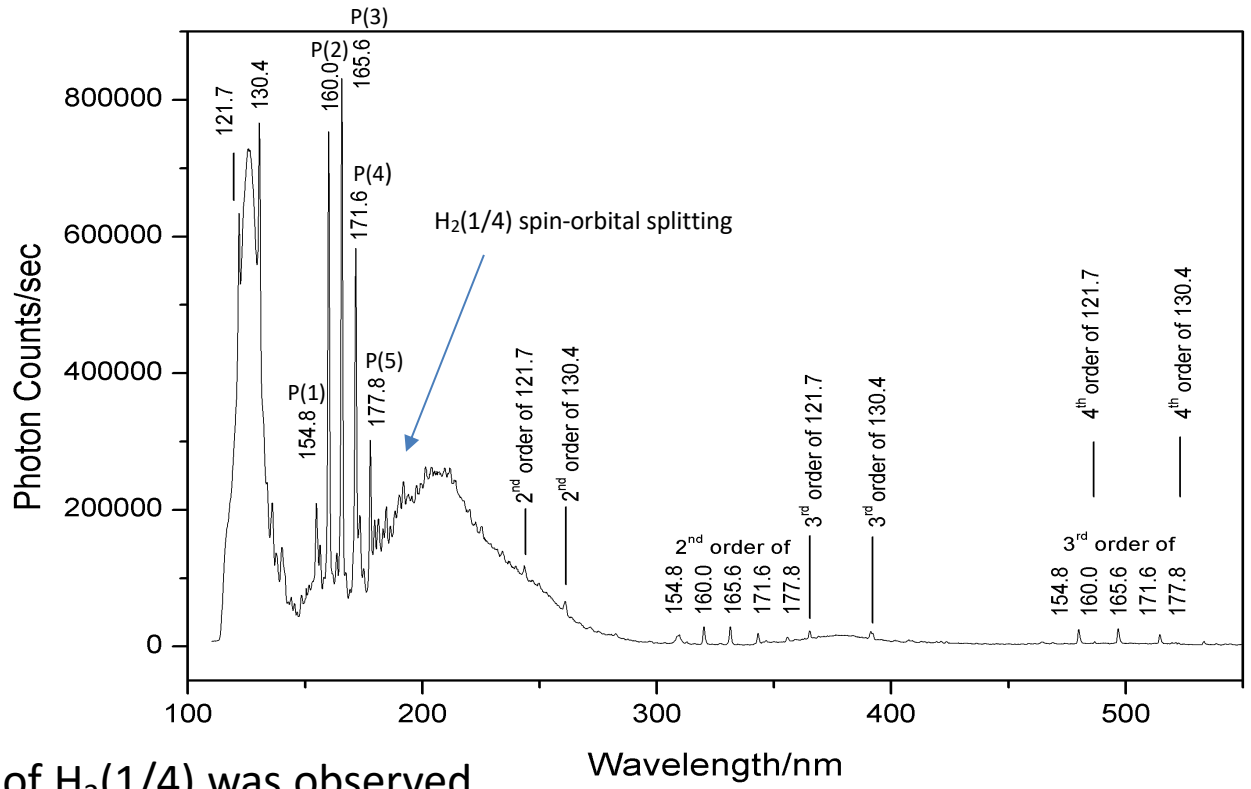

The ro-vibrational spectrum of $H_2(1/4)$ was observed by 6 keV electron beam excitation of argon gas at atmospheric pressure wherein the electron beam passed through a silicon nitride window of the plasma cell. The cutoff of 8.2 eV and the line spacing of 0.25 eV matched the $\nu = 1$ to $\nu = 0$ vibrational transition with the P-branch rotational spectrum of $H_2(1/4)$.

HOH-Argon E-beam Emission Linear Regression

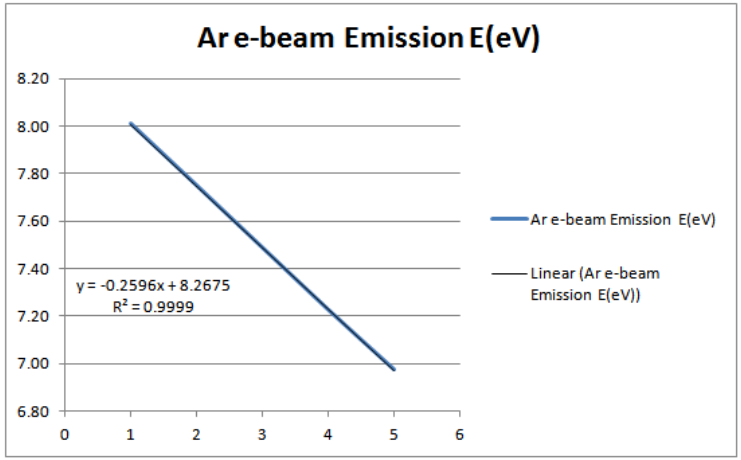

R. L. Mills, K. Akhtar, G. Zhao, Z. Chang, J. He, X. Hu, G. Chu, "Commercializable Power Source Using Heterogeneous Hydrino Catalysts," Int. J. Hydrogen Energy, Vol. 35, (2010), pp. 395–419, doi: 10.1016/j.ijhydene.2009.10.038.

E-beam Emission Hydrino $H_2(1/4)$ Gas Ro-vibrational P Branch

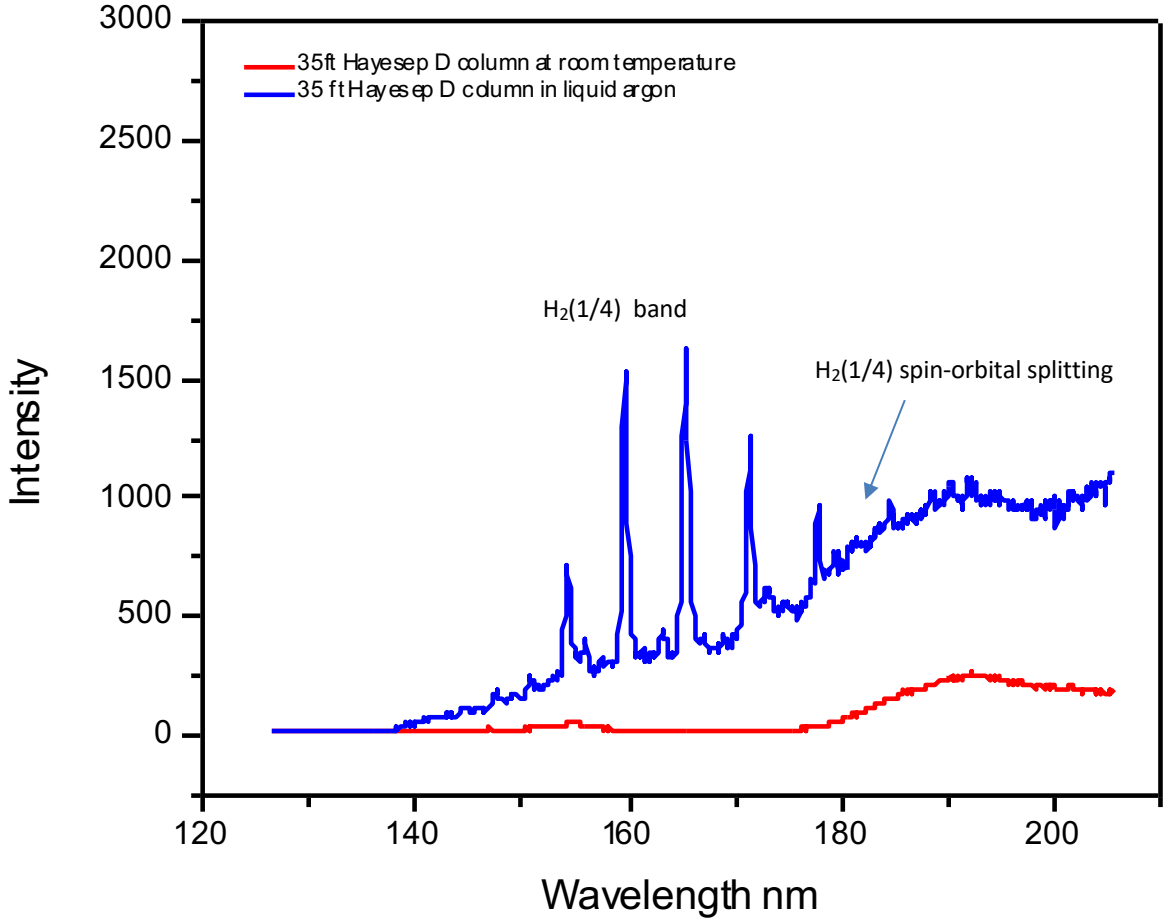

$H_2(1/4)$ gas of an argon/$H_2(1/4)$ mixture formed by recombination of hydrogen and oxygen on a supported noble metal catalyst in an argon atmosphere was enriched on a HayeSep® D chromatographic column cooled to a cryogenic temperature in a liquid argon. The $H_2(1/4)$ enrichment caused a dramatic increase in the ro-vibrational P branch of $H_2(1/4)$ observed by e-beam excitation emission spectroscopy. The spectrum was obtained at room temperature.

E-beam Emission Hydrino $H_2(1/4)$ Gas Ro-vibrational P Branch

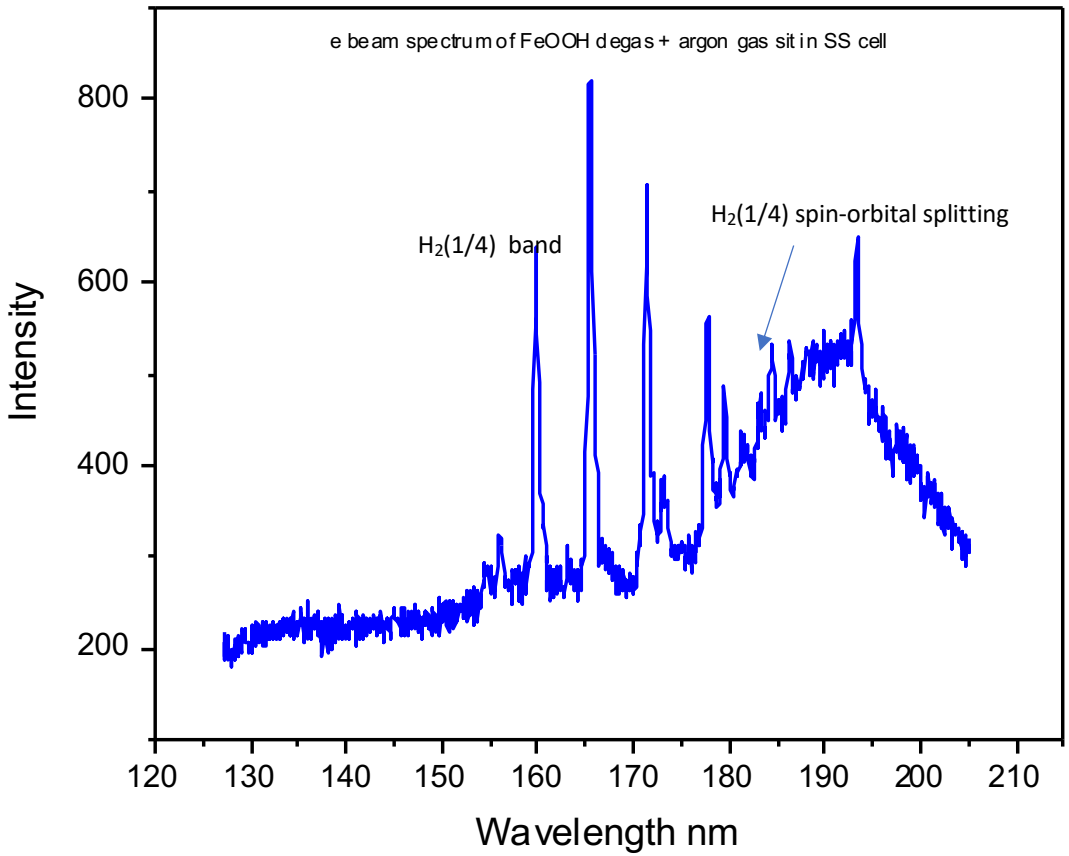

Ultraviolet emission spectrum from electron beam excitation of $H_2(1/4)$ gas released from heating FeOOH:$H_2(1/4)$. The cutoff of 8.2 eV and the line spacing of 0.25 eV matched the $\nu = 1$ to $\nu = 0$ vibrational transition with the P-branch rotational spectrum of $H_2(1/4)$.

E-beam Emission Hydrino $H_2(1/4)$ Gas Ro-vibrational P Branch

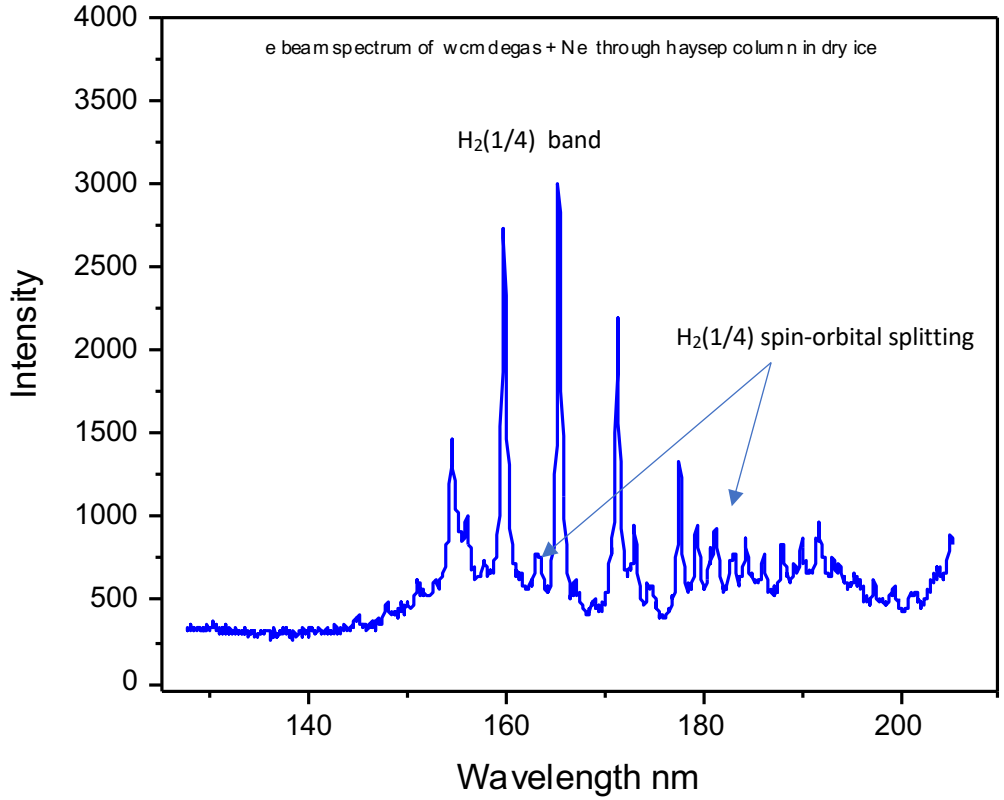

The ro-vibrational spectrum of $H_2(1/4)$ that was observed as ultraviolet emission lines by 12 keV electron beam excitation of thermally released GaOOH:$H_2(1/4)$ gas flowed at atmospheric pressure from a cryogenic chromatography wherein the electron beam passed through a silicon nitride window of the plasma cell. The cutoff of 8.2 eV and the line spacing of 0.25 eV matched the $\nu = 1$ to $\nu = 0$ vibrational transition with the P-branch rotational spectrum of $H_2(1/4)$.

R. Mills, "Hydrino States of Hydrogen", https://brilliantlightpower.com/pdf/Hydrino_States_of_Hydrogen_Paper.pdf.

Matrix-Shifted E-beam Emission Hydrino $H_2(1/4)$ Ro-vibrational P Branch ($H_2(1/4)$ in KCl matrix)

Ultraviolet emission spectrum from electron beam excitation of KCl that was impregnated with hydrino reaction product gas showing the $H_2(1/4)$ ro-vibrational P branch in the crystalline lattice.

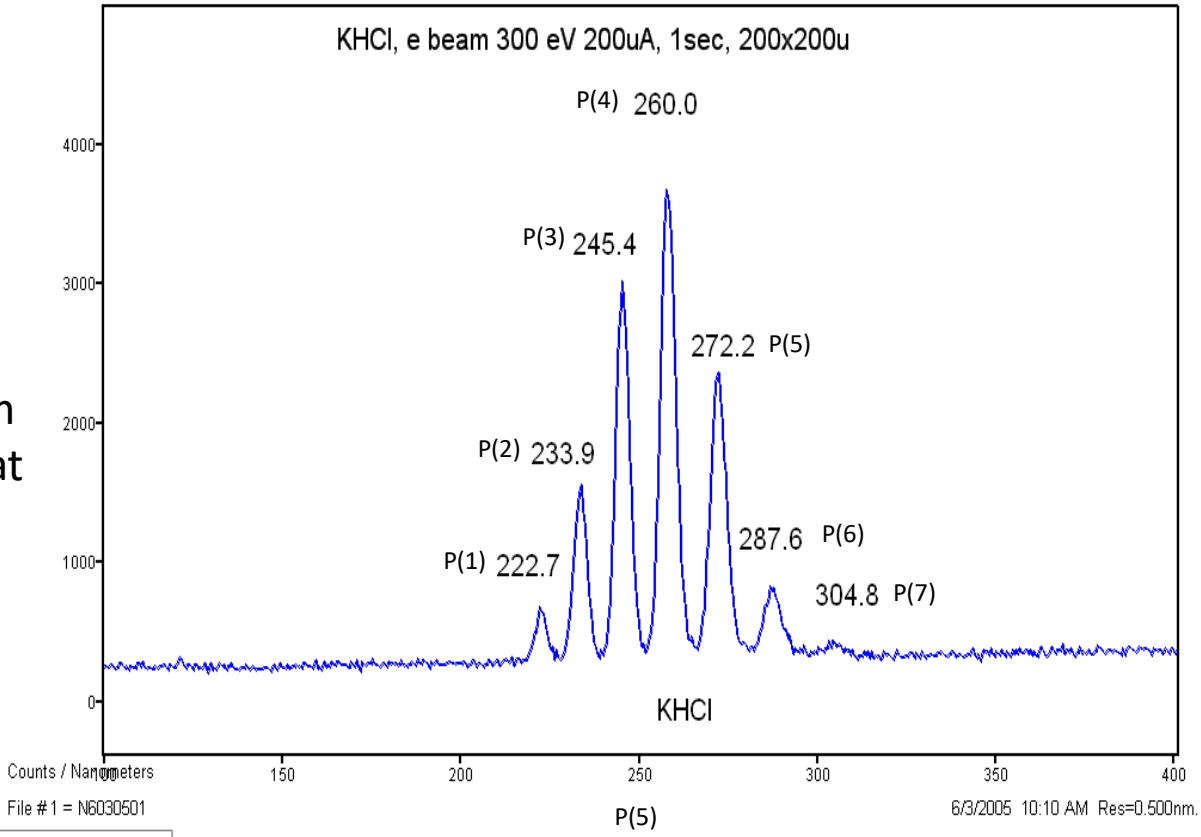

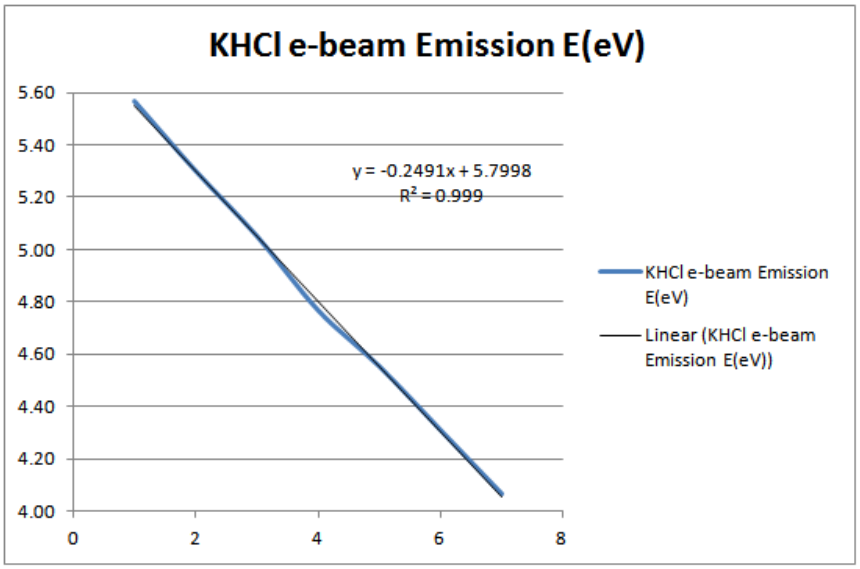

E-beam Emission Linear Regression

R. Mills, X Yu, Y. Lu, G Chu, J. He, J. Lotoski, "Catalyst induced hydrino transition (CIHT) electrochemical cell," (2012), Int. J. Energy Res., (2013), DOI: 10.1002/er.3142.

R. L. Mills, J. He, Z. Chang, W. Good, Y. Lu, B. Dhandapani, "Catalysis of Atomic Hydrogen to Novel Hydrogen Species H-(1/4) and H2(1/4) as a New Power Source," Int. J. Hydrogen Energy, Vol. 32(13), (2007), pp. 2573–2584.

Vibrational and Rotational Predicted Energies

• Hydrogen molecular vibrational energy, E_{vib}, for the $v = 0$ to $v = 1$ transition of hydrogen type molecules $H_2(1/p)$ is

$$E_{vib} = p^2 \times 0.515912\ eV$$

• The rotational energies, E_{rot}, for the J to $J+1$ transition of hydrogen molecules $H_2(1/p)$ is

$$E_{rot} = p^2 \times (J+1) \times 0.01509\ eV$$

•The emitters in both HOH-Ar and a solid impregnated with hydrino gas match emission spacing's and match the rotationally predicted energies for $H_2(1/4)$. The emitter in HOH-Ar matches the vibrationally predicted energy for $H_2(1/4)$.

H2(1/4) in Ar	Experimental Value (eV)	Theoretical Value (eV)
Vibrational Energy (v = 0 to 1)	8.2675	8.2544
Rotational Energy (J = 0 to 1)	0.2596	0.2414

H2(1/4) in KHCl	Experimental Value (eV)	Theoretical Value (eV)
Vibrational Energy (v = 0 to 1)	5.7998	*
Rotational Energy (J = 0 to 1)	0.2491	0.2414

• *The vibrational energy for $H_2(1/4)$ in a solid matrix is shifted due to the increased effective mass from the solid matrix interaction analogous to the cases of H_2 in solid matrices such as Si and Ge as discussed in primary literature.

[1]: R. Mills, The Grand Unified Theory of Classical Physics; September 2016 Edition, posted at http://brilliantlightpower.com/book-download-and-streaming/

Ro-vibrational P Branch from E-beam Emission of Hydrino $H_2(1/4)$ in KCl Matrix is Dependent on Temperature that Confirms Ro-Vibrational Assignment

Emission spectra were recorded using a McPherson grazing incidence EUV spectrometer and a CCD detector during electron-beam excitation of KCl getter exposed to thermal decomposition gas from Ga_2O_3:$H_2(1/4)$ from the SunCell® at 3 keV and 30 uA. The series of peaks matches the $H_2(1/4)$ theoretical ro-vibrational peaks to within an error of less than 1%. The elimination of the emission while cryocooling and its return at lower intensity at room temperature confirmed that the source of the emission was $H_2(1/4)$ ro-vibration with some $H_2(1/4)$ diffusion loss by thermally cycling.

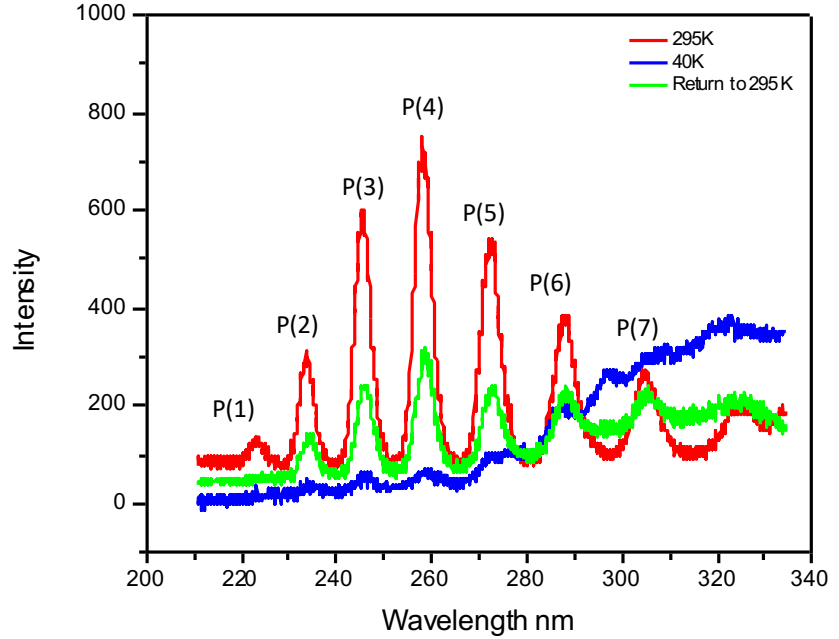

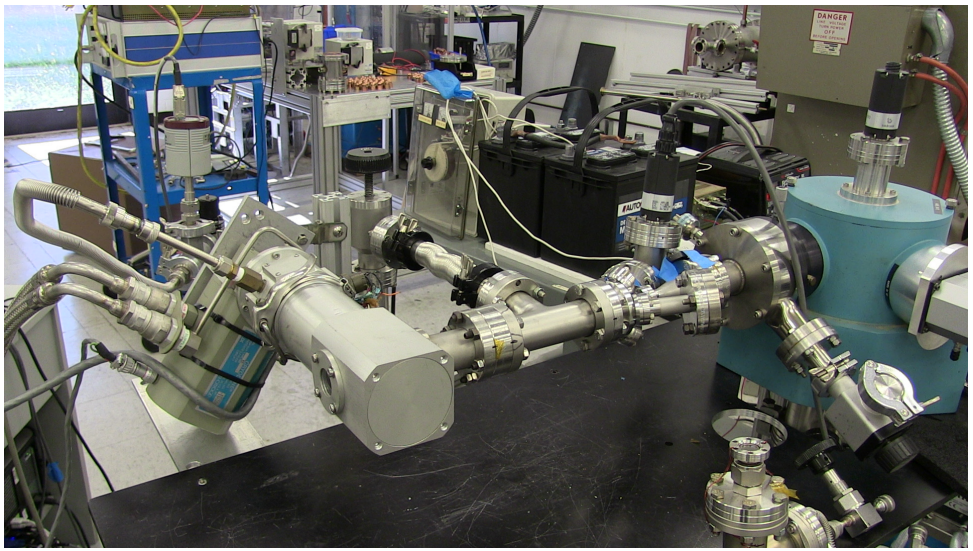

Raman Confirmation of Molecular Hydrino of $H_2(1/4)$ in KCl Matrix Ro-Vibrational Band

- The spin of the molecular hydrino molecular orbital (MO) is ½(↑↑+↓↓) where each arrow designates the spin vector of one electron.
- Due to the unique electronic structure of $H_2(1/4)$ comprising a paired and an unpaired electron in the $H_2(1/4)$ MO requiring spin ½ conservation during transitions, the excitation and decay of ro-vibration states of molecular hydrino involve two-photons, each of ½ the energy of the ro-vibrational state.
- The Raman spectrum of KCl getter exposed to gas from the thermal decomposition of Ga_2O_3:$H_2(1/4)$ collected from the SunCell® wherein the spectrum was recorded with a Horiba Jobin Yvon LabRam ARAMIS spectrometer with a 325nm laser and a 1200 grating over a range of 8000-19,000 cm^{-1} Raman shift.
- The corresponding emission spectrum matched the ½ -energy emission spectrum of the 260nm e-beam band comprising rotational transitions of the matrix-shifted ν=1 to ν=0 vibrational transition.
- A long-pass edge filter confirmed the assignments wherein the series of peaks match the theoretical energies to within an error of less than 1%.

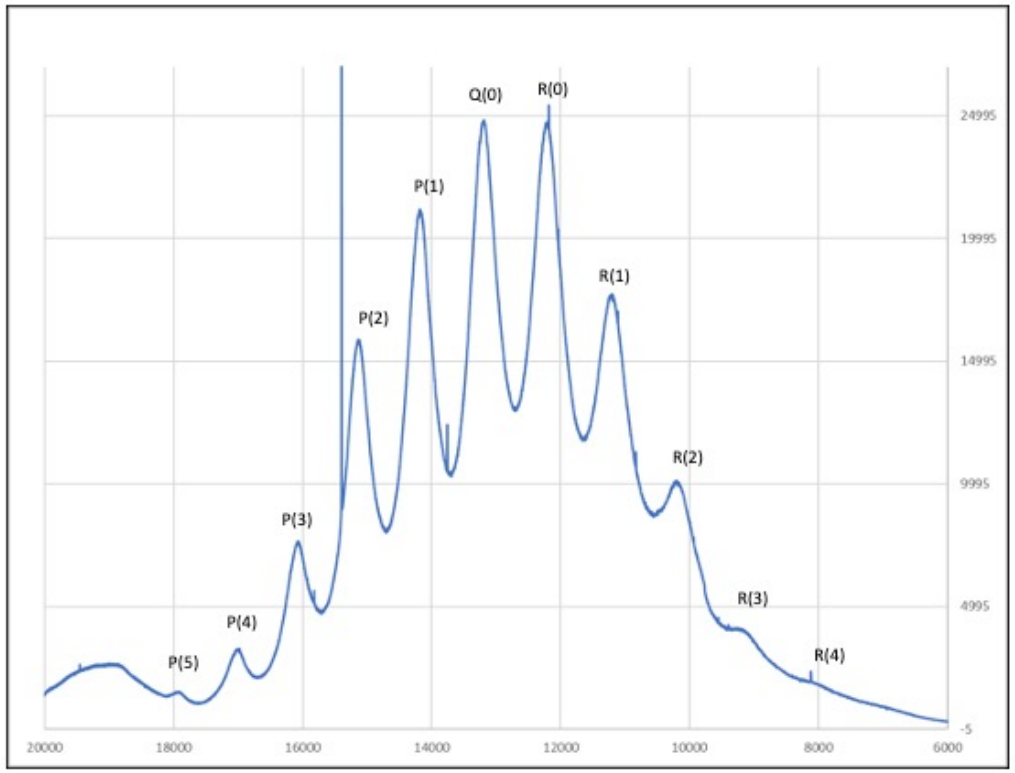

R. Mills, "Hydrino States of Hydrogen", (2022), submitted for publication https://brilliantlightpower.com/pdf/Hydrino_States_of_Hydrogen.pdf.

R. Mills, X Yu, Y. Lu, G Chu, J. He, J. Lotoski, "Catalyst induced hydrino transition (CIHT) electrochemical cell," (2012), Int. J. Energy Res., (2013), DOI: 10.1002/er.3142.

R. Mills, J. Lotoski, J. Kong, G. Chu, J. He, J. Trevey, "High-Power-Density Catalyst Induced Hydrino Transition (CIHT) Electrochemical Cell." Int. J. Hydrogen Energy, 39 (2014), pp. 14512–14530 DOI: 10.1016/j.ijhydene.2014.06.153.

R. Mills, Y. Lu, R. Frazer, "Power Determination and Hydrino Product Characterization of Ultra-low Field Ignition of Hydrated Silver Shots", Chinese Journal of Physics, Vol. 56, (2018), pp. 1667-1717.

R. Mills J. Lotoski, "H_2O-based solid fuel power source based on the catalysis of H by HOH catalyst", Int'l J. Hydrogen Energy, Vol. 40, (2015), 25-37.

Comparison of the theoretical emission energies and assignments, corresponding Raman transition energies, and observed Raman peaks.

Assignment	Emission Calculated (cm^{-1})	Calculated Raman (cm^{-1})	Raman Experimental (cm^{-1})	Difference (%)
P(5)	12,721	18,056	17,873	-1.0
P(4)	13,695	17,082	16,975	-0.6
P(3)	14,668	16,109	16,055	-0.3
P(2)	15,642	15,135	15,106	-0.2
P(1)	16,615	14,162	14,157	0
Q(0)	17,589	13,188	13,188	0
R(0)	18,563	12,214	12,174	-0.3
R(1)	19,536	11,241	11,172	-0.6
R(2)	20,510	10,267	10,159	-1.1
R(3)	21,483	9,294	9,097	-2.1
R(4)	22,457	8,320	8,090	-2.8

Comparison of Spectra of Alkali Hydroxide and Halide Mixture with Spectra of 780 nm Laser Raman Active and Inactive Powders Validated at ThermoFisher

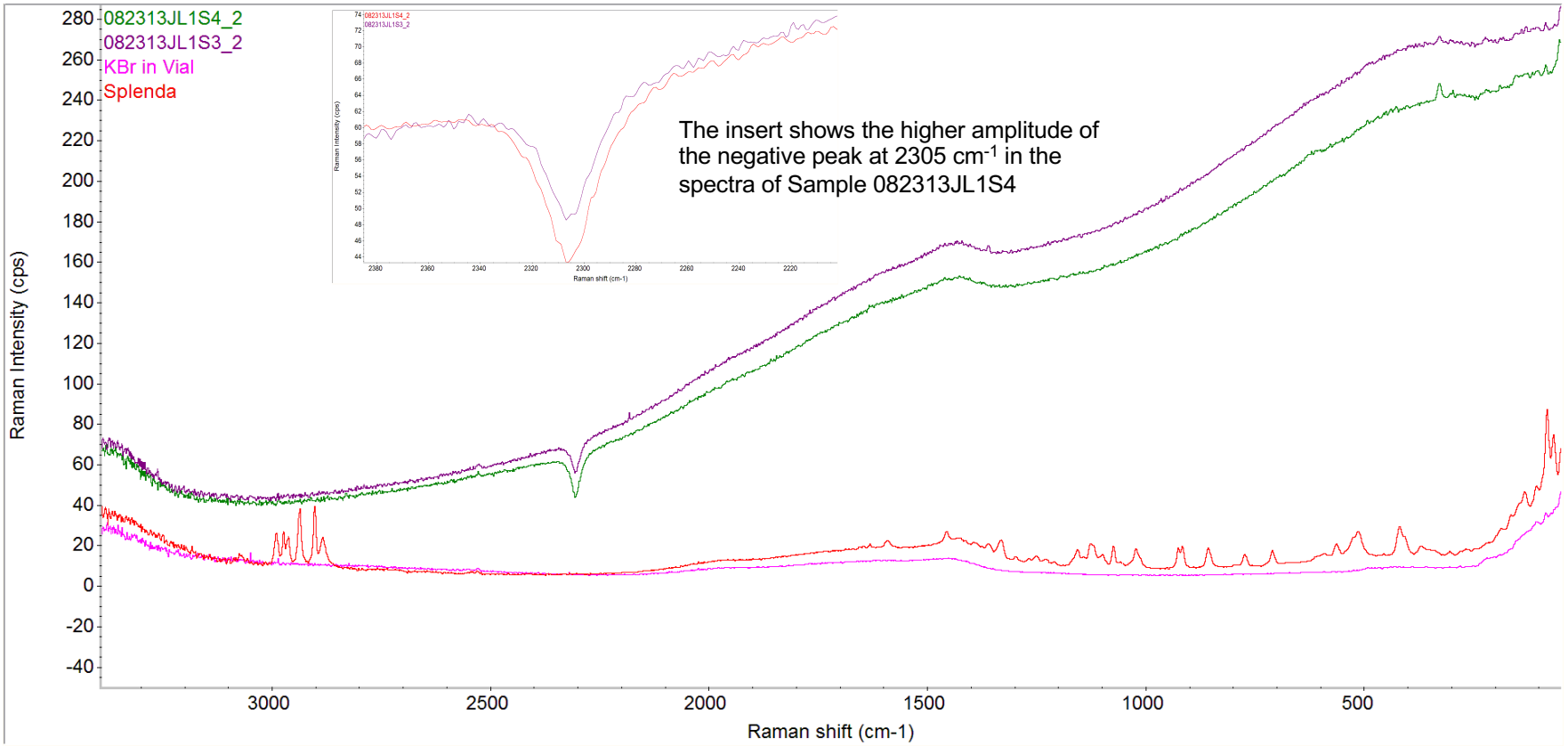

The spectra of the Alkali Hydroxide and Halide Mixture samples shown in a common scale along with reference spectra of KBr (Raman inactive, transparent) and “Splenda” (Raman active, white) powders measured at exactly the same measurement conditions, i.e. the same vial and the measurement parameters. Note: No negative peak at 2305 cm^{-1} is observed in the reference spectra.

ThermoFisher SCIENTIFIC

Alkali Hydroxide and Halide Mixture Spectra of 780 nm Laser Raman Active Powders replicated at University of Texas El Paso

The Raman forbidden $H_2(1/4)$ J = 0 to J =1 rotational transition was observed at 2300 cm^{-1} due to a surface enhanced inverse Raman effect (SEIRE). The free rotor energy of 0.2414 eV (1940 cm^{-1}) has a barrier of about 360 cm^{-1} due to interactions with the solid matrix.

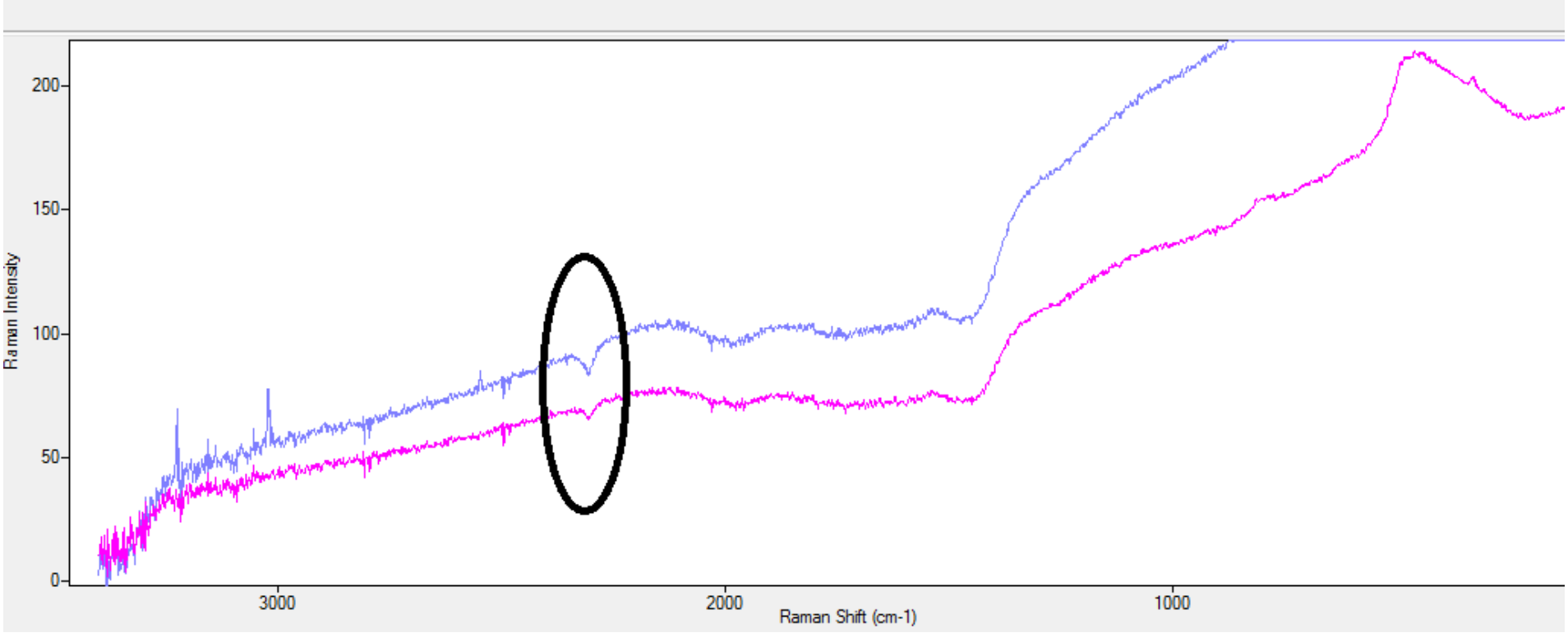

Raman Confirmation of Molecular Hydrino of $H_2(1/4)$ Rotational Energy Allowed by the Surface Enhanced Inverse Raman Effect (SEIRE)

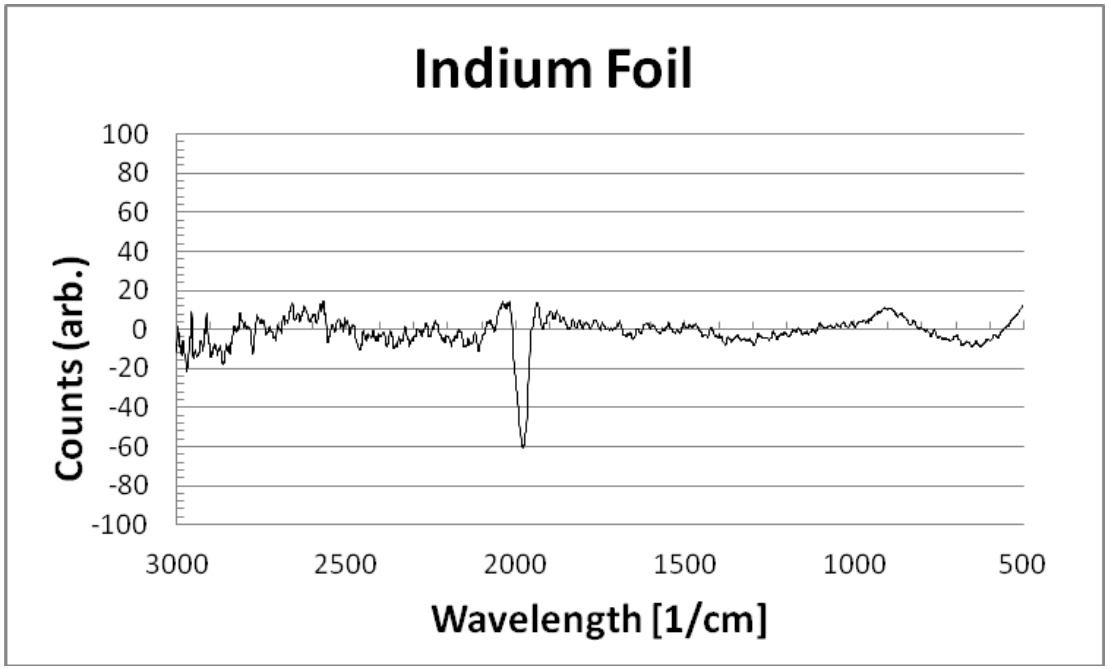

The Raman spectrum obtained on a In metal foil exposed to the product gas from a series of solid fuel ignitions under argon, each comprising 100 mg of Cu mixed with 30 mg of deionized water. Using the Thermo Scientific DXR SmartRaman spectrometer and the 780 nm laser, the spectrum showed an inverse Raman effect peak at 1982 cm^{-1} that matches the free rotor energy of $H_2(1/4)$ (0.2414 eV).

R. Mills J. Lotoski, "H_2O-based solid fuel power source based on the catalysis of H by HOH catalyst", Int'l J. Hydrogen Energy, Vol. 40, (2015), 25-37.

SEIRE Raman Confirmation of Molecular Hydrino of $H_2(1/4)$ Rotational Energy

Raman spectra obtained using the Thermo Scientific DXR SmartRaman spectrometer and the 780 nm laser on copper electrodes pre and post ignition of a 80 mg silver shot comprising 1 mole% H_2O, wherein the detonation was achieved by applying a 12 V 35,000 A current with a spot welder. The spectra showed an inverse Raman effect peak at about 1940 cm^{-1} that matches the free rotor energy of $H_2(1/4)$ (0.2414 eV).

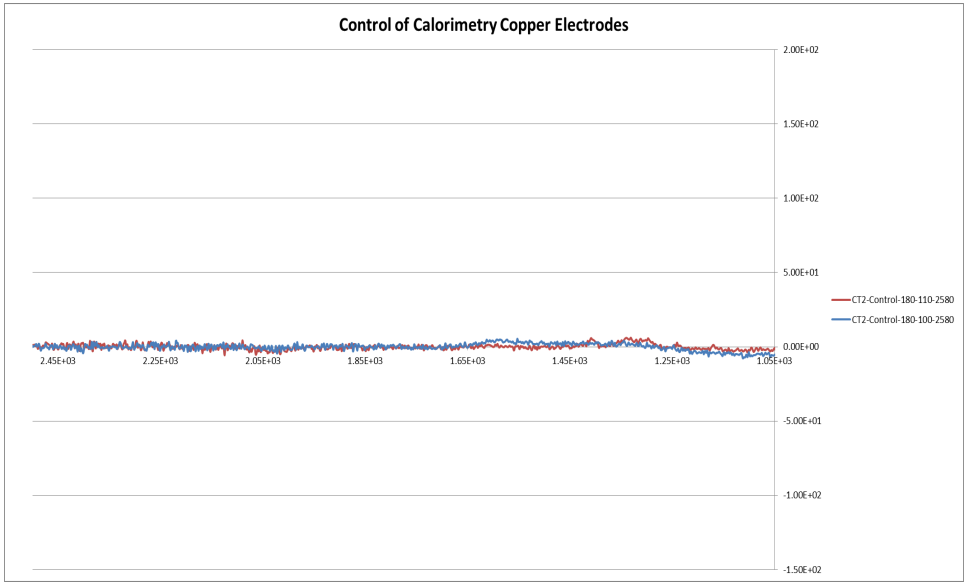

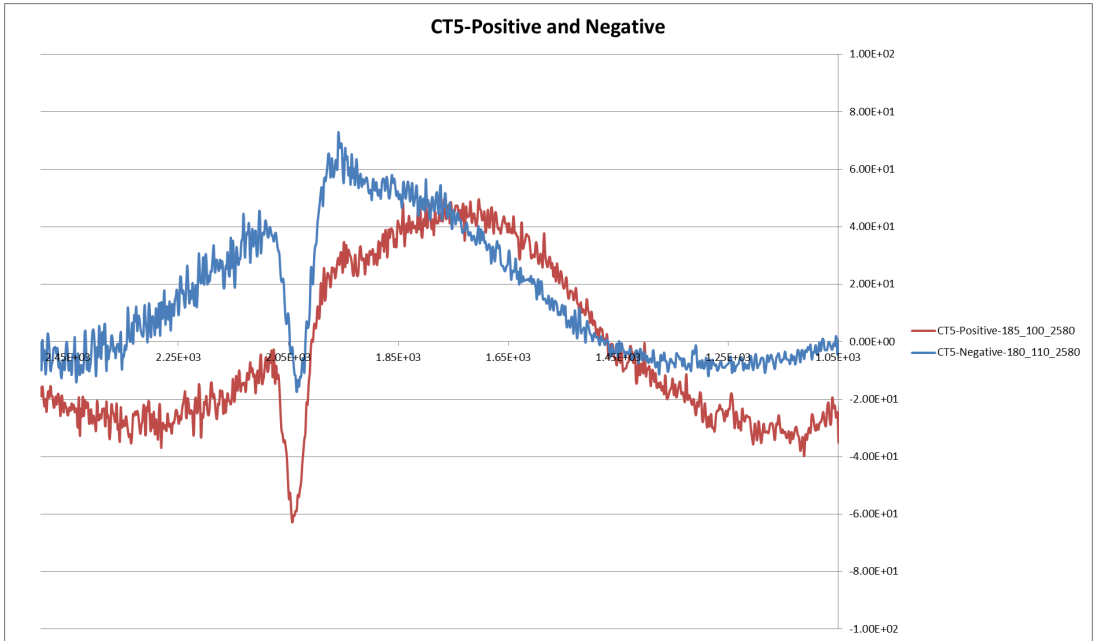

XPS Total Binding Energy of $H_2(1/4)$

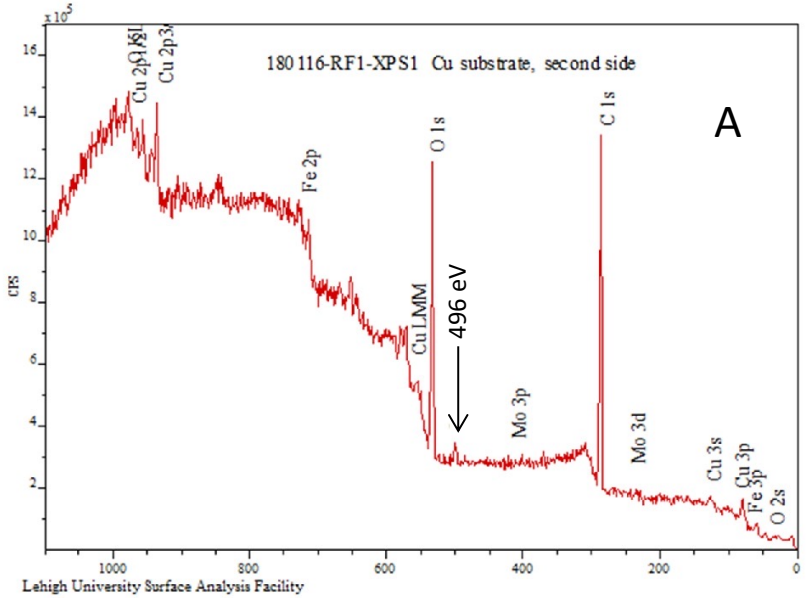

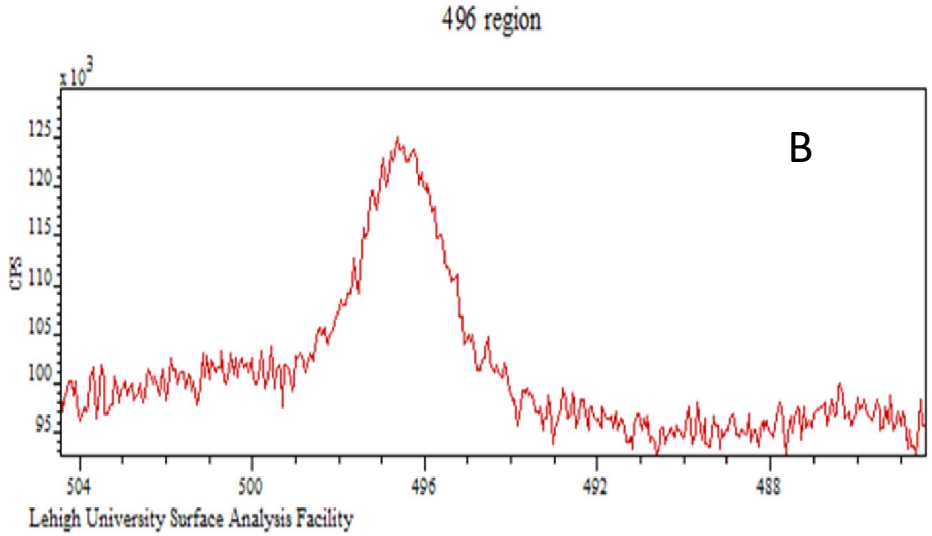

The XPS spectra of the hydrino Mo web compound having a peak at 496 eV assigned to $H_2(1/4)$ wherein other possibilities such Na, Sn, and Zn were eliminated since only Mo, O, and C peaks are present and other peaks of the candidates are absent. Mo 3s which is less intense than Mo3p was at 506 eV with additional samples that also showed the $H_2(1/4)$ 496 eV peak. A. Survey scan. B. High resolution scan in the region of the 496 eV peak of $H_2(1/4)$.

XPS Confirmation of Molecular Hydrino of $H_2(1/4)$ Binding Energy

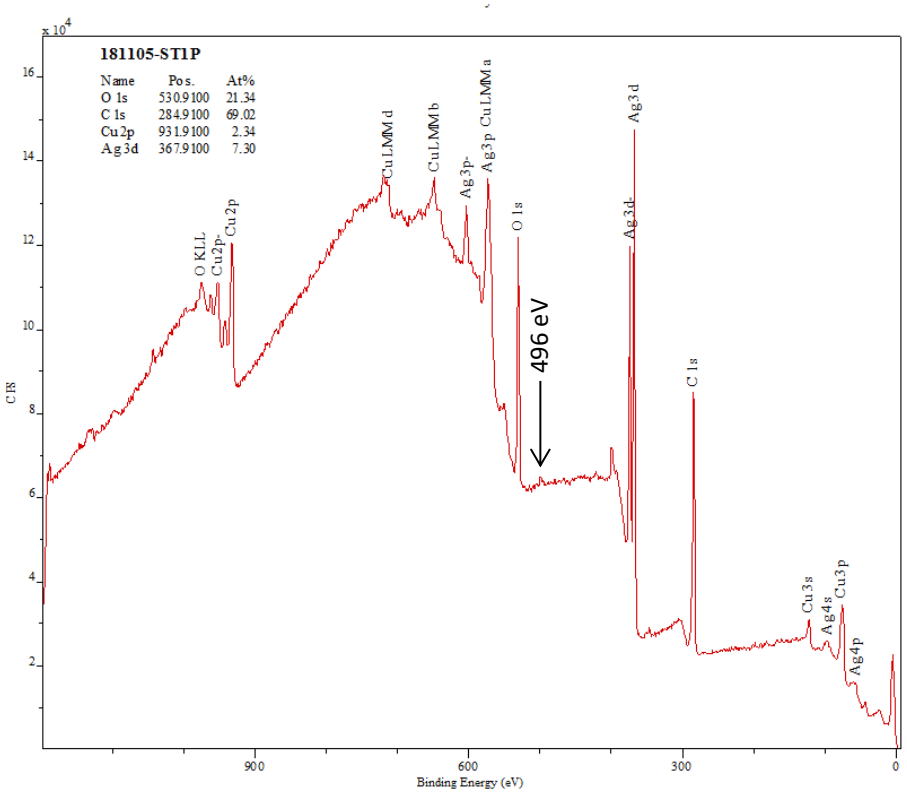

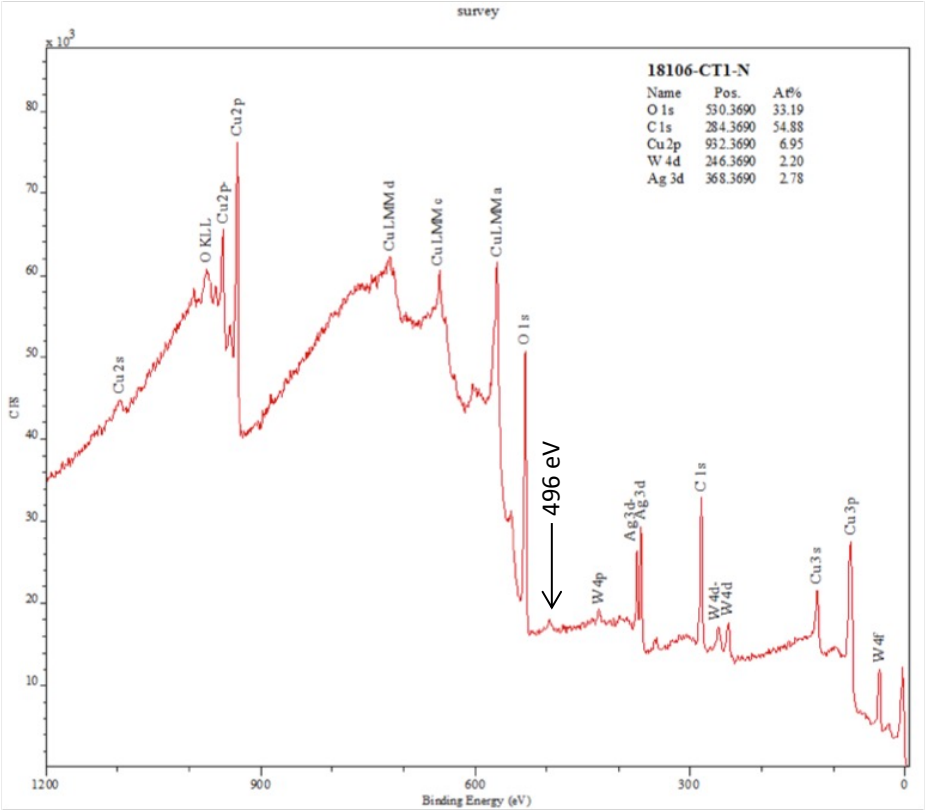

The XPS spectra on copper electrodes post ignition of a 80 mg silver shot comprising 1 mole% H_2O, wherein the detonation was achieved by applying a 12 V 35,000 A current with a spot welder. The peak at 496 eV was assigned to $H_2(1/4)$ wherein other possibilities such Na, Sn, and Zn were eliminated since the corresponding peaks of these candidates are absent. Raman post detonation spectra showed an inverse Raman effect peak at about 1940 cm^{-1} that matches the free rotor energy of $H_2(1/4)$ (0.2414 eV).

Solid Fuel Reaction Product KOH + KCl heated at 80 °C was EPR Active Indicative of the Presence of $H_2(1/4)$ Having an Unpaired Electron

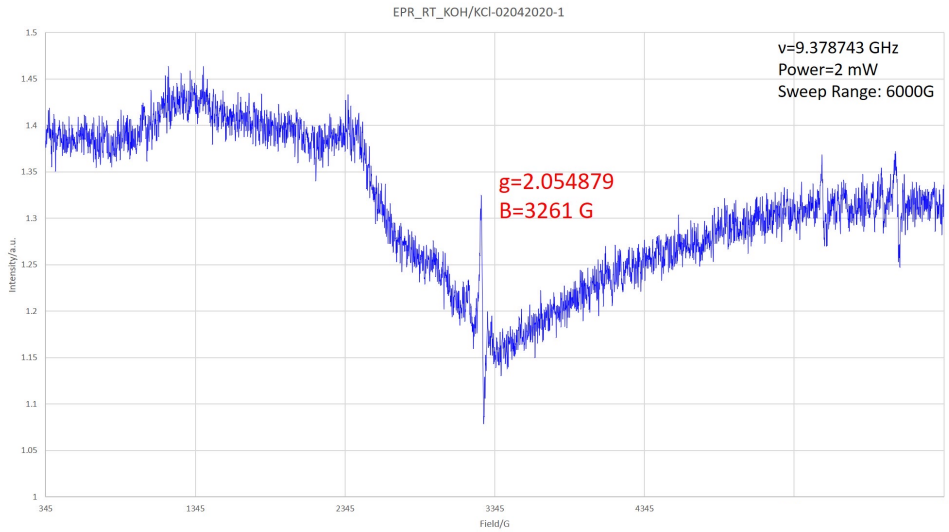

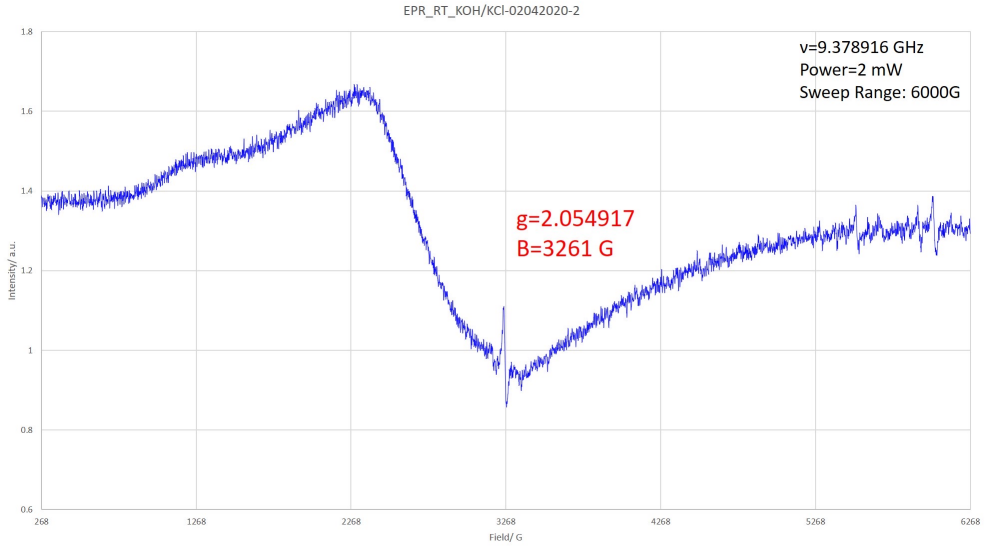

SEM and Energy Dispersive X-ray Spectroscopy (EDS) of white polymeric compound GaOOH:H_2(1/4) comprising H_2(1/4) formed by dissolving Ga_2O_3 collected from a hydrino reaction run in the SunCell® in 4M aqueous KOH, allowing fibers to grow, and float to the surface where they were collected by filtration. Particle size: KOH 100 nm; NaOH 40 nm. The hydrino compound is not soluble in concentrated acid (pH ~0) or concentrated base (pH ~14).

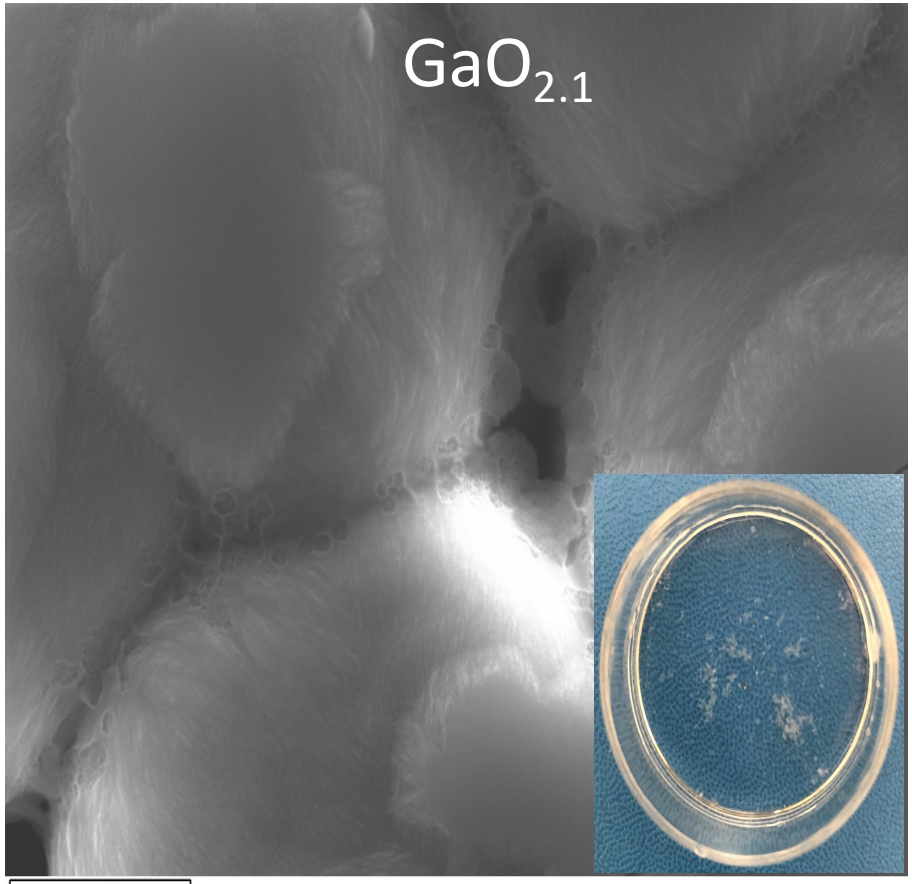

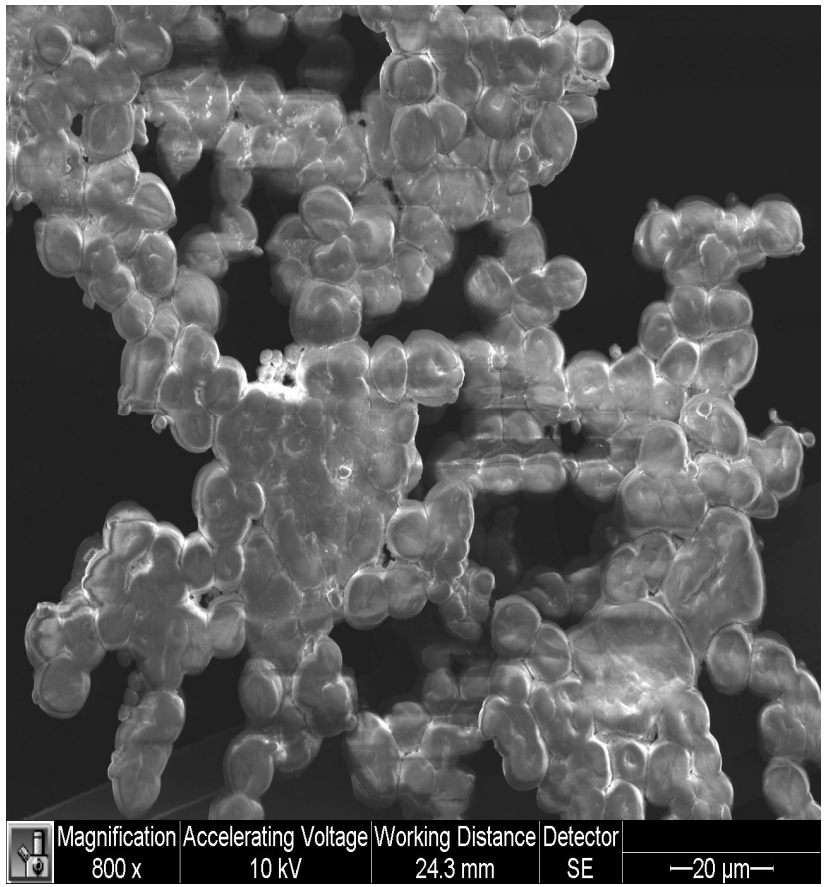

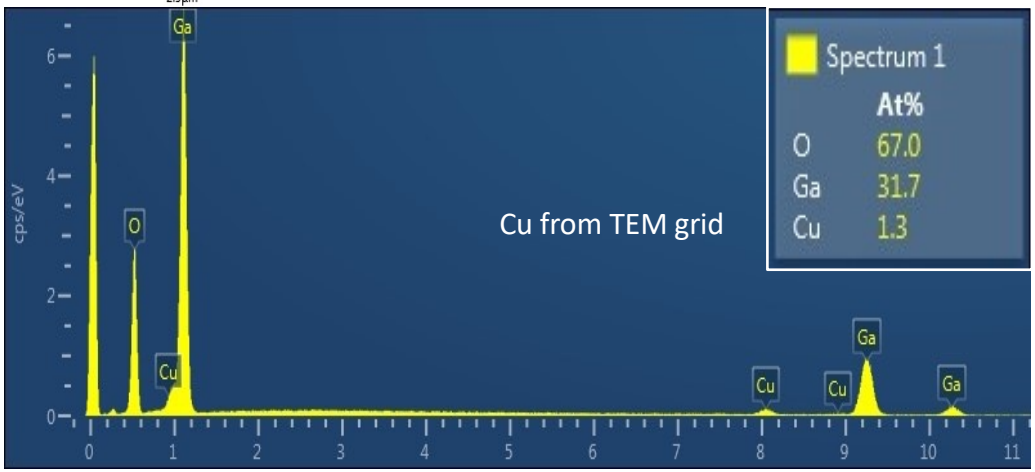

X-ray Diffraction of $GaOOH:H_2(1/4)$ formed by dissolving Ga_2O_3 collected from a hydrino reaction run in the SunCell® in 4M aqueous KOH or 4M NaOH, allowing fibers to grow, and float to the surface where they were collected by filtration. The KOH pattern is shifted to lower 2θ relative to that of NaOH and both patterns are shifted relative to the standard pattern of GaOOH. The particle size of the compound prepared in KOH is 19.4 nm and the particle size of the compound prepared in NaOH is 24.4 nm.

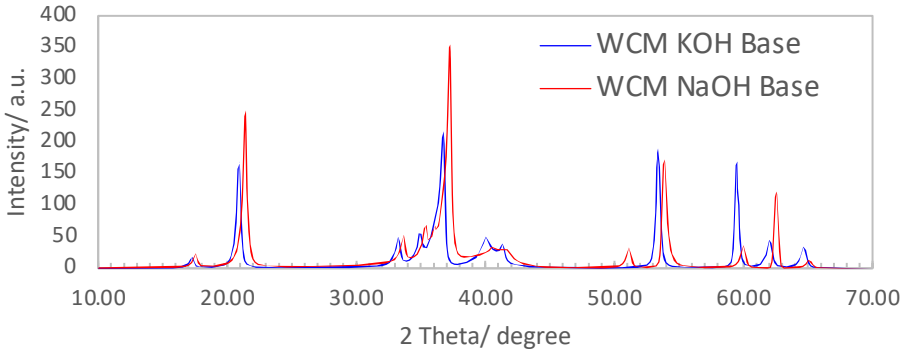

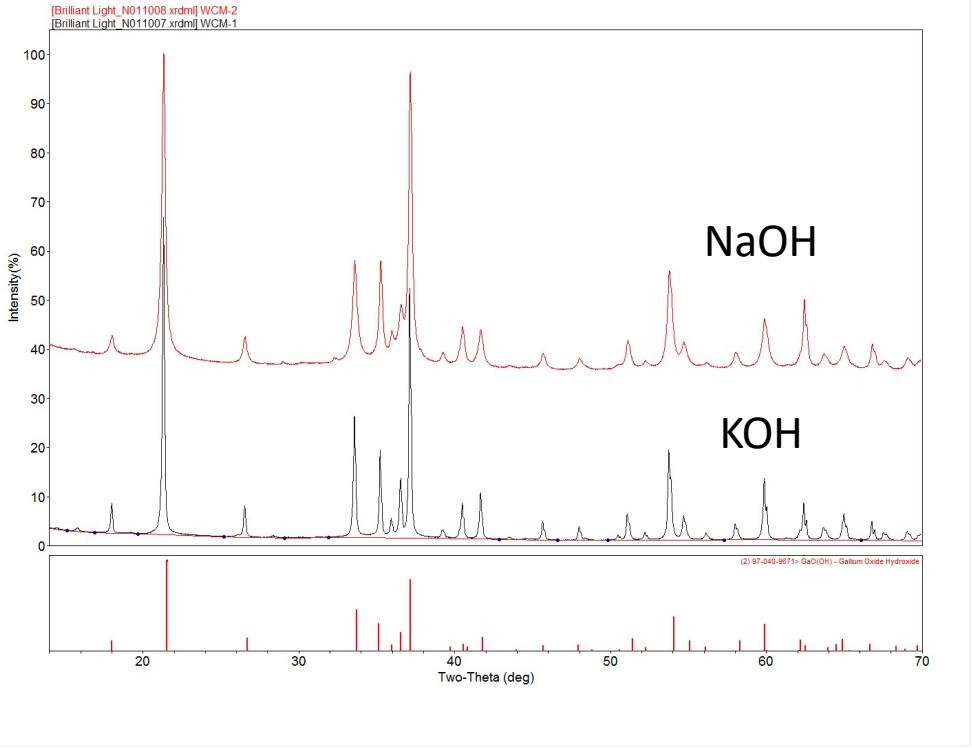

Transmission Electron Microscopy (TEM) Analysis for GaOOH:H_2(1/4) and GaOOH Control

- Talos F200X Scanning/Transmission Electron Microscope used for imaging and selected area electron diffraction (SAED).
- The GaOOH:H_2(1/4) sample was observed by TEM to comprise two different morphological and crystalline forms of GaOOH.
- Observed morphologically polymeric crystals comprising hexagonal crystalline structure were very sensitive to the TEM electron beam; whereas rods having orthorhombic crystalline structure were not electron beam sensitive.
- The rod crystals' morphology and crystalline structure matches those of the literature for control GaOOH that lacks molecular hydrino inclusion.
- XRD crystal system for Tsumgallite (GaOOH) is Orthorhombic.

Polymeric GaOOH:H_2(1/4) TEM Imaging

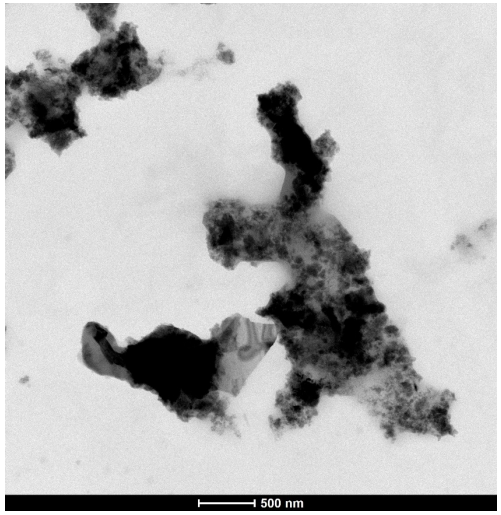

GaOOH:H_2(1/4) SAED Hexagonal Pattern

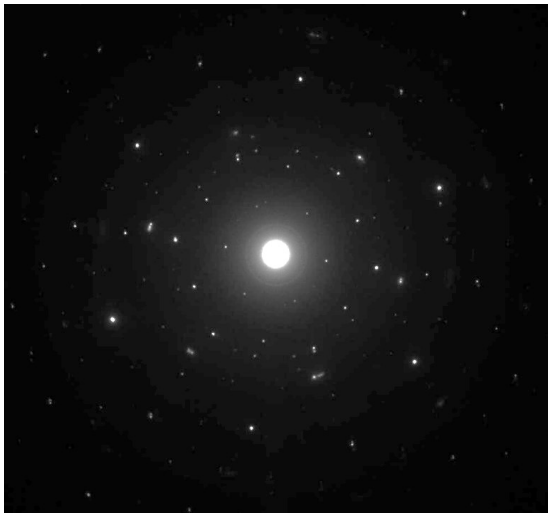

Rod-shaped GaOOH:H_2(1/4) TEM Imaging

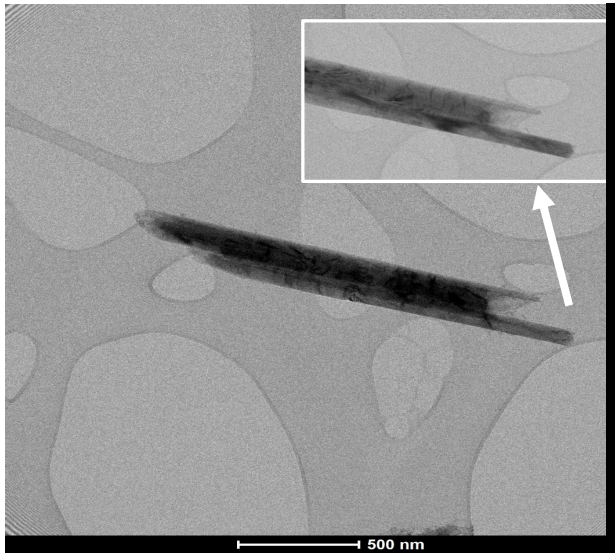

GaOOH:H_2(1/4) SAED Orthorhombic Pattern

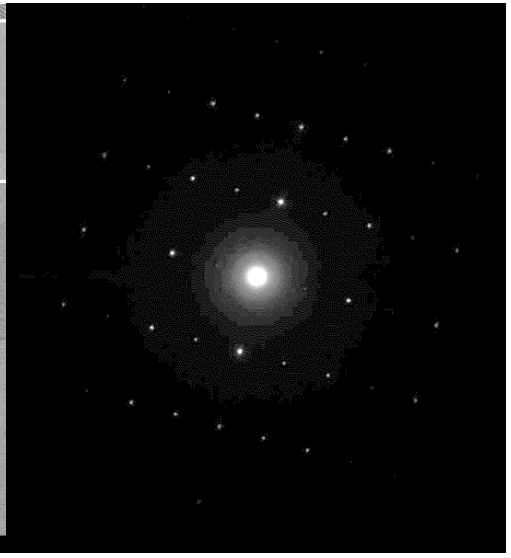

Ga Ion ToF-SIMS

Negative Spectrum showing hydride ion as a dominant ion fragment due to the stability of hydrino hydride ion. The TOF-SIMS confirms the H content supporting the molecular hydrino component. The composition by energy dispersive X-ray spectroscopy (EDS) and Rutherford backscattering spectrometry (RBS) was $GaO_{2.1}$ and $GaO_{1.68}H_{1.32}$, respectively. No hydrocarbons (HC) above adventitious HC were present that could give rise to an EPR spectrum.

Negative Spectrum

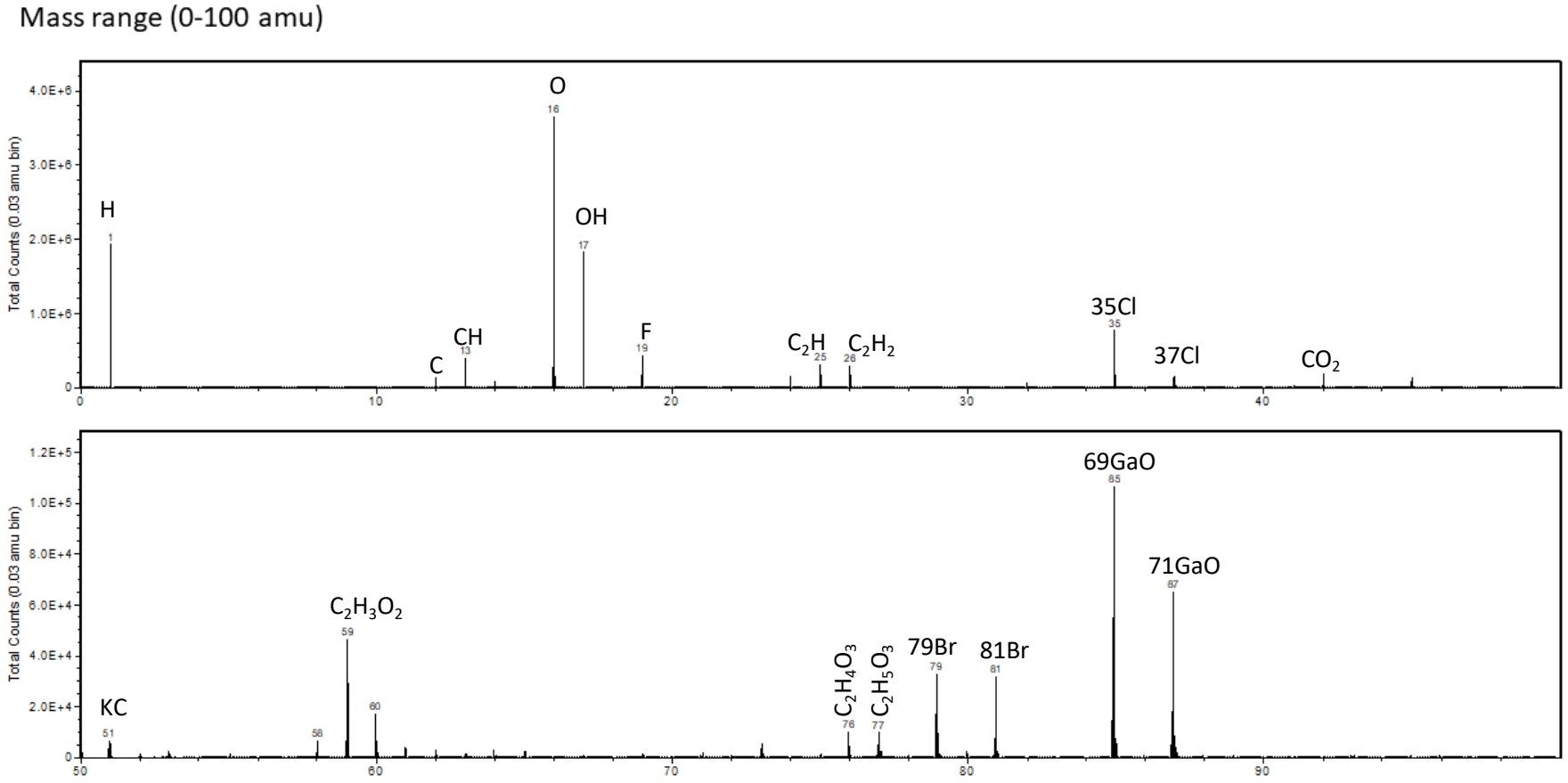

Ga Ion ToF-SIMS

Positive spectrum recorded on the GaOOH:H_2(1/4). Only potassium and gallium were observed in the positive spectrum. No transition metals were present that could give rise to an EPR spectrum.

Positive Spectrum

Mass range (0-100 amu)

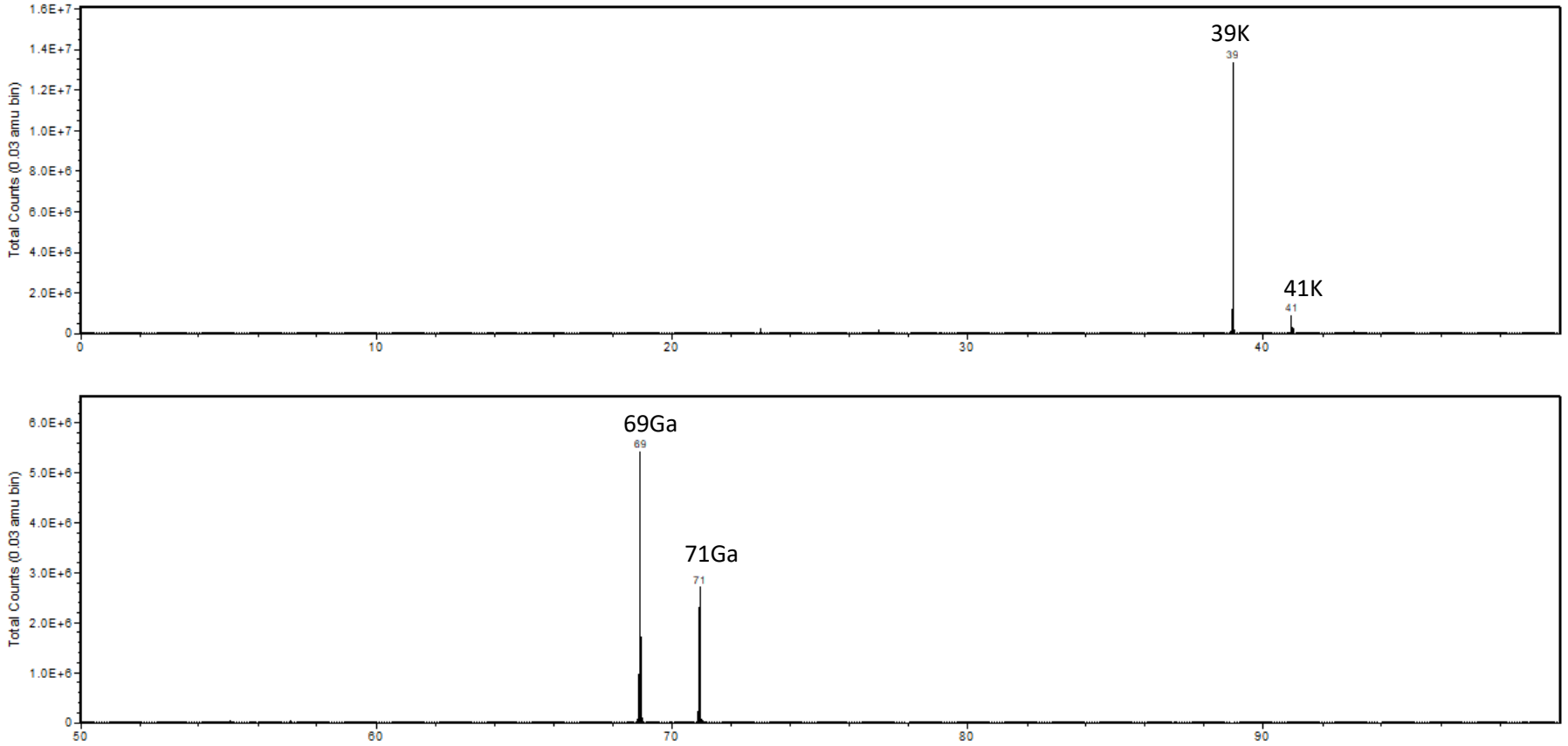

Rutherford Backscattering Spectrometry (RBS) was performed on the $GaOOH:H_2(1/4)$. The RBS result identified the composition as $GaO_{1.68}H_{1.32}$ corresponding to an excess H content, some of which is hydrino hydrogen based on the results of other analytical tests.

	"RBS" Thickness [Å]	Atomic Concentrations [at%]			Assumed Density [at/cc]
		Ga	O	H	
BULK	**-**	**25**	**42**	**33**	**8.56E22**

XPS Total Binding Energy of $H_2(1/4)$

GaOOH:$H_2(1/4)$ was formed by dissolving Ga_2O_3 collected from a hydrino reaction run in the SunCell® in 4M aqueous KOH, allowing fibers to grow, and float to the surface where they were collected by filtration.

The XPS spectrum of GaOOH:$H_2(1/4)$ recorded using a nonmonochromatic Mg Kα (1254 eV) excitation source with the XPS spectra recorded using a SPECS GmbH system with a PHOIBOS 150 hemispherical energy analyzer. The $H_2(1/4)$ total energy peak was observed at 496 eV wherein other possibilities such Sn, W, and Ir were eliminated since the corresponding peaks of these candidates were absent. These alternative elements were also eliminated by ToF-SIMS, EDS, and XRD. Cu is from the TEM grid used to mount the fibers.

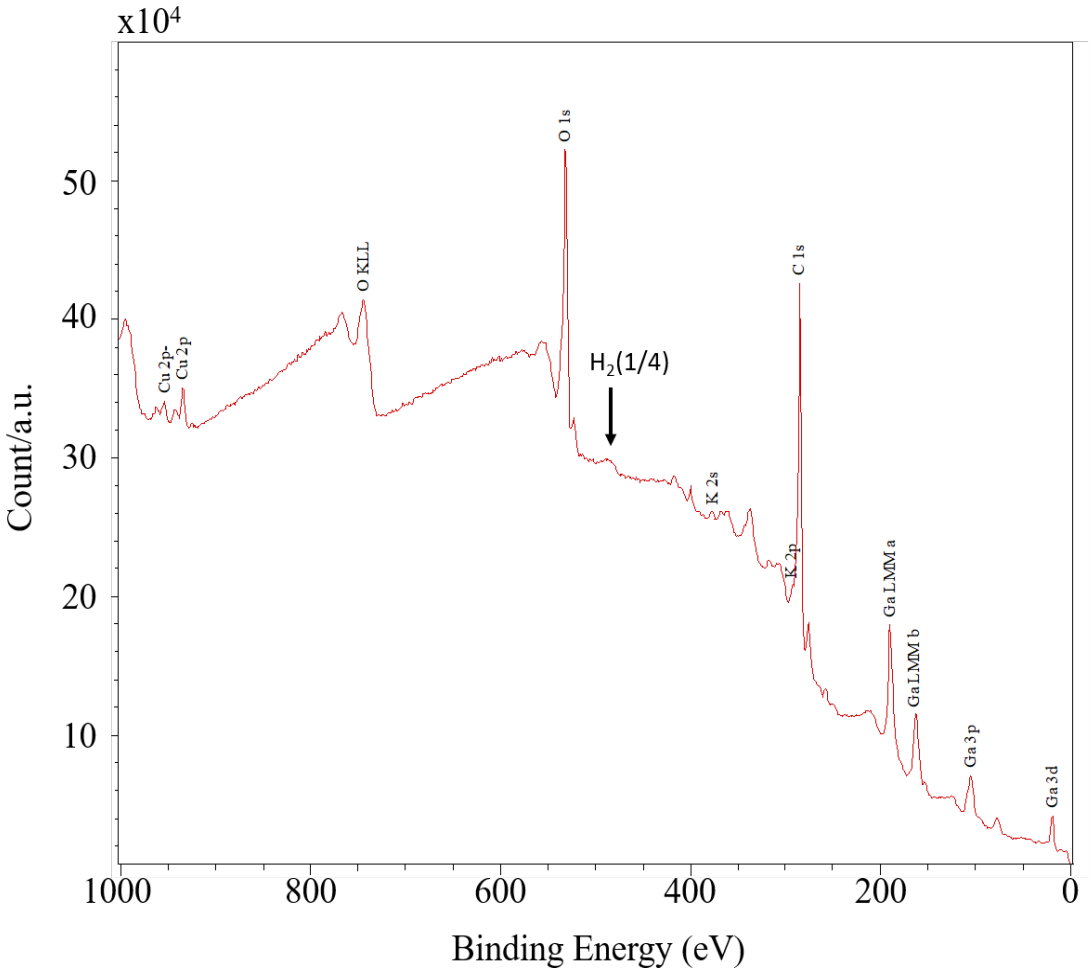

Solution Room Temperature Evaporation Rate Measurement of GaOOH:H_2(1/4) Added to H_2O Versus Controls Shows a Higher Evaporation Rate

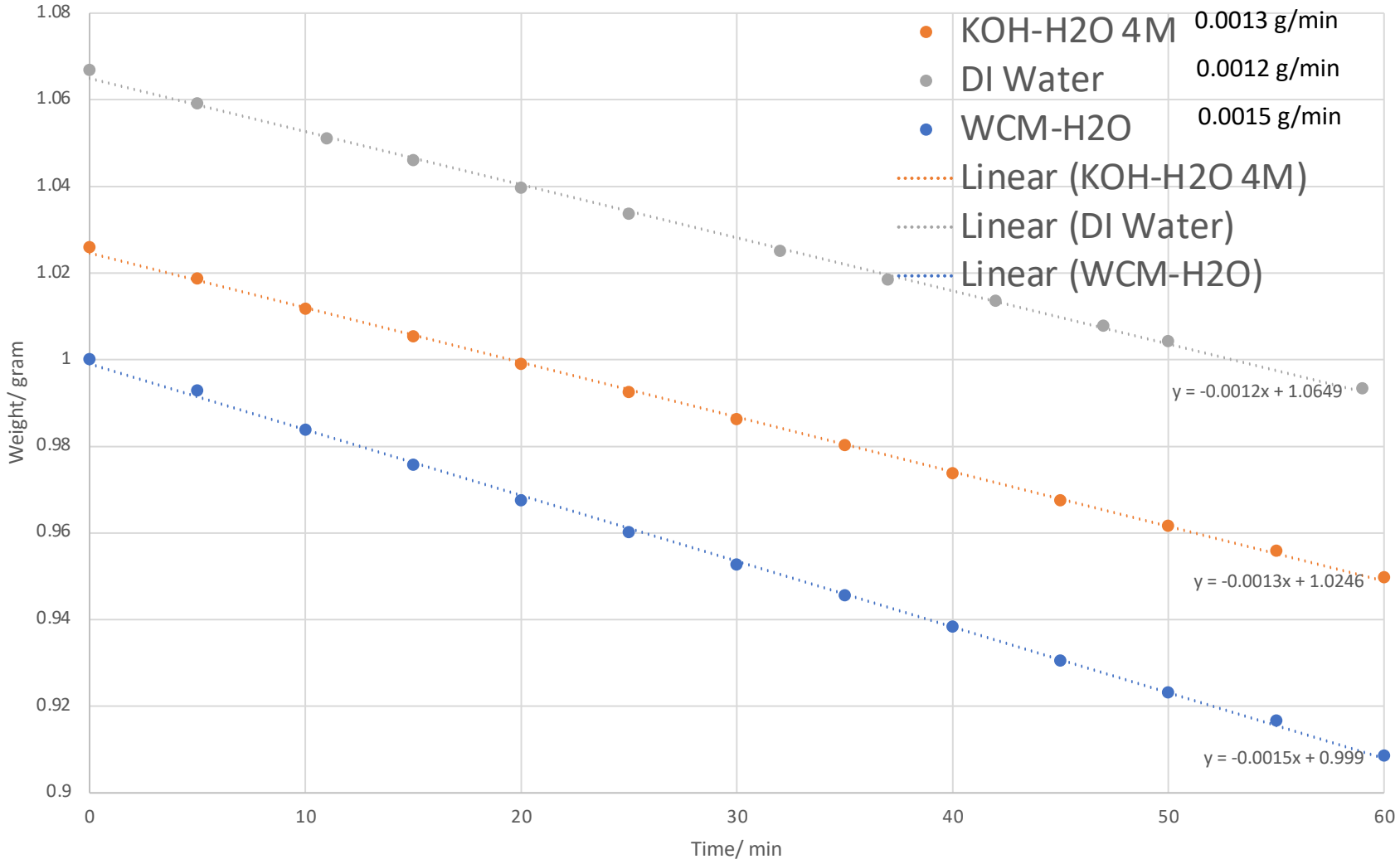

Quantized Magnetic Flux Linkage in Units of h/2e Observed by Visible Emission Spectroscopy of $H^-(1/2)$, Electron Paramagnetic Resonance Spectroscopy of $H_2(1/4)$, and Raman Spectroscopy of $H_2(1/4)$.

- The hydrino hydride ion comprising a paired and unpaired electron in a common atomic orbital demonstrated the phenomena of flux linkage in quantized units of h/2e.

- The pattern of integer-spaced peaks of the EPR spectrum of $H_2(1/4)$ is very similar to the periodic pattern observed in the high-resolution visible spectrum of the hydrino hydride ion.

- Moreover, the same phenomena were observed when the rotational energy levels of $H_2(1/4)$ were excited by laser irradiation during Raman spectroscopy.

- It is extraordinary that the EPR and Raman spectra give the same information about the structure of molecular hydrino in energy ranges that differed by reciprocal of the $H_2(1/4)$ diamagnetic susceptibility coefficient: $1/7X10^{-7} = 1.4X10^6$, wherein the induced diamagnetic orbital magnetic moment active during EPR was replaced by the orbital molecular rotational magnetic moment active during Raman.

Mechanism of Quantized Magnetic Flux Linkage in Units of h/2e Observed by Electron Paramagnetic Resonance Spectroscopy of $H_2(1/4)$

- $H_2(1/4)$ comprises an unpaired electron which enables the electronic structure of this unique hydrogen molecular state to be determined by electron paramagnetic resonance (EPR) spectroscopy.
- Specially, the $H_2(1/4)$ EPR spectrum comprises a principal peak with a g-factor of 2.0046386 that is split into a series of pairs of peaks with members separated by spin-orbital coupling energies that are a function of the corresponding electron spin-orbital coupling quantum numbers.
- The unpaired electron magnetic moment induces a diamagnetic moment in the paired electron of the $H_2(1/4)$ molecular orbital based on the diamagnetic susceptibility of $H_2(1/4)$.
- The corresponding magnetic moments of the intrinsic paired-unpaired current interactions and those due to relative rotational motion about the internuclear axis give rise to the spin-orbital coupling energies.
- The EPR spectral results confirmed the spin-orbital coupling between the spin magnetic moment of the unpaired electron and an orbital diamagnetic moment induced in the paired electron by the unpaired electron that shifted the flip energy of the spin magnetic moment.
- Each spin-orbital splitting peak was further sub-split into a series of equally spaced peaks that matched integer fluxon energies that are a function of the electron fluxon quantum number corresponding to the number of angular momentum components involved in the transition.
- The evenly spaced series of sub-splitting peaks was assigned to flux linkage in units of the magnetic flux quantum h/2e during the coupling between the paired and unpaired magnetic moments while a spin flip transition occurred.
- Additionally, the spin-orbital splitting increased with spin-orbital coupling quantum number on the downfield side of the series of pairs of peaks due to magnetic energies that increased with accumulated magnetic flux linkage by the molecular orbital.

Mechanism of Quantized Magnetic Flux Linkage in Units of h/2e Observed by Raman Spectroscopy of $H_2(1/4)$

- The Raman transition rotation of $H_2(1/4)$ is about a semiminor axis perpendicular to the internuclear axis.
- The intrinsic electron spin angular momentum aligns either parallel or perpendicular to the corresponding molecular rotational angular momentum along the molecular rotational axis, and a concerted rotation of the spin current occurs during the molecular rotational transition.
- The interaction of the corresponding magnetic moments of the intrinsic spin and the molecular rotation give rise to the spin-orbital coupling energies that are a function of the spin-orbital quantum number.
- The Raman spectral results confirmed the spin-orbital coupling between the spin magnetic moment of the unpaired electron and the orbital magnetic moment due to molecular rotation.
- The energies of the rotational transitions were shifted by these spin-orbital coupling energies as a function of the corresponding electron spin-orbital coupling quantum numbers.
- Molecular rotational peaks shifted by spin-orbital energies are further shifted by integer fluxon linkage energies with each energy corresponding to its electron fluxon quantum number dependent on the number of angular momentum components involved in the rotational transition.
- The observed sub-splitting or shifting of Raman spectral peaks was assigned to flux linkage in units of the magnetic flux quantum h/2e during the spin-orbital coupling between spin and molecular rotational magnetic moments while the rotational transition occurred.
- Additionally, the fluxon sub-splitting increased with the integer number of fluxons linked on the downfield side of a series of sub-split peaks due to magnetic energies that increased with accumulated magnetic flux linkage by the molecular orbital.

Hydrino Hydride Ion $H^-(1/2)$ Characteristic Signature

Wavelength-calibrated spectrum (3900-4090 Å) of a hydrino-reaction-plasma formed by heating KNO_3 and dissociating H_2 using a tungsten filament overlaid with a hydrogen microwave plasma. The emission due to $H^-(1/2)$ formation in the bound-free region is not a continuum as in the case of ordinary hydride ion. $H^-(1/2)$ comprises an unpaired electron such that upon the binding of a free electron by H(1/2) to form $H^-(1/2)$, flux is linked by H(1/2) in integer units of the magnetic flux quantum h/2e. Consequently, the bound-free spectrum comprises a series of hyperfine lines corresponding to quantized energy levels given by the sum of the fluxon energy, the spin-spin energy, and the binding energy.

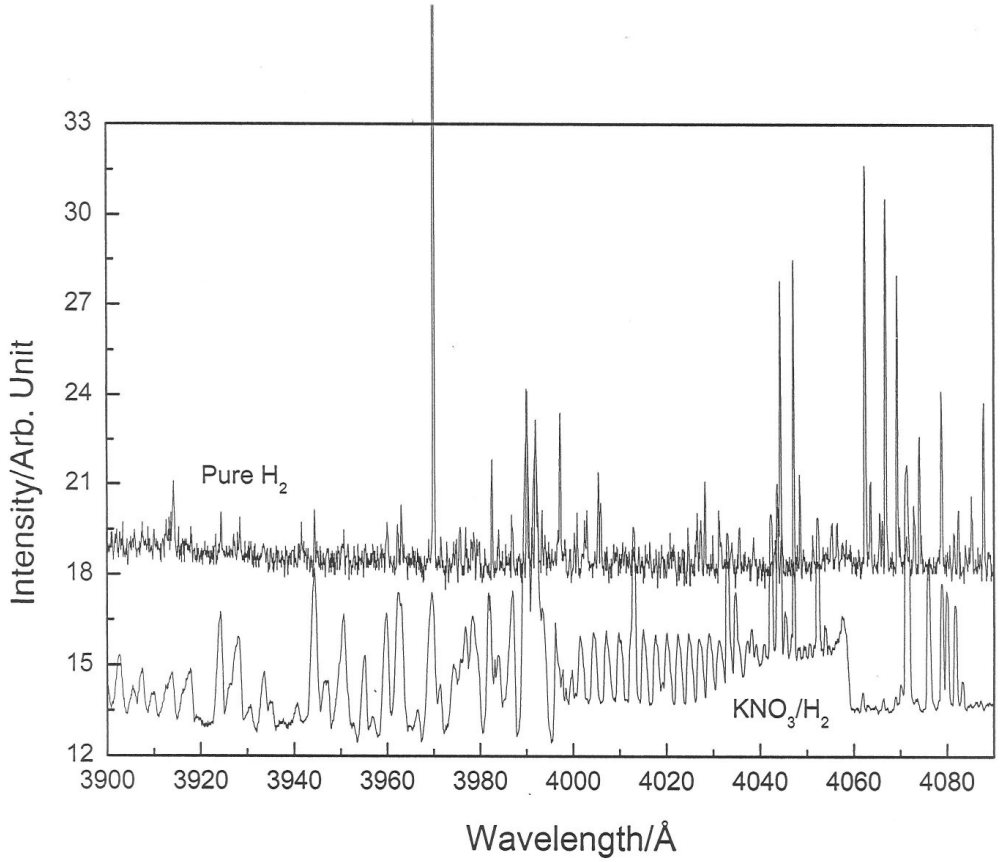

R. L. Mills, J. He, Y. Lu, M. Nansteel, Z. Chang, B. Dhandapani, "Comprehensive Identification and Potential Applications of New States of Hydrogen," Int. J. Hydrogen Energy, Vol. 32(14), (2007), 2988–3009.

High Resolution Electron Paramagnetic Resonance (EPR) Spectrum of a Molecular Hydrino (Data courtesy of prof dr Wilfred R Hagen TU Delft)

The 9.73855 GHz EPR spectrum (3445 G to 3495 G region) of a hydrino reaction product $GaOOH:H_2(1/4)$. This reaction product was formed by dissolving Ga_2O_3 collected from a hydrino reaction run in the SunCell® in aqueous KOH, and allowing polymeric fibers to grow, and float to the surface where they were collected by filtration.

The spectrum demonstrates splitting into two main peaks at 3467.9 G and 3470.9 G corresponding to a 4.1 G separation, wherein the two main peaks comprised sub-splitting into a series of evenly separated peaks of 0.31 G separation.

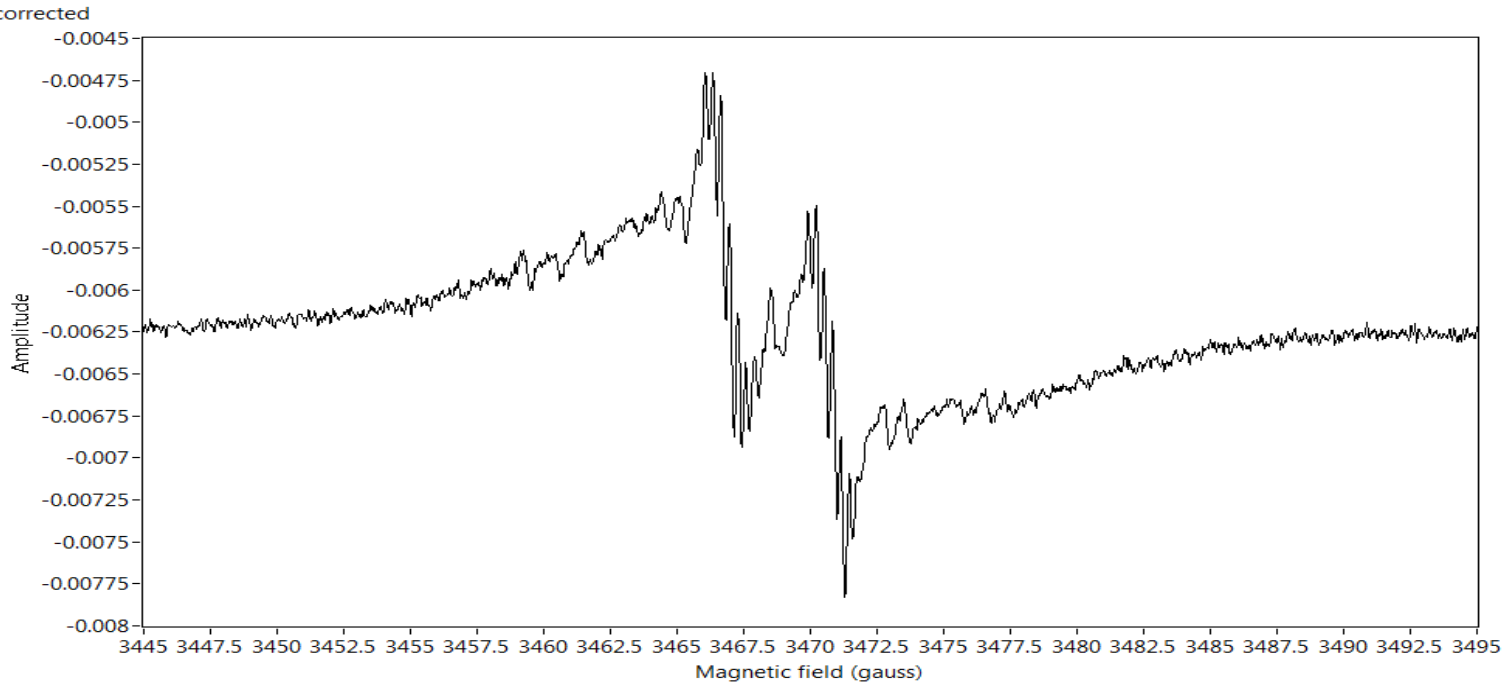

Theory Chapter 16: https://brilliantlightpower.com/GUT/GUT-CP-2020-Ed-Volume2-Web.pdf
Wilfred R. Hagen, Randell L. Mills, "Electron Paramagnetic Resonance Proof for the Existence of Molecular Hydrino", Vol. 47, No. 56, (2022), pp. 23751-23761; https://www.sciencedirect.com/science/article/pii/S0360319922022406.

High Resolution Electron Paramagnetic Resonance (EPR) Spectrum of a Molecular Hydrino (Data courtesy of prof dr Wilfred R Hagen TU Delft)

The sub-splitting into the series of evenly spaced peaks of 0.31 G separation is apparent in the high-resolution 9.7385 GHz EPR spectrum in the region of 3464.5 G to 3468.5 G acquired at modulation amplitude of 0.025 G with averaging of 1000, 20 s scans (top) and in the corresponding filtered spectrum (bottom).

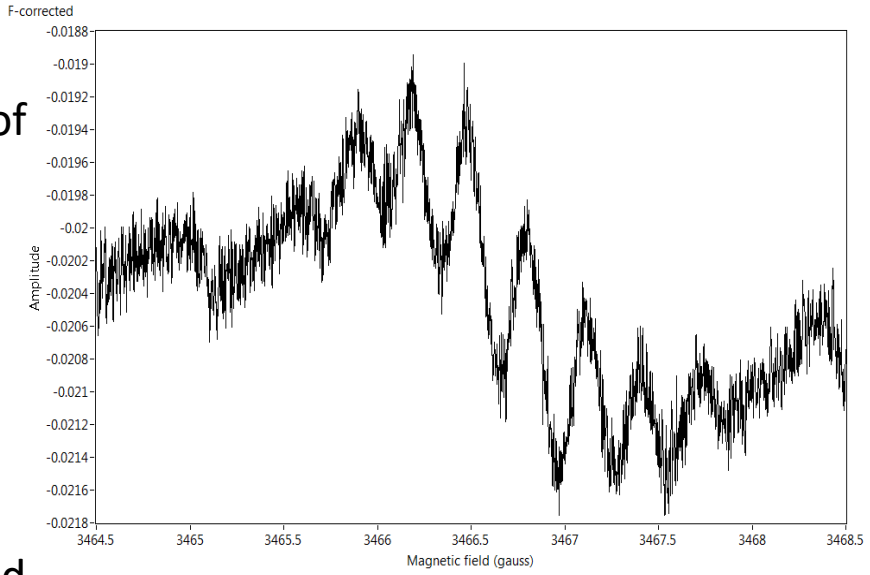

The spectra match theory identically wherein the two main peaks arise from spin-orbital coupling between the spin magnetic moment of the unpaired electron and an orbital diamagnetic moment induced in the paired electron by the flip of the spin magnetic moment.

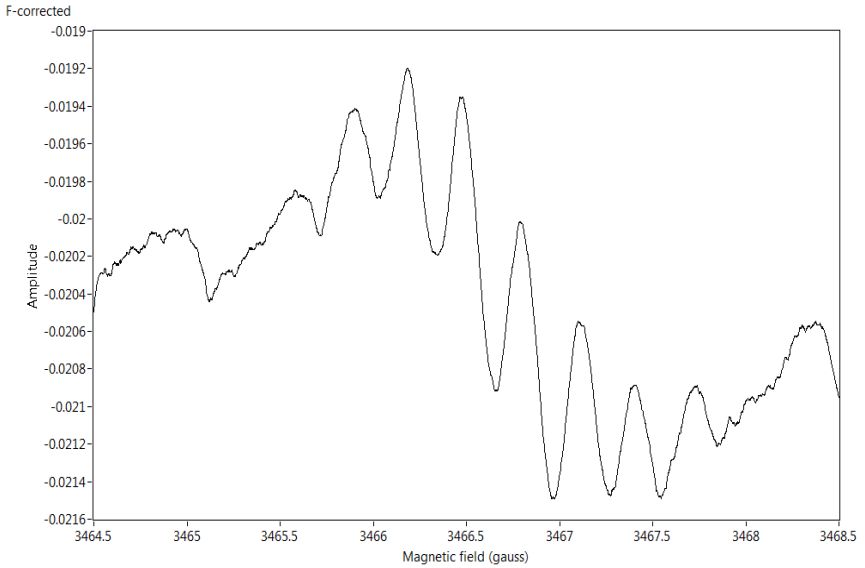

By a common mechanism as the hydrino hydride ion, the evenly spaced series of sub-splitting peaks is due to flux linkage during the coupling between the paired and unpaired magnetic moments in units of the magnetic flux quantum h/2e while a spin flip transition occurs. The splitting energies are too low to match any prior known assignment.

The EPR spectrum of GaOOH:H_2(1/4) was replicated by Bruker using two instruments.

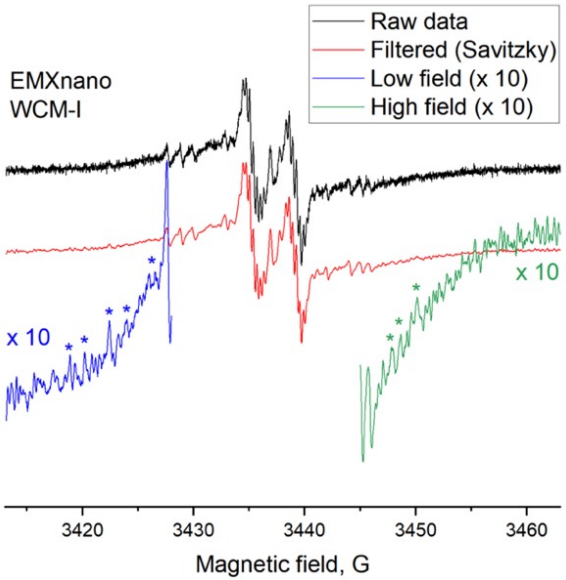

EMXnano data.

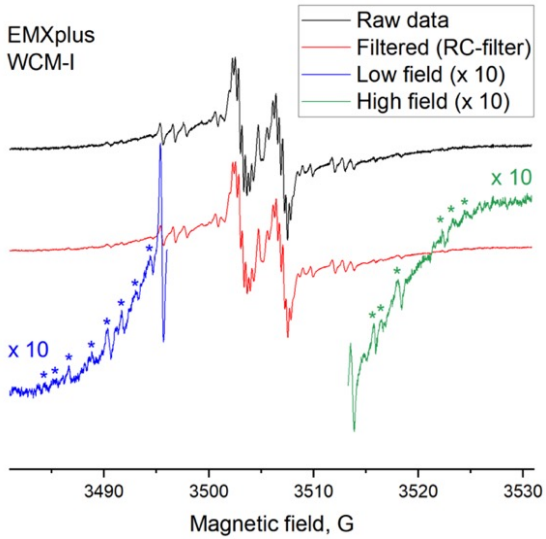

EMXplus data.

Expansion of EMXplus data, 3503 G - 3508 G region.

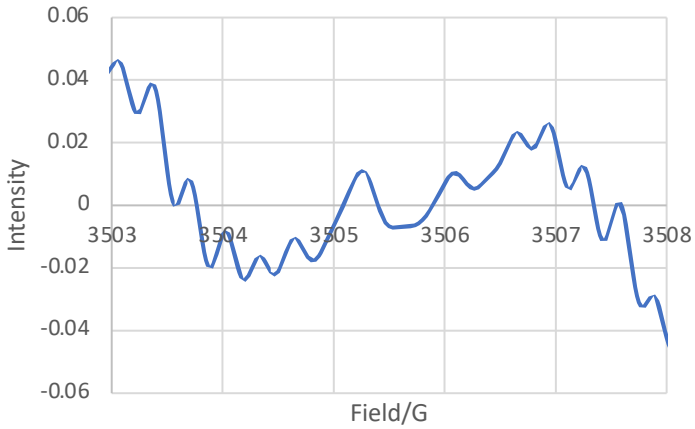

Deuterium Substitution Confirmed the Purely Electronic Spin-Orbital and Fluxon Splitting Assignments of the EPR Spectrum

- The EPR spectrum of the deuterated analog showed a singlet with no fine structure; thus, eliminating any possible nuclear splitting assignment.

- GaOOH:H_2(1/4) comprised a hexagonal phase having a complex EPR spectrum of lines assigned to spin-orbital and fluxon splitting. It also comprised an orthorhombic phase having a singlet EPR spectrum.

- The g factor and profile of GaOOH:HD(1/4) matched that of the singlet of GaOOH:H_2(1/4) wherein the singlet in both cases was due to the orthorhombic phase. The XRD of the deuterated analog matched that of the hydrogen analog, both comprising gallium oxyhydroxide. TEM confirmed that the deuterated analog comprised 100% orthorhombic phase. The phase preference of the deuterated analog may be due to a different hydrino concentration and kinetic isotope effect which could have also reduced the concentration.

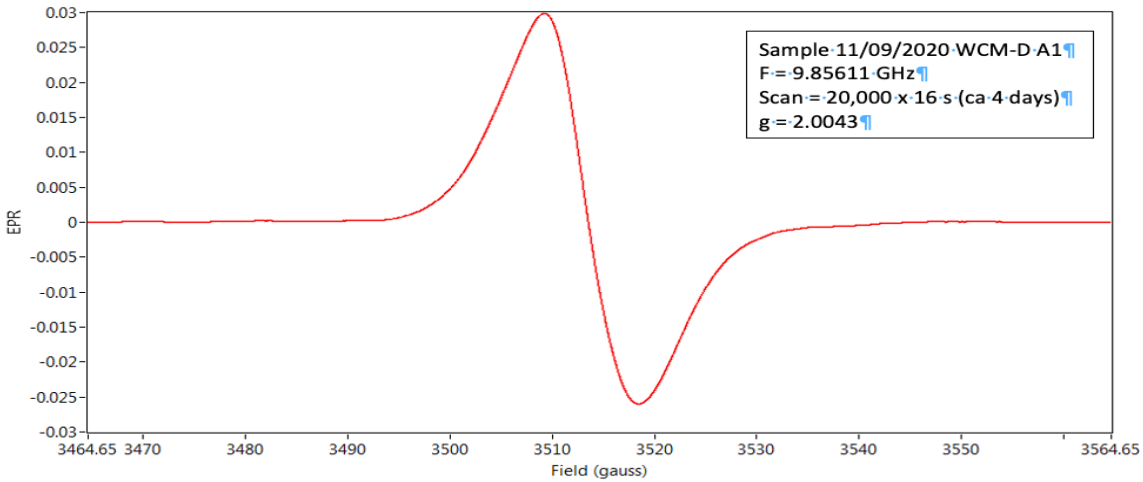

EPR spectrum of GaOOH:HD(1/4) (3464.65 G - 3564.65 G) region.

R. Mills, "Hydrino states of hydrogen", https://brilliantlightpower.com/pdf/Hydrino_State_of_Hydrogen_Paper.pdf.

Molecular Hydrino such as $H_2(1/4)$ Forms Dimers at Elevated Temperature (e.g. $[H_2(1/4)]_2$)

- Two very different types of EPR spectra were observed from molecular hydrino samples, ZnO@$H_2(1/4)$ prepared by Zn wire detonation in humidified air atmosphere (blue trace) comprising $H_2(1/4)$ dimers and Ga(O)OH@$H_2(1/4)$ prepared by aqueous KOH treatment of gallium oxide collected following a plasma reaction in a SunCell comprising molten gallium as one of the electrodes (red trace) wherein Ga(O)OH@$H_2(1/4)$ comprised individual $H_2(1/4)$ molecules trapped in a gas-like state.
- Control experiment ($KHCO_3$, KCl) showing the generation of the broad EPR signal of H2(1/4) in a sample produced in a tungsten carbide ball mill. The test shows that the signal is not associated with iron contamination from the mill, nor from contaminants in the original chemicals. EPR conditions: microwave frequency, 9.84 GHz; modulation amplitude, 10 Gauss; temperature, 293 K.

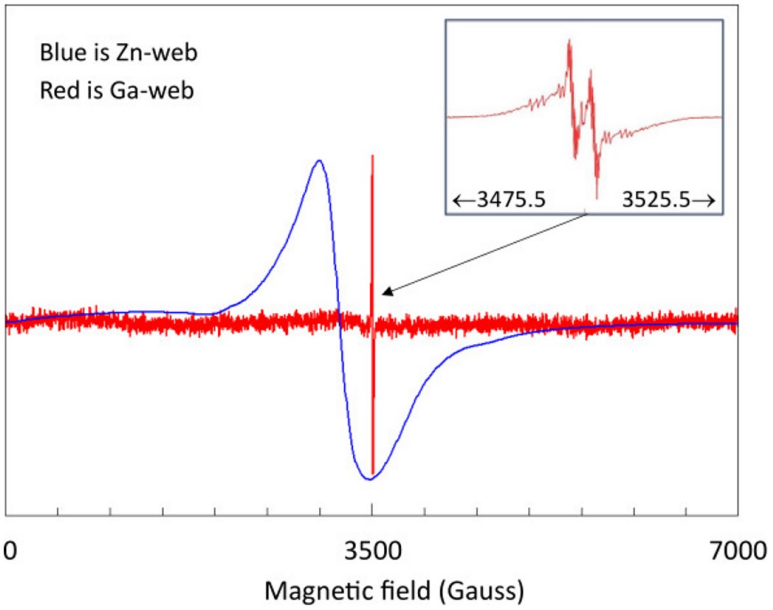

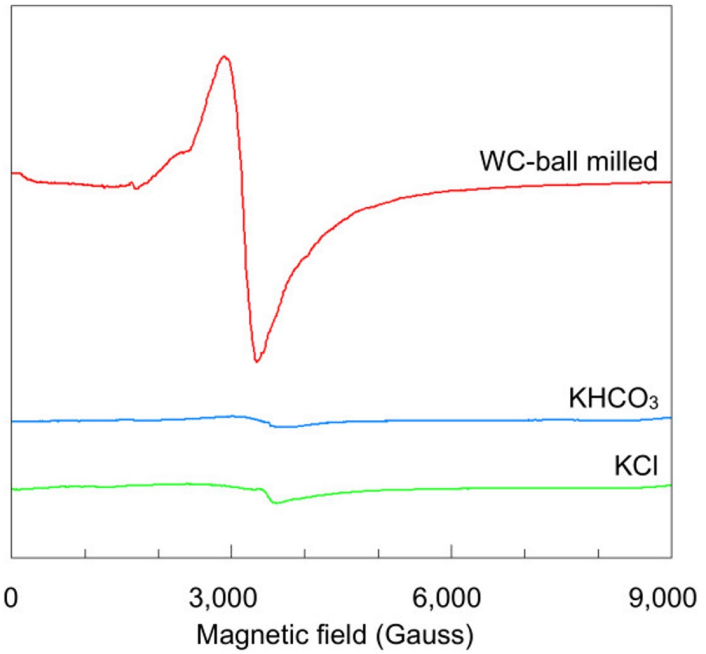

Wilfred R. Hagen, Randell L. Mills, "General EPR pattern from molecular hydrino produced in various reactors", (2024), submitted; https://brilliantlightpower.com//pdf/General_EPR_pattern_from_molecular_hydrino_produced_in_various_reactors.pdf.

Wilfred R. Hagen, Randell L. Mills, "Electron Paramagnetic Resonance Proof for the Existence of Molecular Hydrino", Vol. 47, No. 56, (2022), pp. 23751-23761; https://www.sciencedirect.com/science/article/pii/S0360319922022406.

Molecular Hydrino such as $H_2(1/4)$ Forms Dimers at Elevated Temperature (e.g. $[H_2(1/4)]_2$)

- Multi-frequency spectra of the $H_2(1/4)@Zn(OH)_2$ compound. EPR conditions: the L- (1.43101 GHz) and S-band (4.09267 GHz) spectra were taken with a modulation amplitude of 25 Gauss and were 9 times averaged; X-band EPR (9.62135 GHz); for Q-band (35.22700 GHz) the modulation amplitude was 10 Gauss and the microwave power was 12.6 mW. All spectra were taken at a temperature of 293 K. Positions of the zero crossing of the main line and of a special inflection point (S-band: in yellow) are indicated.
- Multi-frequency spectra of the compound NaHCO3/NaCl/Ga 47.5/47.5/5 wt%. Frequencies are given in the figure. Positions of the zero crossing of the main line and of an extra line (in yellow) in Q-band are indicated.
- A large down-field singlet signature and temperature dependencies were recorded by EPR that confirm the theoretical prediction of the formation of molecular Hydrino dimers $[H_2(1/p)]_2$ as an extension of ordinary hydrogen chemistry. H_2 is known to form dimers $[H_2]_2$ at cryogenic temperatures whereas $[H_2(1/p)]_2$ was shown to be stable at elevated temperatures.

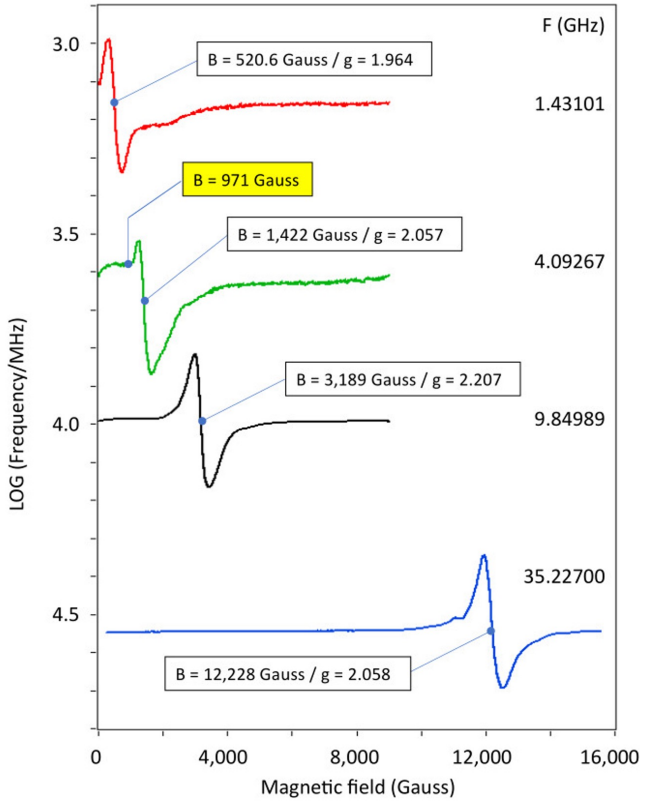

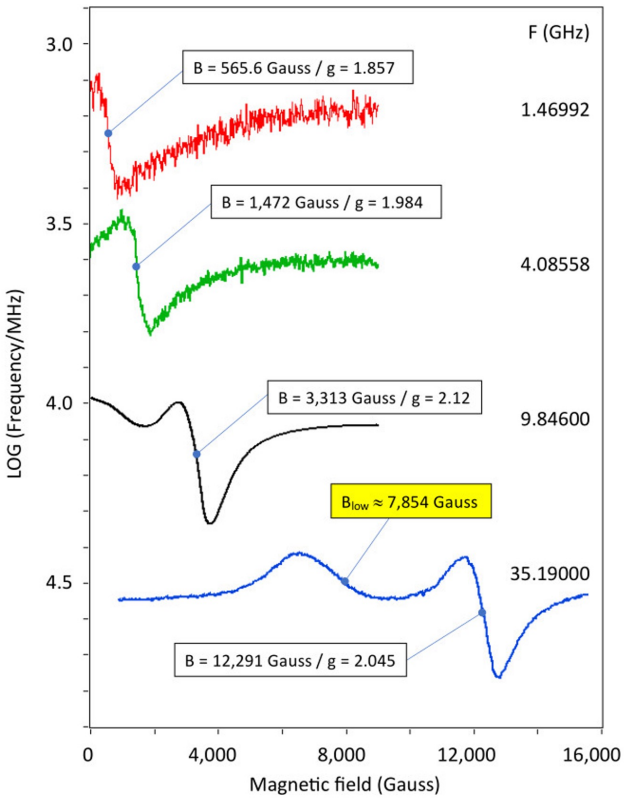

Molecular Hydrino such as $H_2(1/4)$ Forms Dimers at Elevated Temperature (e.g. $[H_2(1/4)]_2$)

- Relative population of the H(1/4)2@Zn(OH)$_2$paramagnet measured as EPR intensity times temperature versus temperature. For an S = 1/2 system or an isolated ground state this graph should be a straight horizontal line. EPR intensity was measured as height times width of the central line. A small transition range around 107 K is ignored. The black line is a single-exponential fit to the T greater than or equal to 116 K data. The figure indicates that even at room temperature the spin system has not reached its maximal population by far.
- At low temperatures, it was observed that $[H_2(1/4)]_2$ dimers side to side anti-paired to form tetramers that were not EPR active. As the temperature was raised the EPR singlet for the dimer reappeared at the predicted temperature.

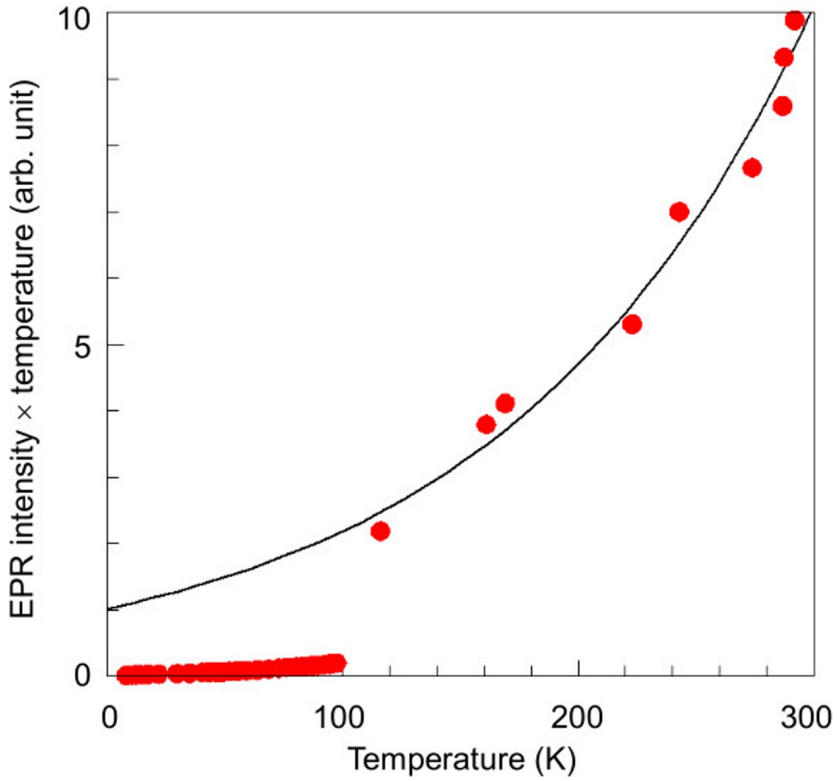

Molecular Hydrino such as $H_2(1/4)$ Forms Dimers at Elevated Temperature (e.g. $[H_2(1/4)]_2$)

- Multi-frequency results for compound 'Zn', that is $H_2(1/4)@Zn(OH)_2$ and compound 'Ga', that is $H_2(1/4)@NaHCO_3/NaCl/Ga$. Comparison of experimental and calculated peak positions for molecular hydrino dimers $[H_2(1/4)]_2$.
- $[H_2(1/8)]_2$ dimers were also observed indicating greater release of energy than production of H2(1/4).
- The theoretical prediction of the formation of a dimer between molecular hydrino $H_2(1/4)$ and H_2 ($[H_2\text{-}H_2(1/4)]$) and the temperature dependence of hydrogen release explains the massive hydrogen gas release observed from common salts with embedded molecular hydrino that indicates a new hydrogen storage technology.

	Frequency /GHz	Resonance field/Gauss	dipole-corrected field/Gauss	predicted peak position/Gauss	Observed peak position/Gauss
'Zn'					
	35.22700	12,573	12,071	12,071	12,288
	9.62135	3,429	2,927	2,927	3,189
	4.09267	1,458	956	956	971[a]
	1.43101	510	8	502	521[b]
'Ga'					
	35.19000	12,542	12,040		12,291
	35.19000	12,542	8,496	8,496	7,854[c]
	9.84660	3,509	3,008		3,313
	4.08558	1,456	954		1,472
	1.46992	524	22		566

[a] EPR frequency is resonant with dipole shift within the line width; it starts with negative slope; peak position taken at zero crossing.
[b] EPR frequency is resonant with dipole shift; increased initial slope of Lorentzian line shape.
[c] Molecular hydrino dimer $[H_2(1/8)]_2$.

SunCell® hydrino power generator comprising a single electromagnetic pump injector and electrode in an injector reservoir electrode, a vertically aligned counter electrode, and a glow discharge cell connected to a top flange to form HOH catalyst and atomic H.

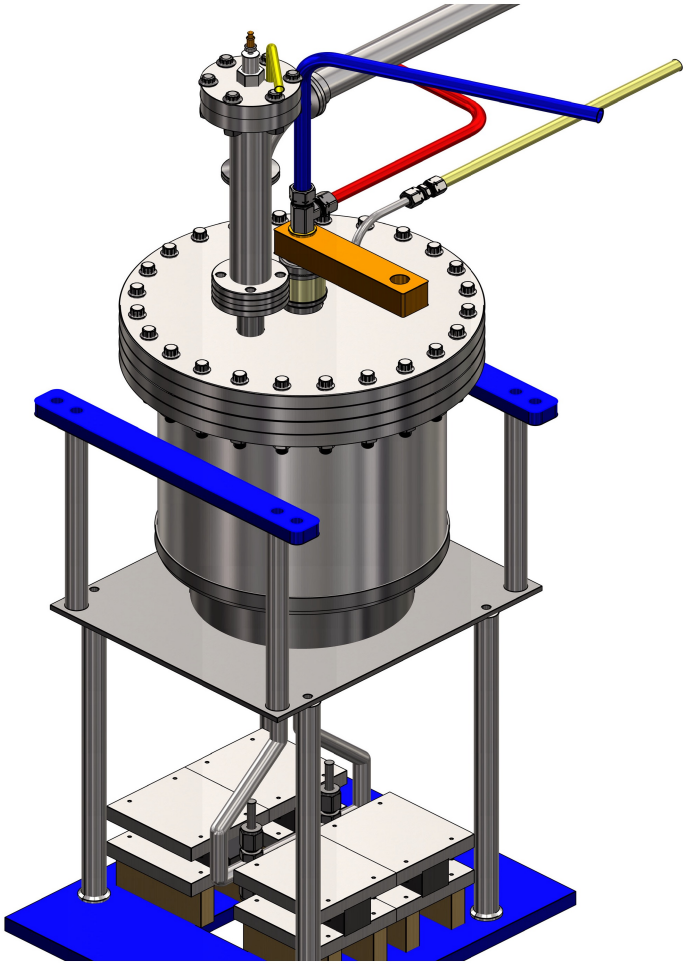

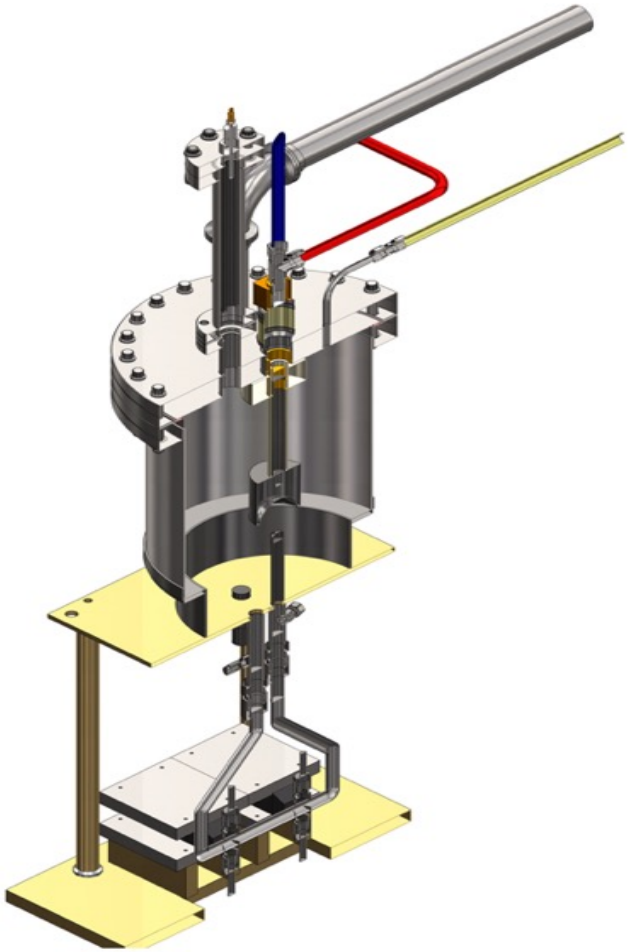

Confirmation of Molecular Hydrino $H_2(1/4)$ by Raman Spectroscopy

- Raman spectra obtained using a Horiba Jobin Yvon LabRam ARAMIS spectrometer with a 785 nm laser on a Ni foil prepared by immersion in the molten gallium of a SunCell that maintained a hydrino plasma reaction for 10 minutes. A. 2500 cm^{-1} to 11,000 cm^{-1} region. B. 8500 cm^{-1} to 11,000 cm^{-1} region.

- All of the novel high-energy emission lines matched the double transition for final rotational quantum numbers $J'_p = 3$ and $J'_c = 0,1,2$.

- Corresponding spin-orbital coupling and fluxon coupling were also observed.

- The novel lines were eliminated by a Semrock long-pass edge filter (BLP01-785R-25) having an edge wavelength of 805 nm and $T_{avg} > 93\%$ 812.1 – 1200 nm placed between the sample and the detector confirming the assignment to high energy emission rather than low energy Raman transitions

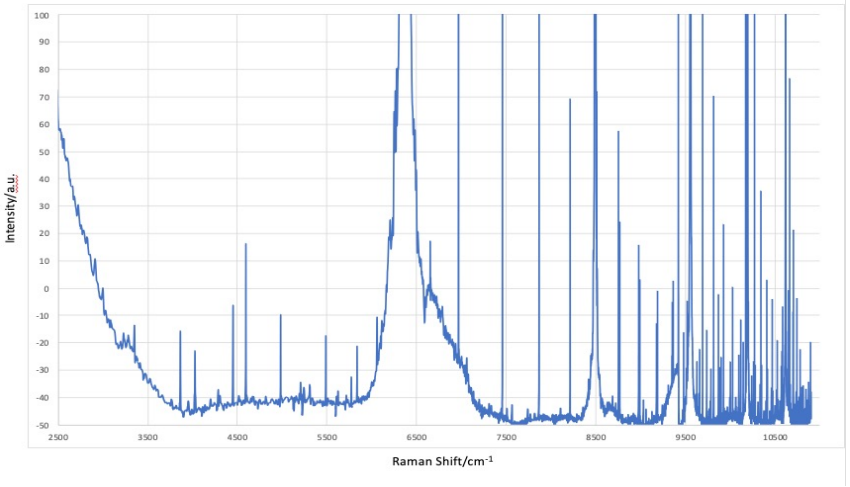

(A)

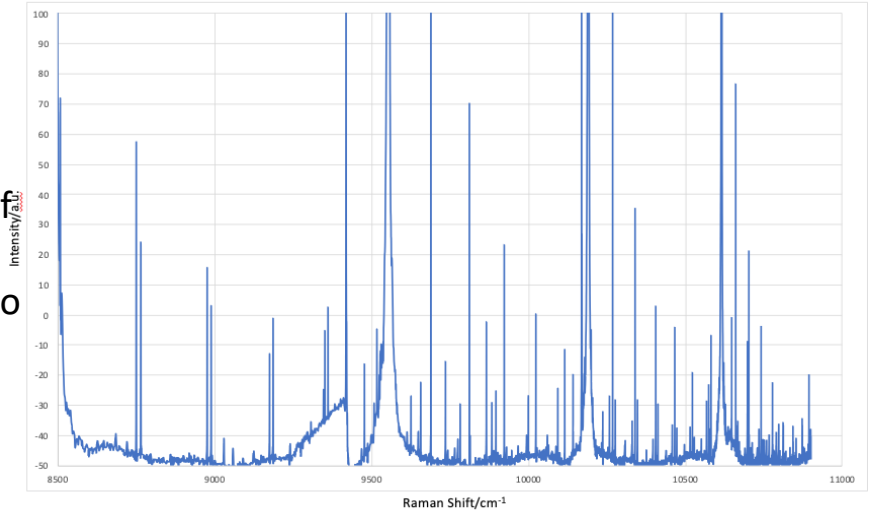

(B)

R. Mills, "Hydrino States of Hydrogen", https://brilliantlightpower.com/pdf/Hydrino_States_of_Hydrogen_Paper.pdf.

Control Sample for Confirmation of Molecular Hydrino $H_2(1/4)$ by Raman Spectroscopy

Raman spectra obtained using a Horiba Jobin Yvon LabRam ARAMIS spectrometer with a 785 nm laser on a Ni_3Ga alloy sample prepared by immersion of the Ni foil in the molten gallium of a SunCell that maintained a hydrino plasma reaction for 10 minutes. No lines were observed which confirmed that the novel lines observed in the Ni foil are real and not an artifact.

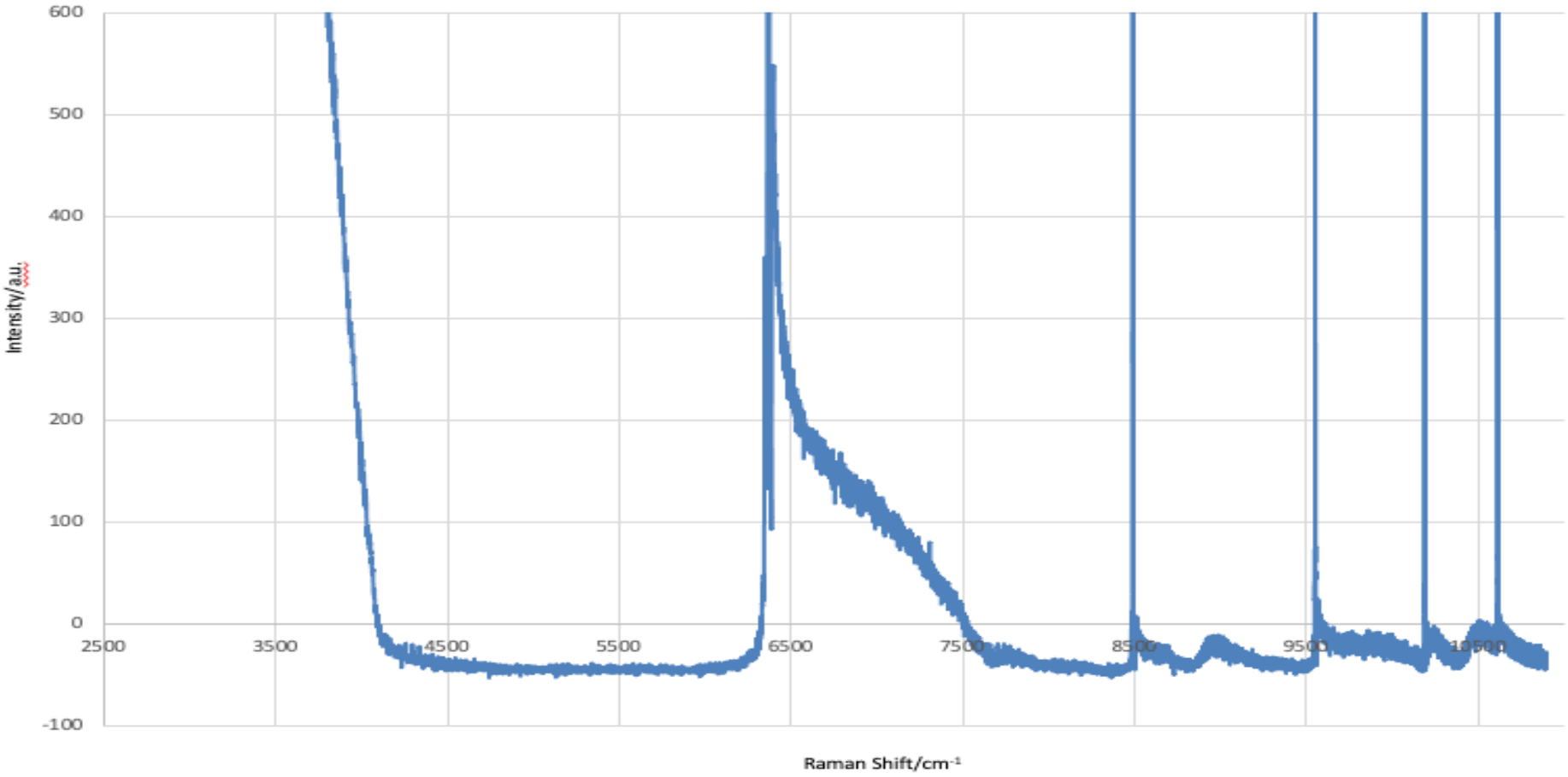

Confirmation of Molecular Hydrino $H_2(1/4)$ by Raman Spectroscopy

Raman spectra (2200 cm^{-1} to 11,000 cm^{-1}) obtained using a Horiba Jobin Yvon LabRam ARAMIS spectrometer with a 785 nm laser on GaOOH:H2(1/4) showing $H_2(1/4)$ rotational transitions with spin-orbital coupling and fluxon linkage shifts.

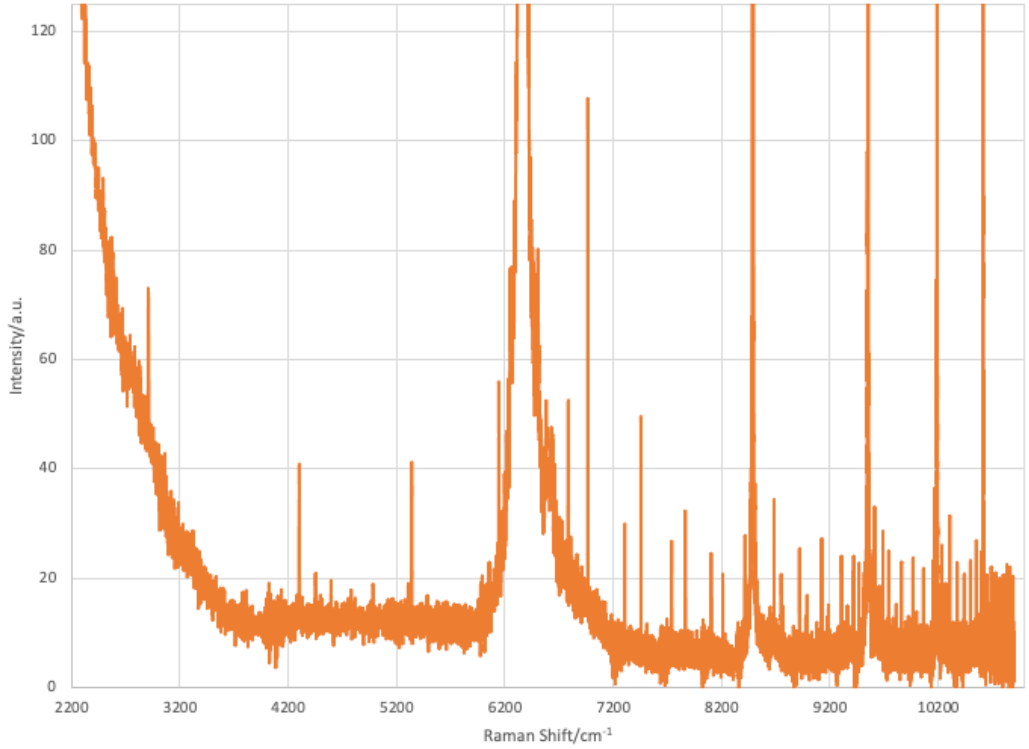

Confirmation of Molecular Hydrino $H_2(1/4)$ by Raman Spectroscopy

Raman spectra (2200 cm^{-1} to 11,000 cm^{-1}) obtained using a Horiba Jobin Yvon LabRam ARAMIS spectrometer with a 785 nm laser on a silver shot electrode post detonation showing $H_2(1/4)$ rotational transitions with spin-orbital coupling and fluxon linkage shifts.

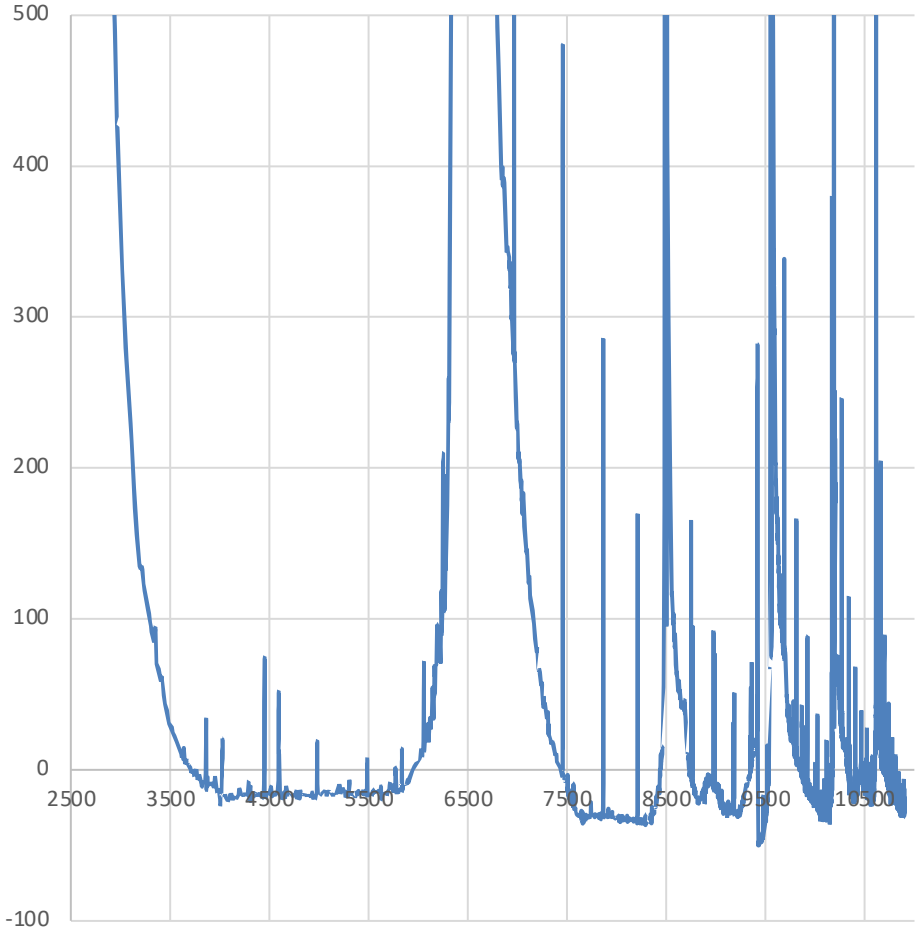

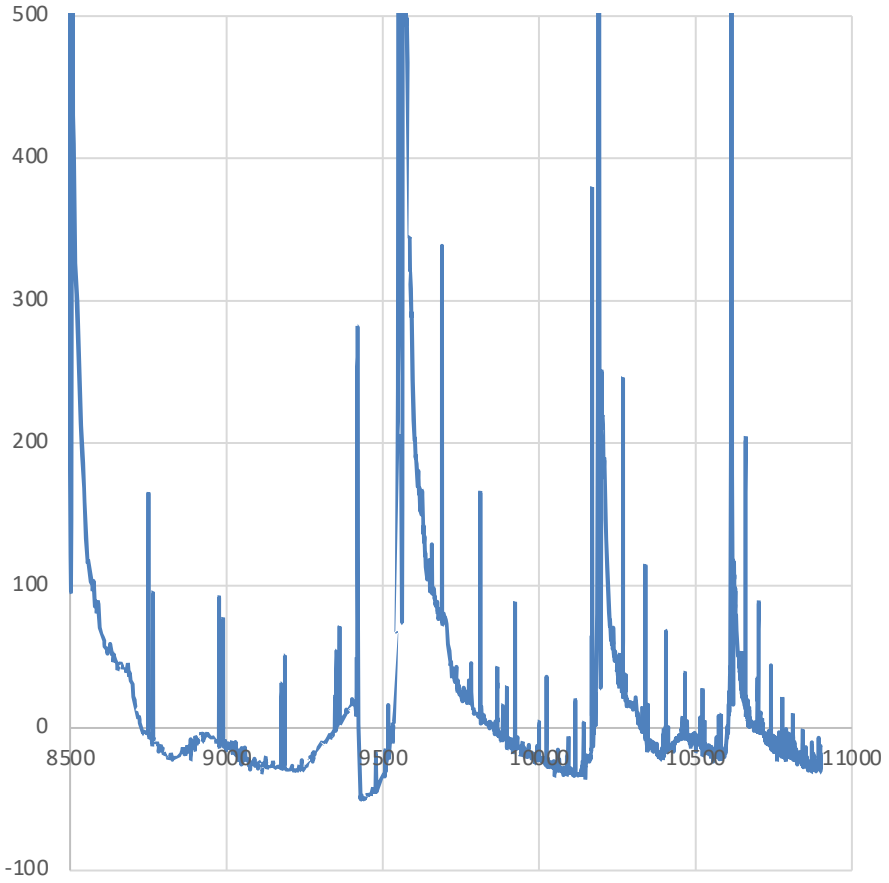

Confirmation of Molecular Hydrino HD(1/4) by Raman Spectroscopy

Raman spectra obtained using a Horiba Jobin Yvon LabRam ARAMIS spectrometer with a 785 nm laser on GaOOH:HD(1/4). A. 2500 cm^{-1} to 11,000 cm^{-1} region. B. 8000 cm-1 to 11,000 cm-1 region. All of the novel high-energy emission lines matched the double transition for final rotational quantum numbers J'_p =2(3) and J'_c = 1(0,1,2). Corresponding spin-orbital coupling and fluxon coupling were also observed. The rotational peaks shifted as predicted for the change in reduced mass of HD(1/4) compared to that of H_2(1/4).

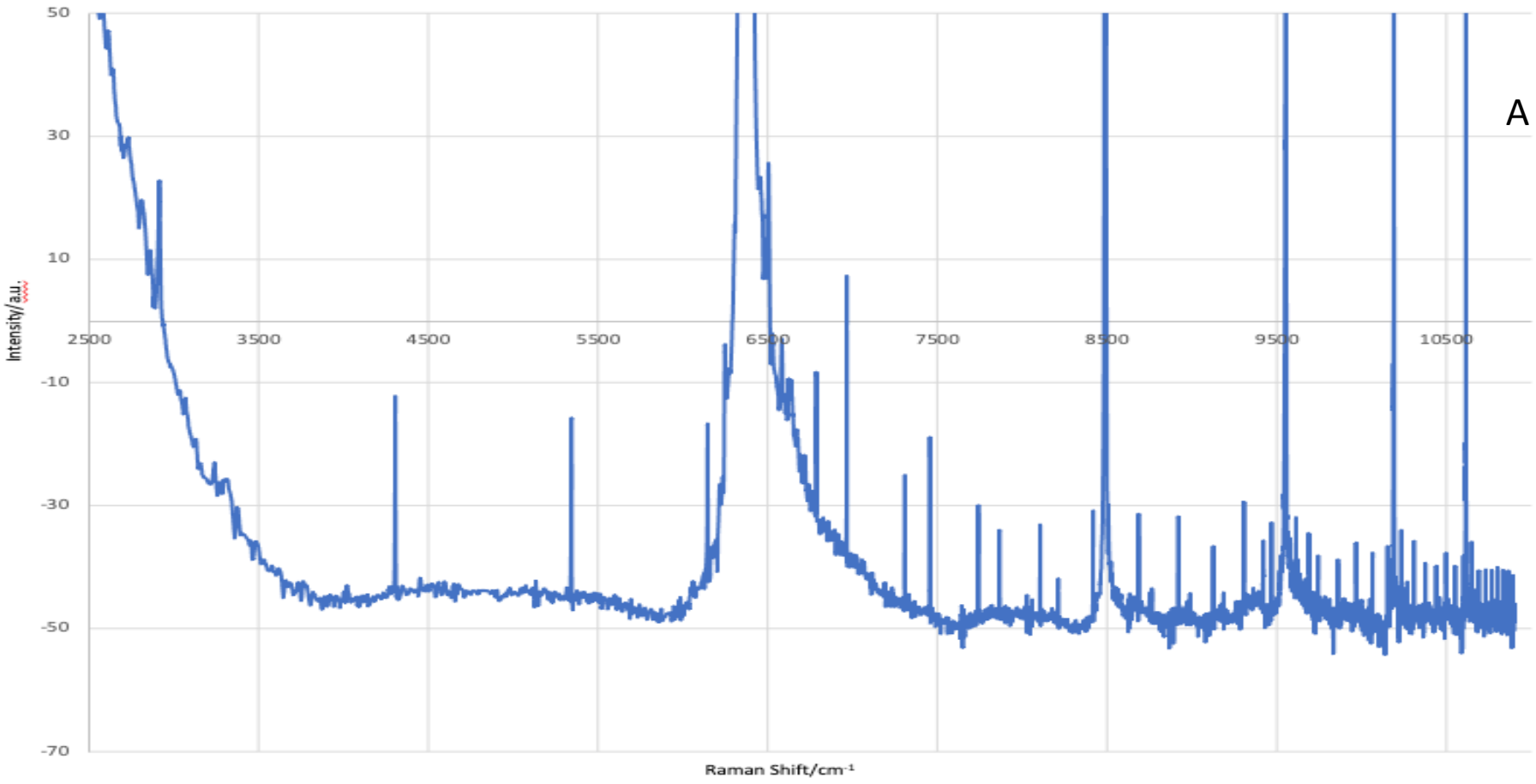

Confirmation of Molecular Hydrino HD(1/4) by Raman Spectroscopy Cont'd

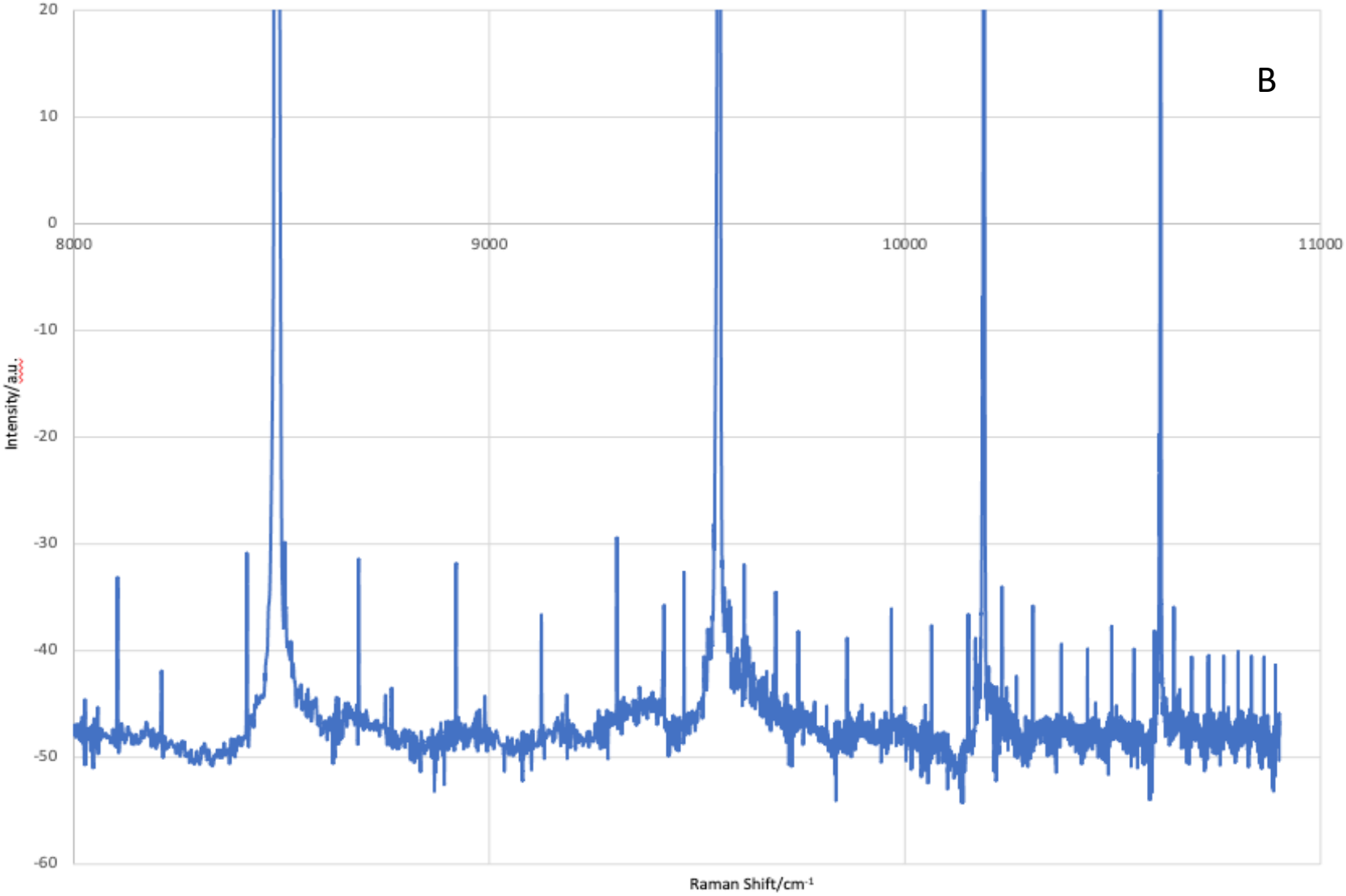

FTIR spectrum recorded on KI:H_2(1/4)

- The ability of interactions with a crystalline site to permit H_2(1/4) to be FTIR active due to an induced dipole was tested by embedding H_2(1/4) in a KI lattice.
- The high resolution (0.5 cm^{-1}) FTIR spectrum (490–4000 cm^{-1}) of KI:H_2(1/4) showing unique sharp peaks assigned to H_2(1/4).
- A major sharp peak was observed by FTIR on KI:H_2(1/4) at 1943 cm^{-1} that matched near identically the J = 0 to J' = 1 rotational transition of H_2(1/4).
- Other sharp peaks in the FTIR spectrum matched this rotational transition with spin-orbital and fluxon linkage splitting.

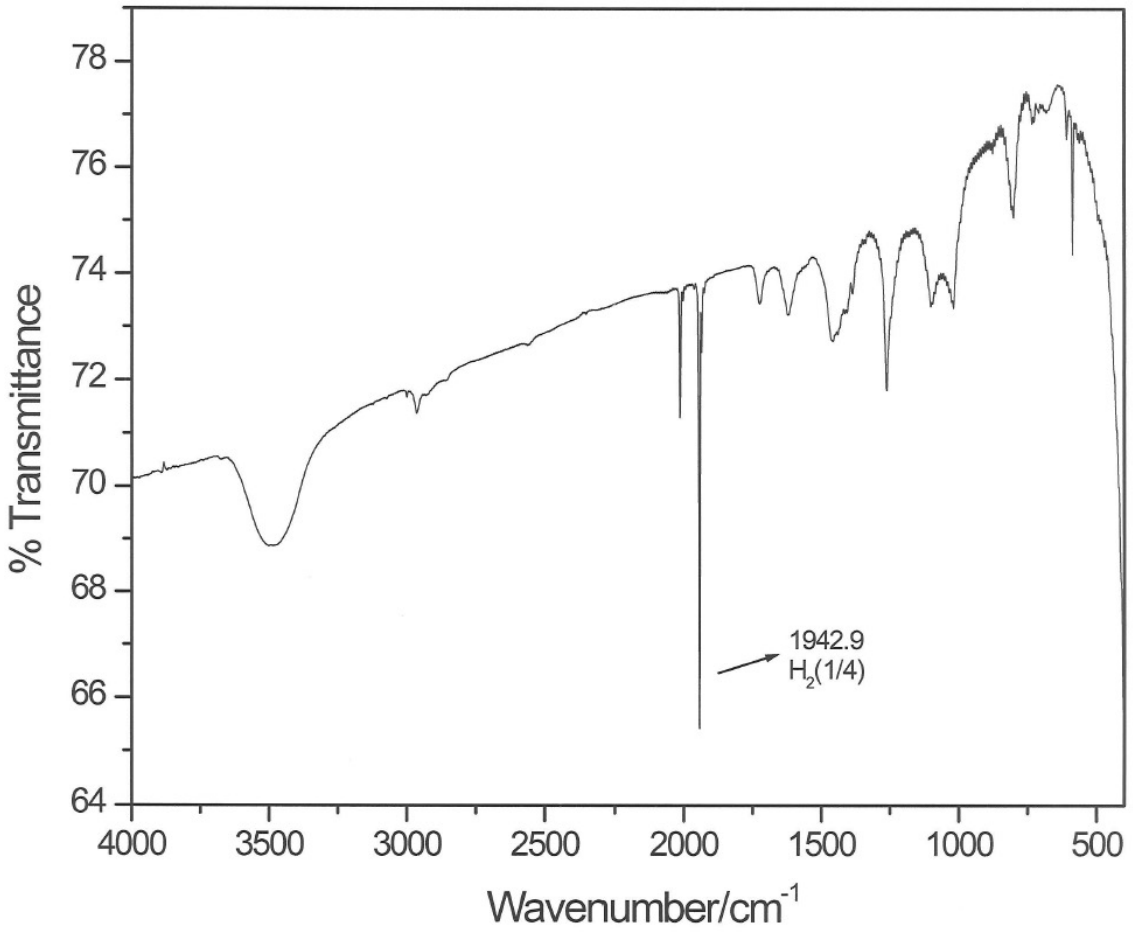

The effect of the application of a magnetic field on the FTIR spectrum (200 cm^{-1} to 8000 cm^{-1}) recorded on GaOOH:H_2(1/4).

- Infrared transitions of H_2(1/4) are forbidden because of its symmetry that lacks an electric dipole moment. However, H_2(1/4) has an unpaired electron resulting in the observation of rotational infrared excitation by coupling to the magnetic dipole of H_2(1/4), enhanced by an external applied magnetic field as well as through spin-orbital coupling.
- The application of a magnetic field gave rise to a significantly increased FTIR peak at 4164 cm^{-1}, too high an energy to be a known peak considering that H_2 was eliminated as possibility. The peak is an exact match to the concerted rotational transition J=0 to J'=1 with spin-orbital coupling.
- In addition, a substantial increased intensity of a sharp peak at 1801 cm^{-1} was observed. This peak was is not observed in the FTIR of control GaOOH. The peak matched the lowest energy concerted rotational transition with spin orbital and fluxon linkage coupling.

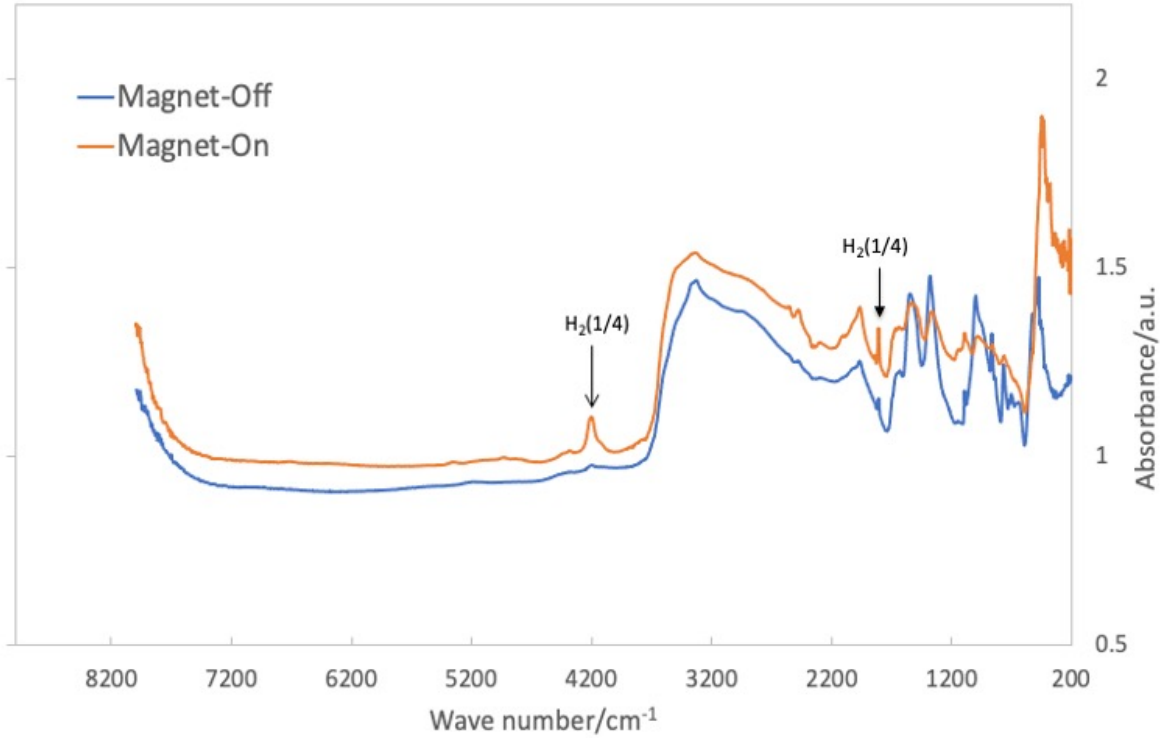

The effect of the application of a magnetic field on the FTIR spectrum recorded on GaOOH:H_2(1/4) Cont'd.

FTIR spectra (4000-8500 cm^{-1}) recorded on GaOOH:H_2(1/4) showed addition peaks having the very high energies of 4899 cm^{-1}, 5318 cm^{-1}, and 6690 cm^{-1} matching H_2(1/4) rotational and spin-orbital transitions wherein the intensity was increased due to the applied magnetic field, Control GaOOH showed no features.

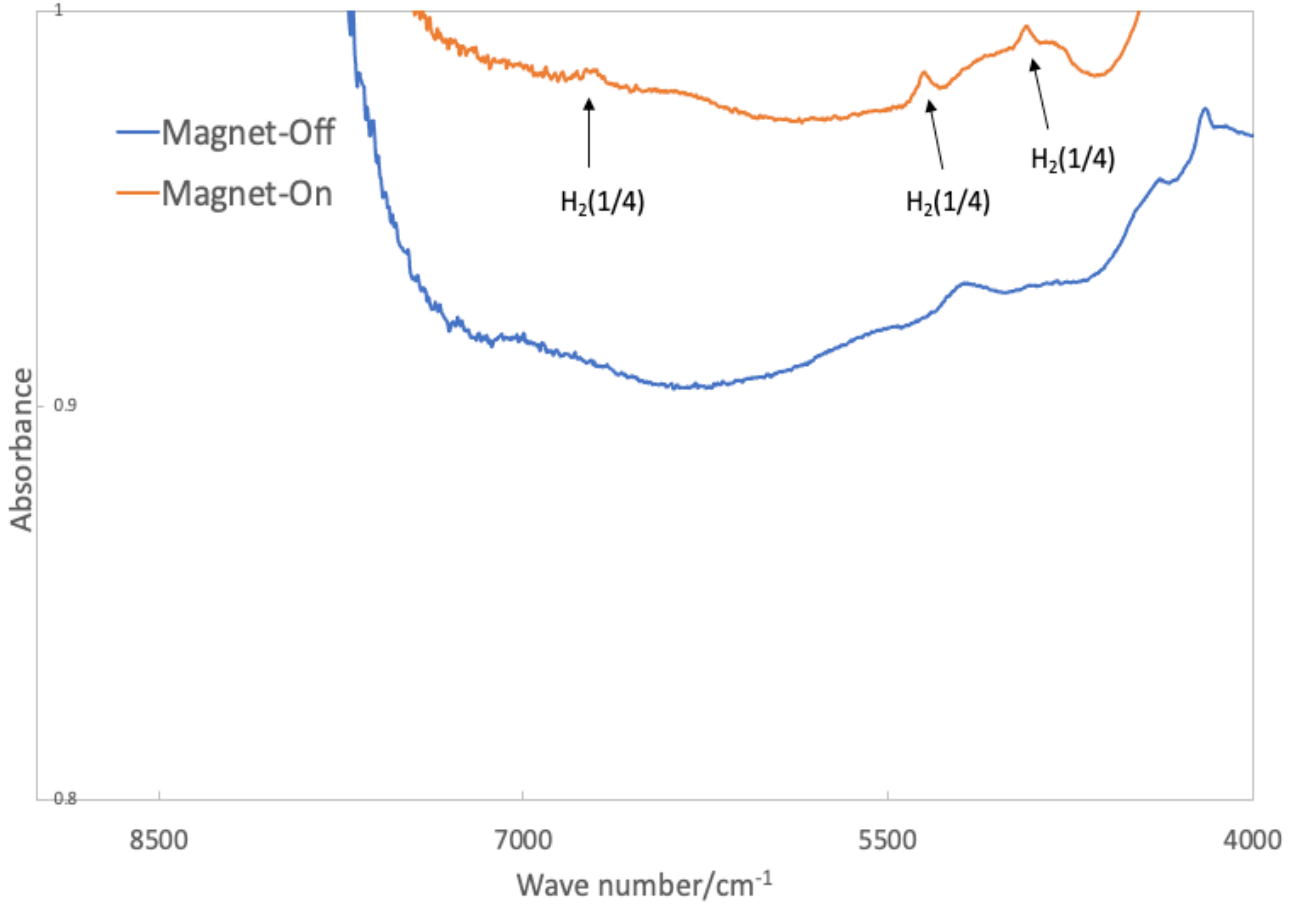

Confirmation of Molecular Hydrino $H_2(1/4)$ by Its Raman Allowed J = 0 to J = 2 Rotational Transition

The Raman allowed $H_2(1/4)$ J = 0 to J' =2 rotational transition with spin orbital coupling was observed on Fe_2O_3:$H_2(1/4)$ the product of FeOOH solid fuel hydrino reaction product using a Horiba Jobin Yvon LabRam ARAMIS with a 785 nm laser. The peak at 1062 cm^{-1} is due to silicate of the Raman slide and the other lines are multi-order 785 nm laser lines. Due to the extraordinary high energy, the peak assigned to $H_2(1/4)$ rotation cannot be assigned to any prior known compound. (R. Mills, J. Lotoski, W. Good, J. He, "Solid Fuels that Form HOH Catalyst," Int'l J. Hydrogen Energy, Vol. 39 (2014), pp. 11930–11944 DOI: 10.1016/j.ijhydene.2014.05.170.0

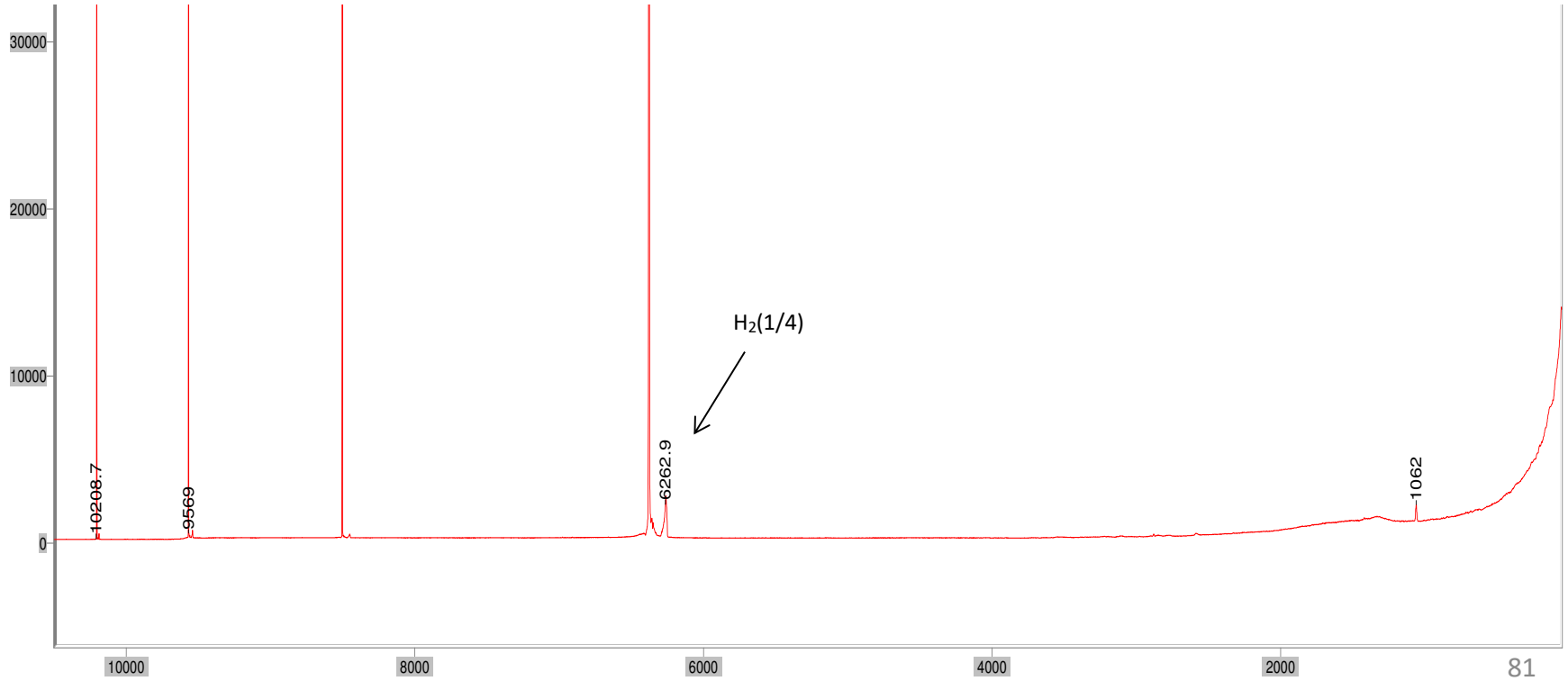

The Raman spectrum (3500 cm^{-1} to 8000 cm^{-1}) obtained using a Horiba Jobin Yvon LabRam ARAMIS spectrometer with a 785 nm laser on solid FeOOH powder prepared by ball milling for 10 hours showing the series of peaks assigned to the second and third order emission of fluxon linkages during the $H_2(1/4)$ double rotational and spin-orbital transition for final rotational, spin-orbital, and fluxon quantum numbers J'_p=3 and J'_c=2, m=-1.5, and $m_{\Phi 3/2}$ =2, respectively.

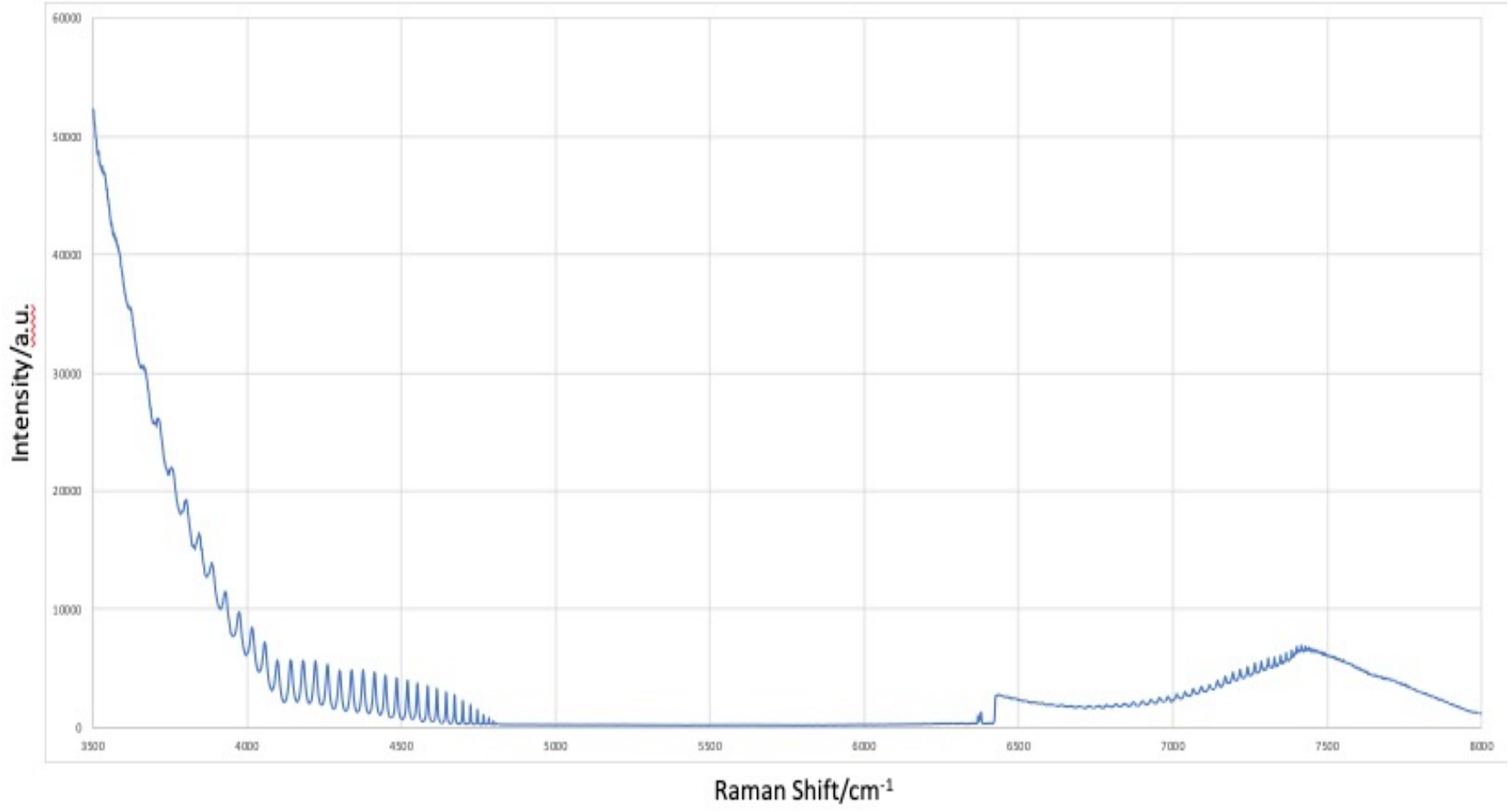

The Raman spectrum (3420 cm^{-1} to 4850 cm^{-1}) obtained using a Horiba Jobin Yvon LabRam ARAMIS spectrometer with a 785 nm laser on solid web-like fibers (Fe web) prepared by wire detonation of an ultrahigh purity Fe wire in air maintained with 20 Torr of water vapor showing a periodic series of peaks assigned to the second order emission of fluxon linkages during the $H_2(1/4)$ double rotational and spin-orbital transition for final rotational, spin-orbital, and fluxon quantum numbers $J'_p=3$ and $J'_c=2$, m=-1.5, and $m_{\Phi 3/2}=2$, respectively.

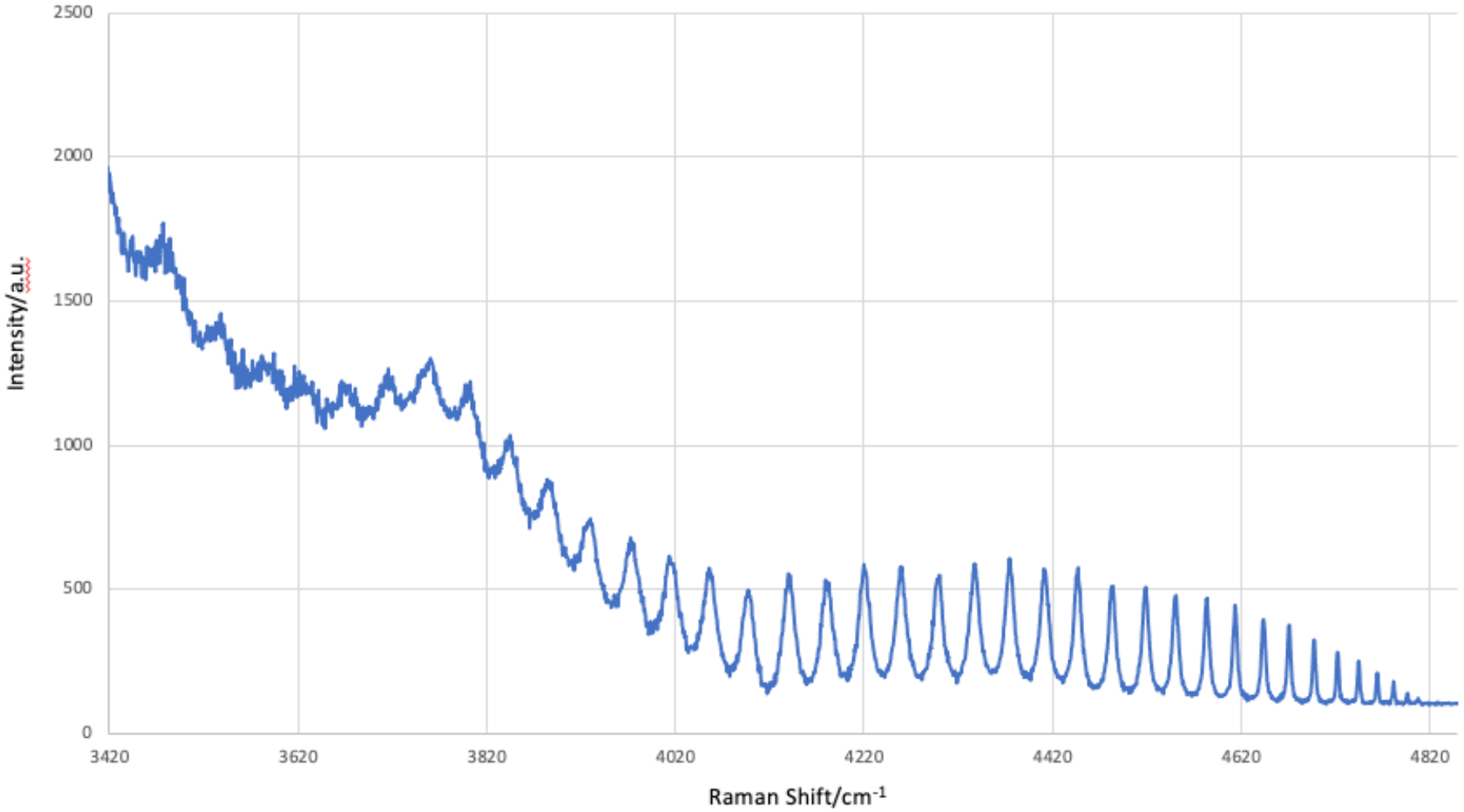

The Raman spectrum (6000 cm^{-1} to 7600 cm^{-1}) obtained on solid FeOOH:H_2(1/4) showing the details of the series assigned to the third order emission of fluxon linkages during the H_2(1/4) double rotational and spin-orbital transition for final rotational, spin-orbital, and fluxon quantum numbers J'_p=3 and J'_c=2, m=-1.5, and $m_{\Phi 3/2}$=2, respectively.

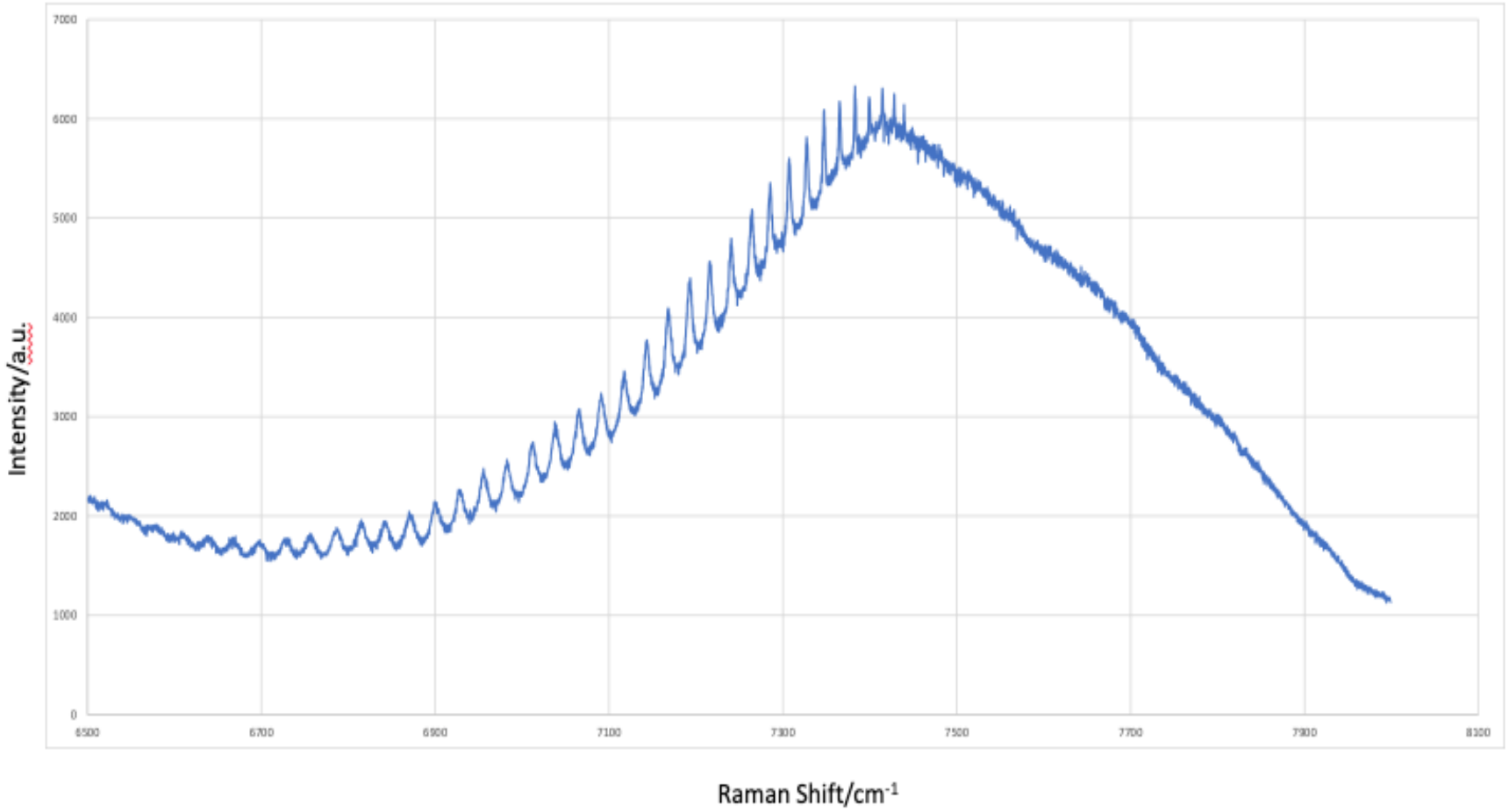

Raman anti-Stokes (-50 cm^{-1} to -8000 cm^{-1}) of the ball milled FeOOH sample recorded with 25% and 50% 300 mW 785 nm laser power and 100X objective.

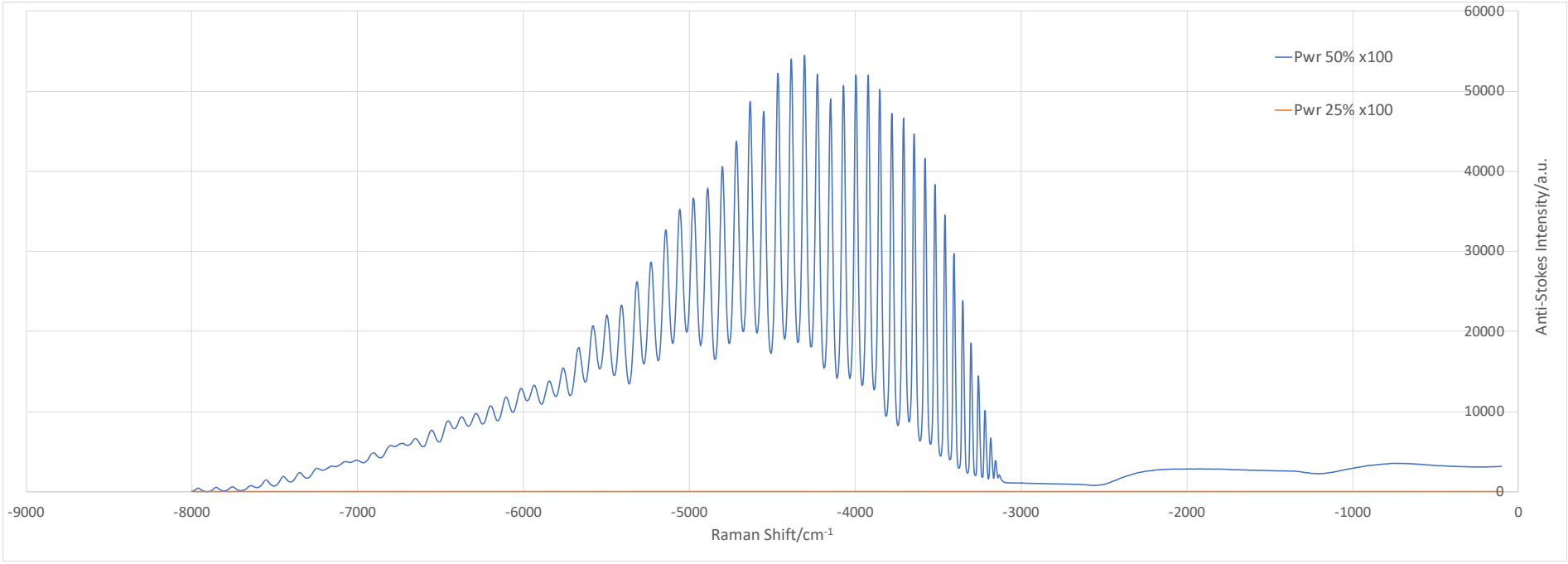

Raman Stokes (100 cm^{-1} to 8000 cm^{-1}) of the ball milled FeOOH sample recorded with 25% and 50% 300 mW 785 nm laser power and 100X objective.

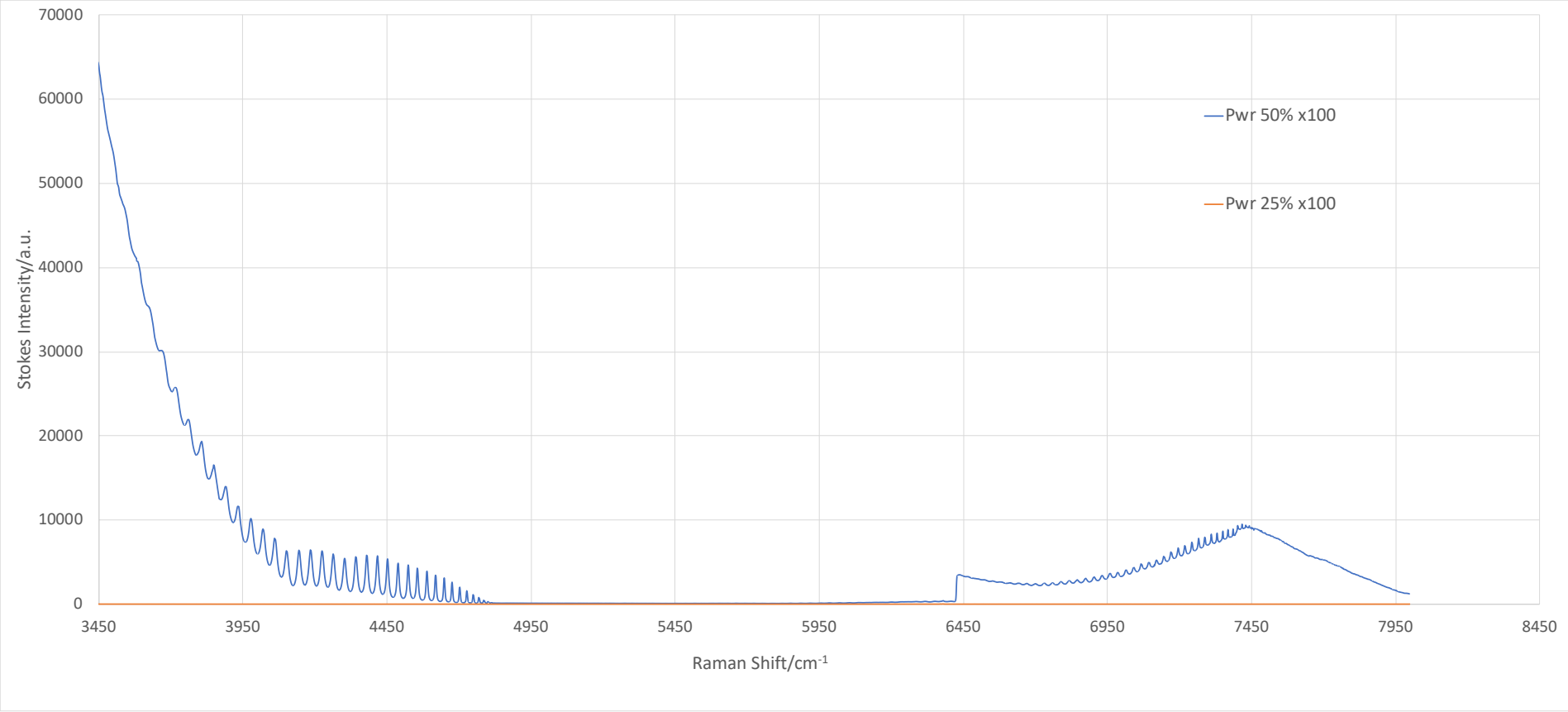

Raman anti-Stokes (-50 cm^{-1} to -8000 cm^{-1}) and Stokes (100 cm^{-1} to 8000 cm^{-1}) of the ball milled FeOOH sample recorded with 25% and 50% 300 mW 785 nm laser power and 100X objective. The anti-Stokes emission is the source of the Stokes-spectral lines assigned to second and third order high-energy emission.

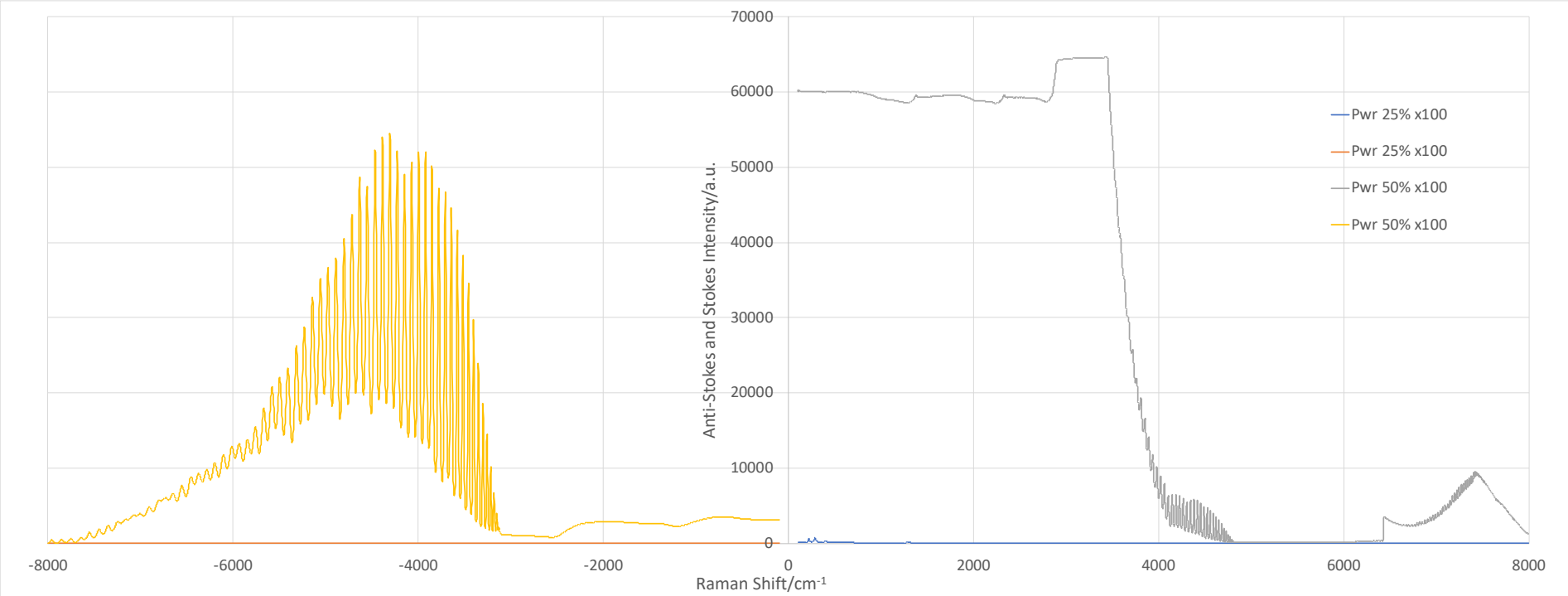

- The anti-Stokes and Stokes spectra are remarkable in that the energy ranges are higher than any prior recorded, there is a threshold laser intensity to observe the emission lines, and the first, second, and third order peaks are observed that match the rotational transitions of $H_2(1/4)$ and not any known source.

- The Raman results provide strong confirmation of $H_2(1/4)$ and the two-photon excitation mechanism of the rotational energy levels of $H_2(1/4)$.

Raman anti-Stokes (-50 cm^{-1} to -8000 cm^{-1}) of ball milled CoOOH and ball milled non-magnetic chemical mixture KI-NH_4NO_3 recorded with 50% of 300 mW 785 nm laser power and 100X objective. The anti-Stokes emission that was only observed on the CoOOH product with a magnetic matrix is the source of the Stokes-spectral lines assigned to second and third order high-energy emission.

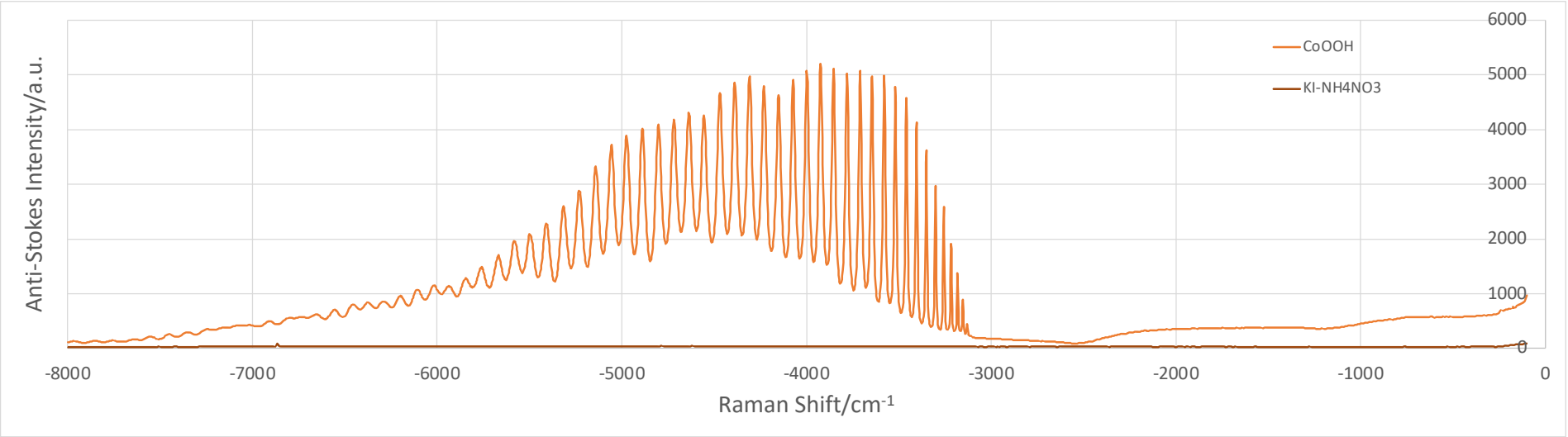

Raman Stokes (4000 cm-1 to 8000 cm-1) of ball milled CoOOH recorded with 50% of 300 mW 785 nm laser power and 100X objective. The peaks match the corresponding second and third order lines of the anti-Stokes lines.

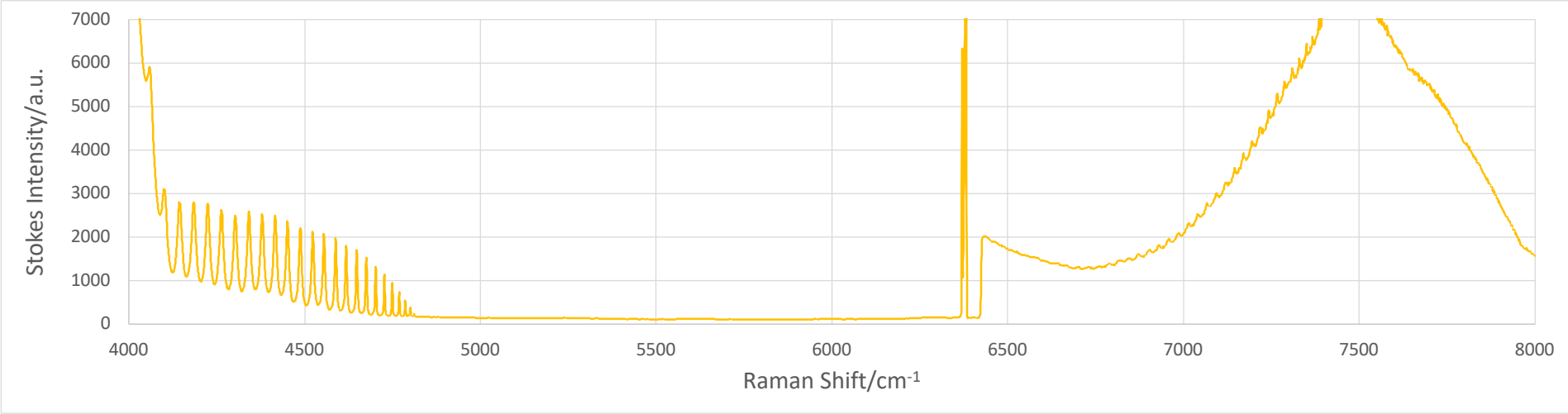

Raman anti-Stokes (-50 cm^{-1} to -8000 cm^{-1}) of the Ni and tin-coated Ni foil samples run in the SunCell® and control Ni foil recorded with 50% of 300 mW 785 nm laser power and 100X objective. The anti-Stokes emission is the source of the Stokes-spectral lines assigned to second and third order high-energy emission. The results demonstrate that the reaction of H_2 to $H_2(1/4)$ is the source of SunCell® power gain.

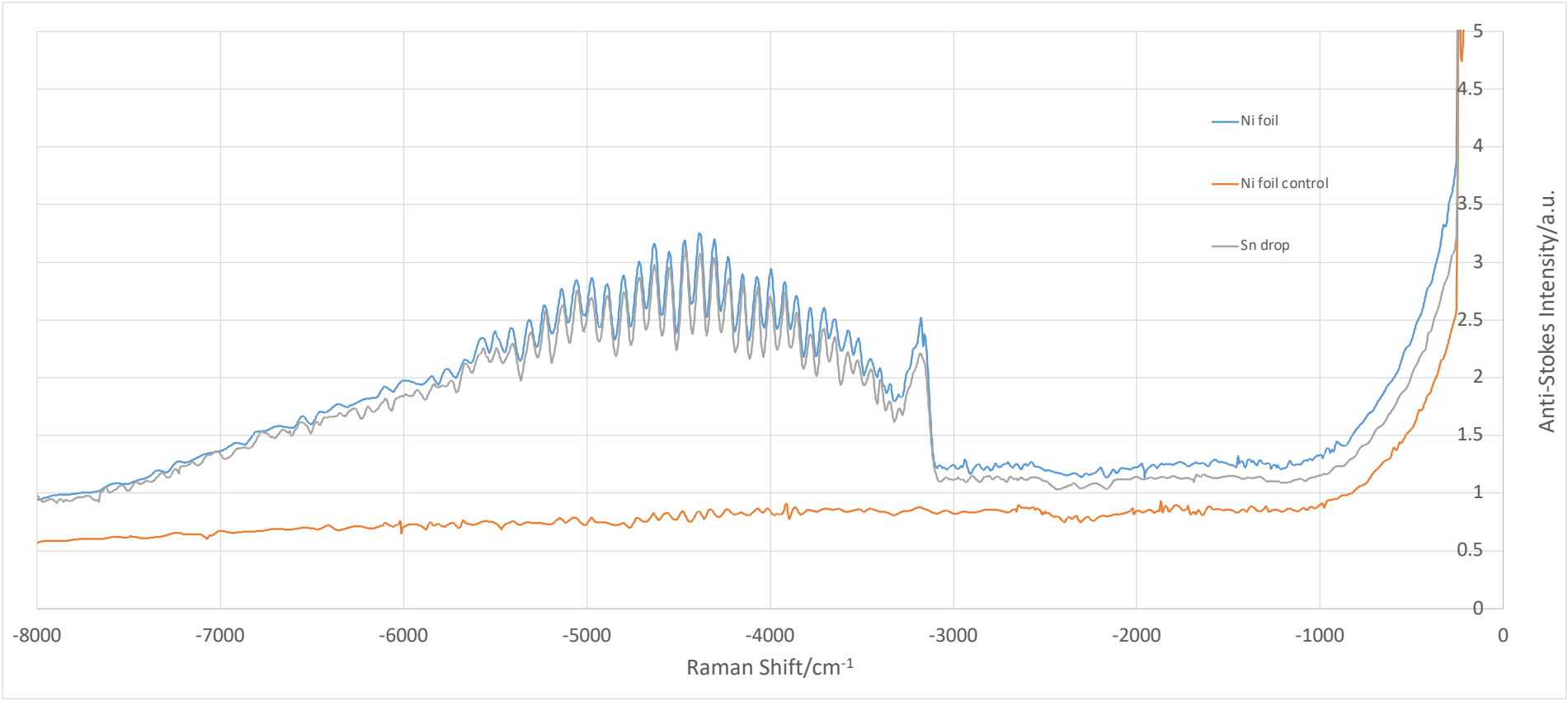

Raman Stokes (3000 cm^{-1} to 8000 cm^{-1}) of the Ni and tin-coated Ni foil samples run in the SunCell® and control Ni foil recorded with 50% of 300 mW 785 nm laser power and 100X objective. The peaks match the corresponding second and third order lines of the anti-Stokes lines.

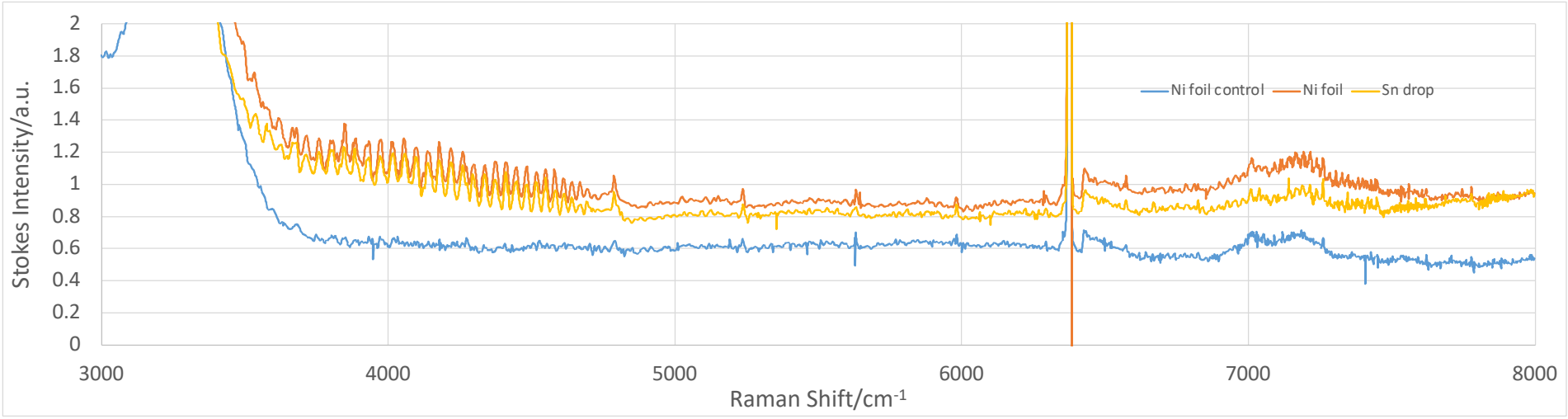

Raman Spectroscopy of $H_2(1/4)$ With Application of a Magnetic Field

- Raman spectra obtained using a Horiba Jobin Yvon LabRam ARAMIS spectrometer with an 11 mW laser 785 nm laser on a Ni foil prepared by immersion in the molten gallium of a SunCell that maintained a hydrino plasma reaction for 10 minutes. A. 2500 cm^{-1} to 11,000 cm^{-1} region. B. 3700 cm-1 to 5500 cm-1 region with Ni foil magnetized with a 1 T neodymium magnet.

- $H_2(1/4)$ showed a series of SQUID-like fluxon transitions of a single rotational and spin-orbital spilt level as high-energy emission observed by Raman spectroscopy on magnetic Fe_2O_3 and FeOOH samples.

- Ni foil samples run at a temperature above the Ni Curie temperature and then magnetized by the application of 1T magnetic flux, switched from discrete high-energy emission lines corresponding to $H_2(1/4)$ rotational transitions slit by spin-orbital and fluxon linkage transitions to the series of fluxon transitions of a single rotational and spin-orbital spilt level that matches the spectra of magnetic Fe_2O_3 and FeOOH samples.

- The high energy emission assignments were confirmed by elimination of the lines by an 805 nm long-pass edge filter between the sample and the detector.

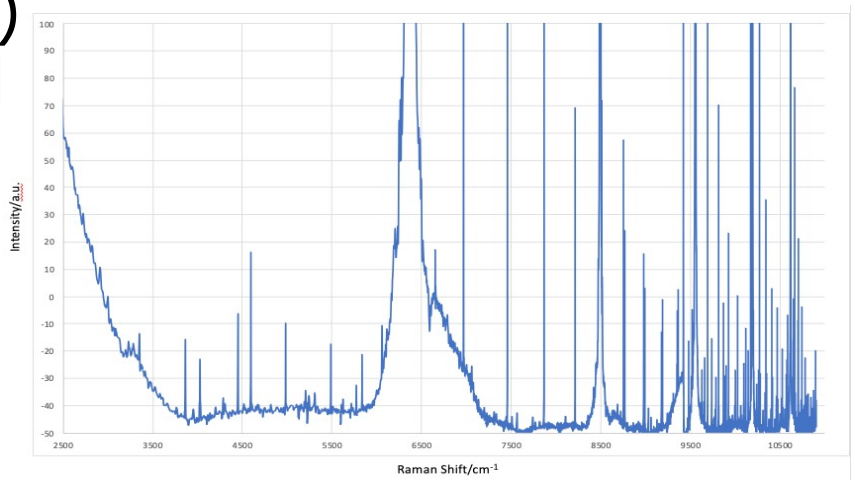

(A)

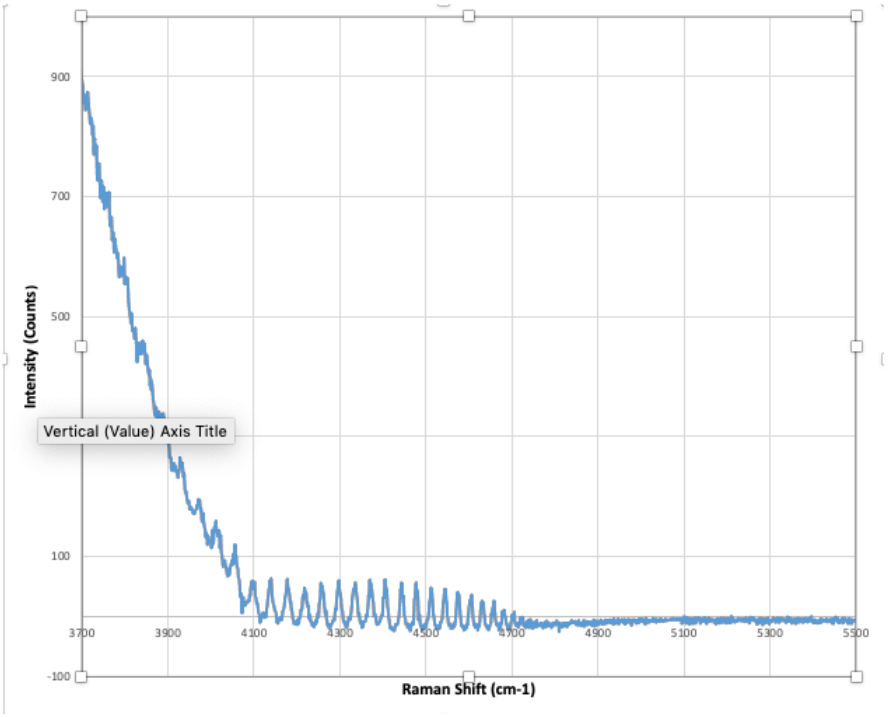

(B)

R. Mills, "Hydrino States of Hydrogen", https://brilliantlightpower.com/pdf/Hydrino_States_of_Hydrogen_Paper.pdf.

High-Energy Emission Lines (16,800-16,100 cm^{-1}) of GaOOH:H_2(1/4):H_2O

- Raman spectra (14,000-14,700 cm^{-1}) of 50:50 vol% GaOOH:H_2(1/4):H_2O and controls recorded using a Horiba Jobin Yvon LabRam ARAMIS with a 325 nm laser.
- GaOOH:H_2(1/4) was formed by dissolving Ga_2O_3 collected from a hydrino reaction run in the SunCell® in 4M aqueous KOH, allowing fibers to grow, and float to the surface where they were collected by filtration.
- GaOOH:H_2(1/4):H_2O was formed by suspending GaOOH:H_2(1/4) in H_2O at 50:50 vol% .
- Based on the absence of a change in the spectrum with a 331 long-pass edge filter placed between the laser and the sample and placed between the sample and the detector, the series of peaks observed on GaOOH:H_2(1/4):H_2O was assigned to 587.8 nm laser line excitation with emission from the H_2(1/4) J_p'=3, J_c'=1 double rotational transition level split by spin-orbital coupling and fluxon linkages.
- The peaks were absent in controls 4M KOH and deionized water.
- Seventeen of the lines of the emission spectrum match members of the Diffuse Interstellar Medium (DIBs).

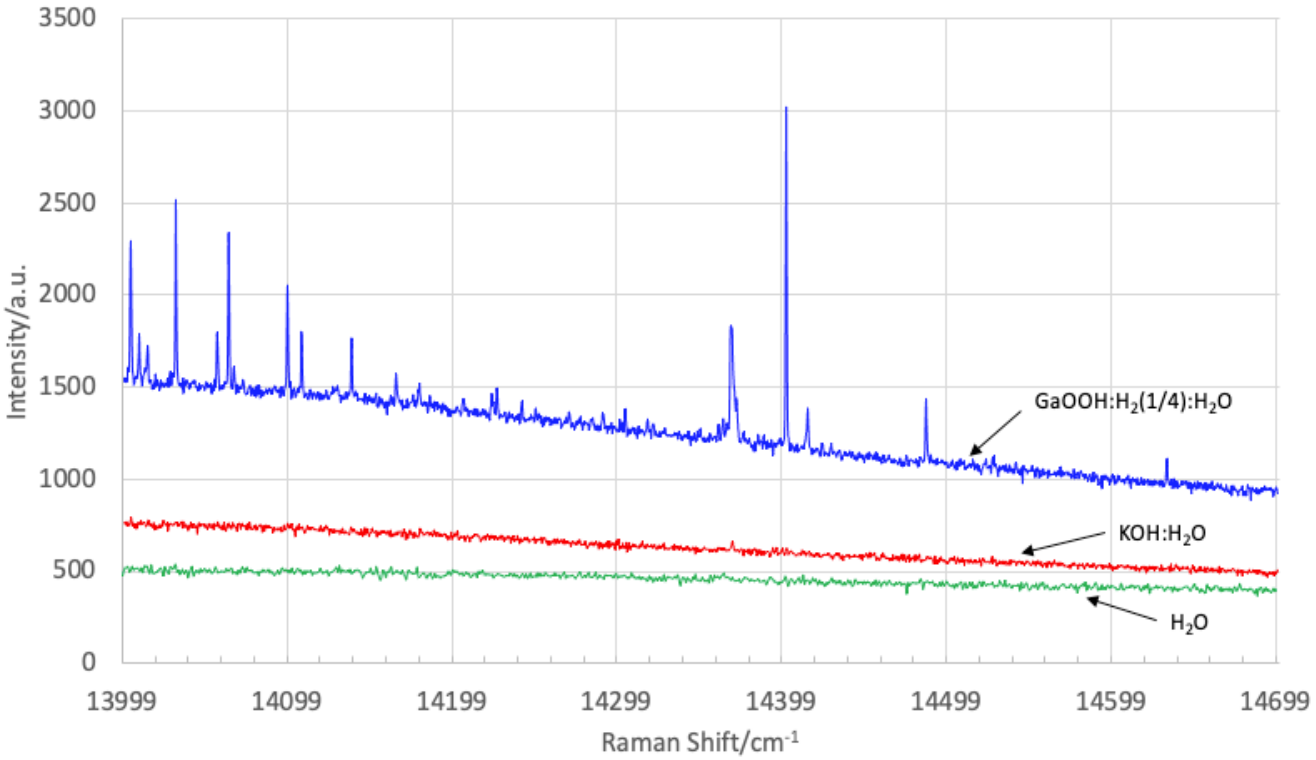

High-Energy $H_2(1/4)$ Ro-Vibrational Emission Lines (17,900-16,200 cm^{-1})

- 325 nm Raman spectra (12,250-14,750 cm^{-1}) were obtained on the plasma and molten gallium exposed surfaces of a Ni foil maintained in a SunCell® during a hydrino plasma reaction for 10 minutes.
- The corresponding series of emission peaks (17,900-16,200 cm^{-1}) observed on the plasma exposed side was assigned to 587.8 nm laser line excitation with emission from the $H_2(1/4)$ $J_p'=3$, $J_c'=1,2$ double rotational transition levels split by spin-orbital coupling and fluxon linkages.
- Many of the peaks matched those recorded on $GaOOH:H_2(1/4):H_2O$.
- Forty-five of the lines of the combined emission spectra match members of the Diffuse Interstellar Medium (DIBs).

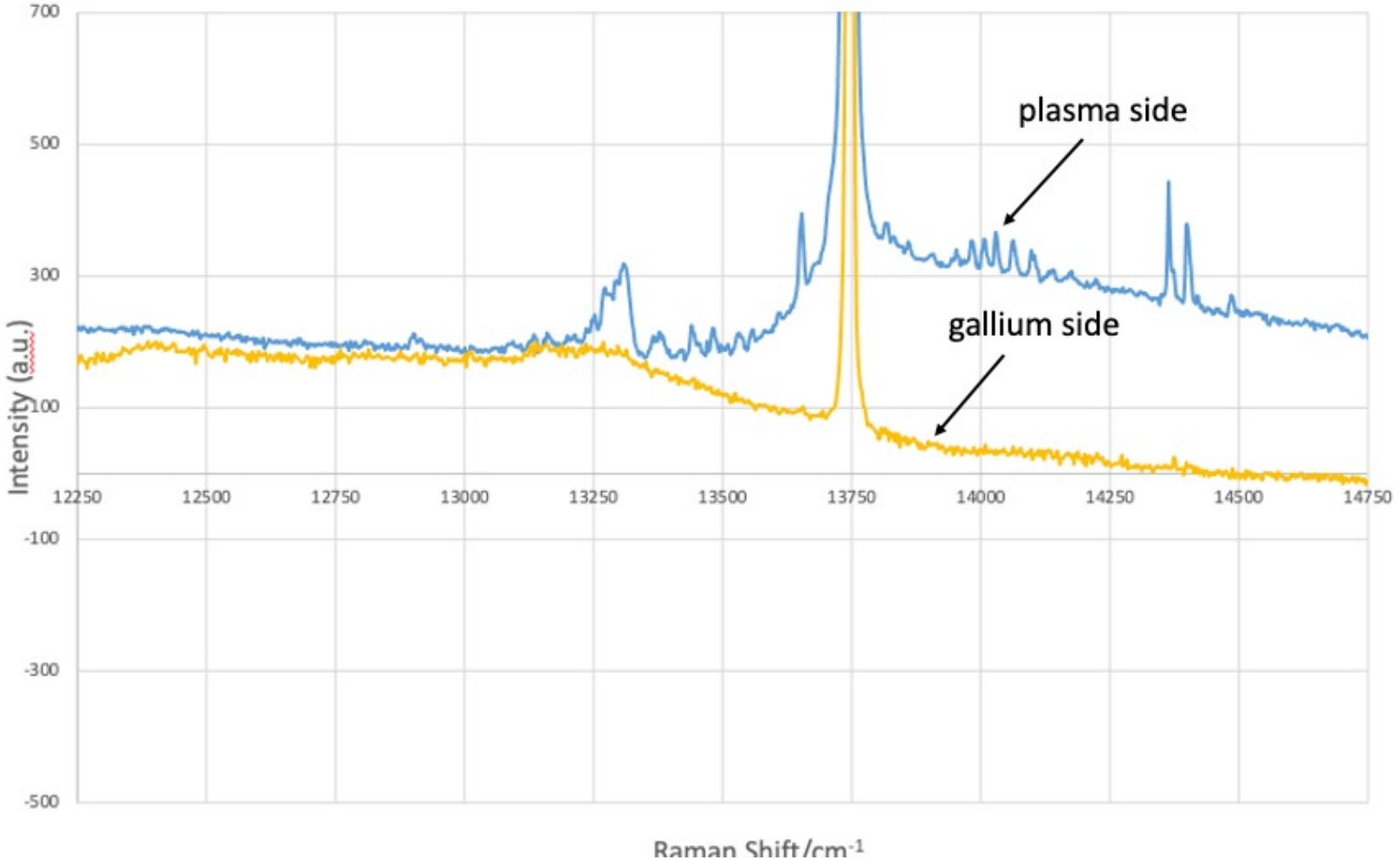

High-Energy $H_2(1/4)$ Ro-Vibrational Emission Lines (17,900-16,200 cm^{-1})

- 325 nm Raman spectra (12,250-14,750 cm^{-1}) were obtained on the plasma and molten tin exposed surfaces of a Ni foil maintained in a SunCell® during a hydrino plasma reaction for 10 minutes.
- The corresponding observed series of emission peaks (17,900-16,200 cm^{-1}) was assigned to 587.8 nm laser line excitation with emission from the $H_2(1/4)$ $J_p'=3$, $J_c'=1,2$ double rotational transition levels split by spin-orbital coupling and fluxon linkages.
- The results further demonstrate that the reaction of H_2 to $H_2(1/4)$ is the source of SunCell® power gain.

High-Energy $H_2(1/4)$ Ro-Vibrational Emission Lines (15,750-16,750 cm^{-1})

- 442 nm Raman spectra (13,000-15,000 cm^{-1}) were obtained on the Ni foils used to recorded the 325 nm Raman results.
- The corresponding series of emission peaks (15,750-16,750 cm^{-1}) was assigned to 442 nm laser line excitation with emission from the $H_2(1/4)$ $J_p'=3$, $J_c'=1$ double rotational transition levels split by spin-orbital coupling and fluxon linkages.
- First order and second order emission peaks were observed.
- The 442 nm results confirm the excitation mechanism of the 325 nm Raman spectra.
- Ten of the lines of the 442 emission spectrum match members of the Diffuse Interstellar Medium (DIBs).

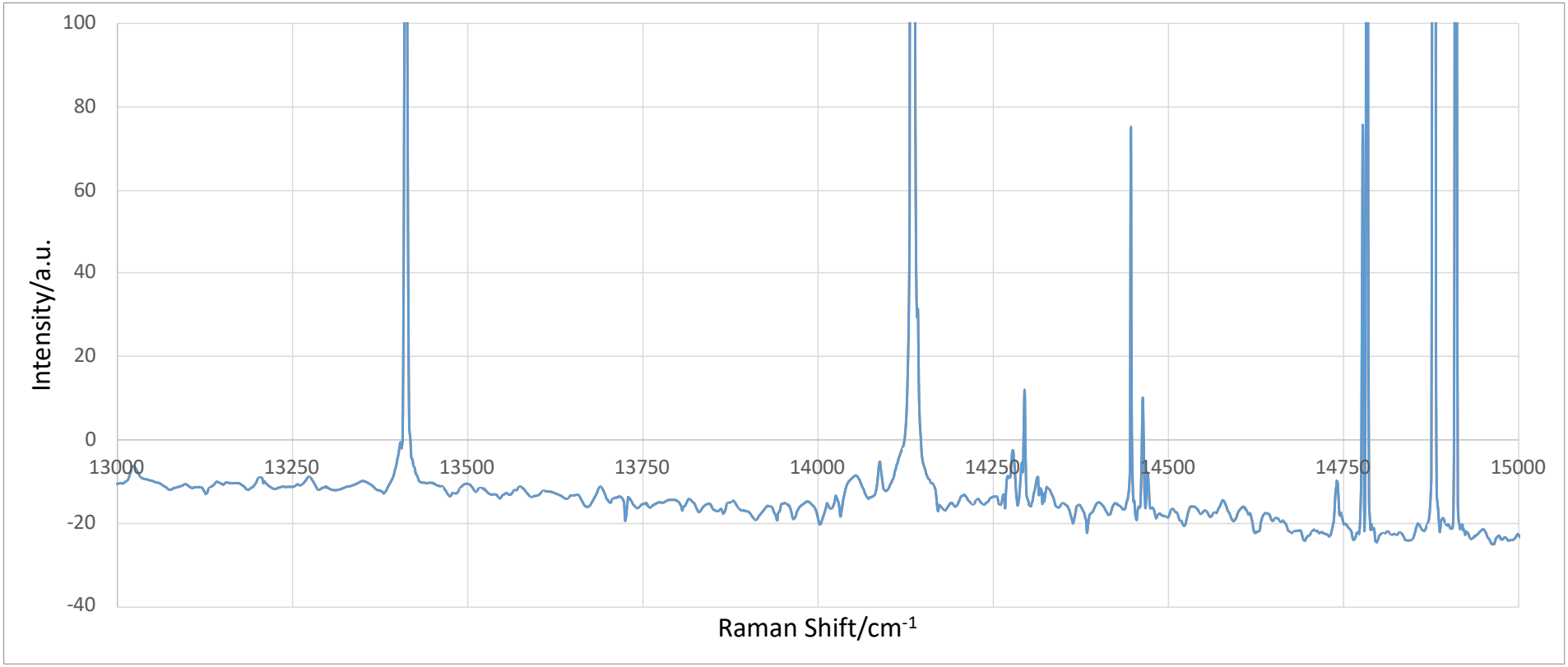

MoWeb: Vibrating Sample Magnetometer

- Paramagnetic material responds linearly with the induced magnetism.
- The observed “S” shape is characteristic of super paramagnetic, a hybrid of ferromagnetism and para magnetism.
- It is exception that the induced magnetism peaks at 5K Oe and declines with higher applied field.

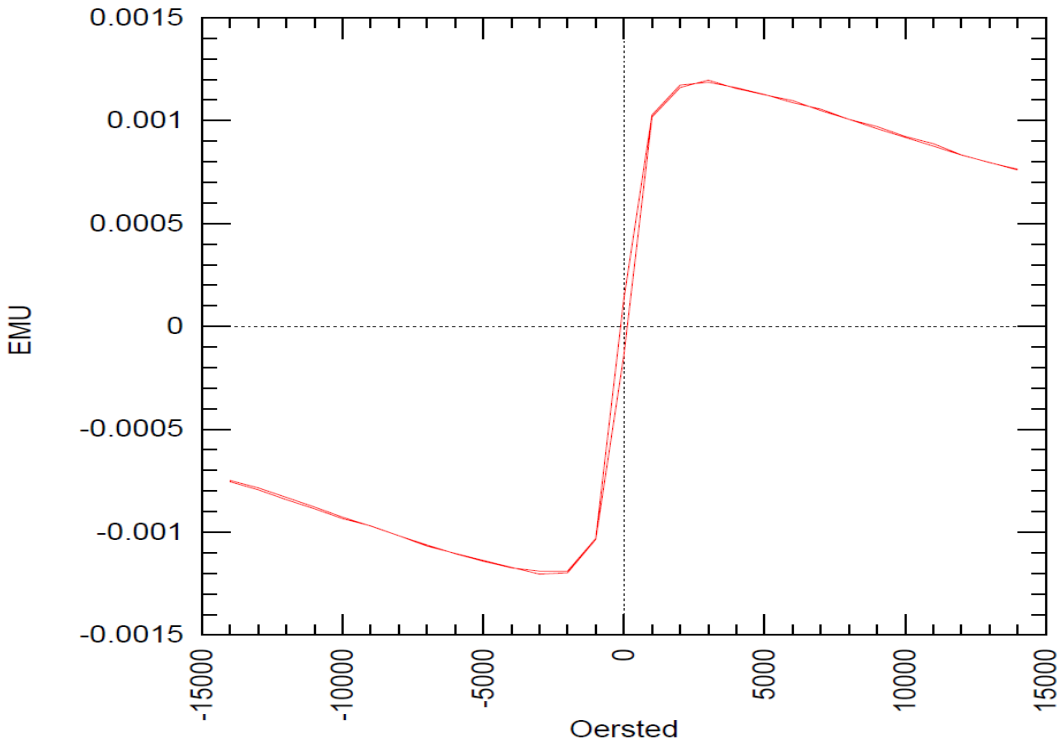

^{1}H MAS NMR Spectra

^{1}H MAS NMR spectrum relative to external TMS of the KCl getter exposed to hydrino gas that shows upfield shifted matrix peak a -4.6 ppm due to the magnetism of molecular hydrino.

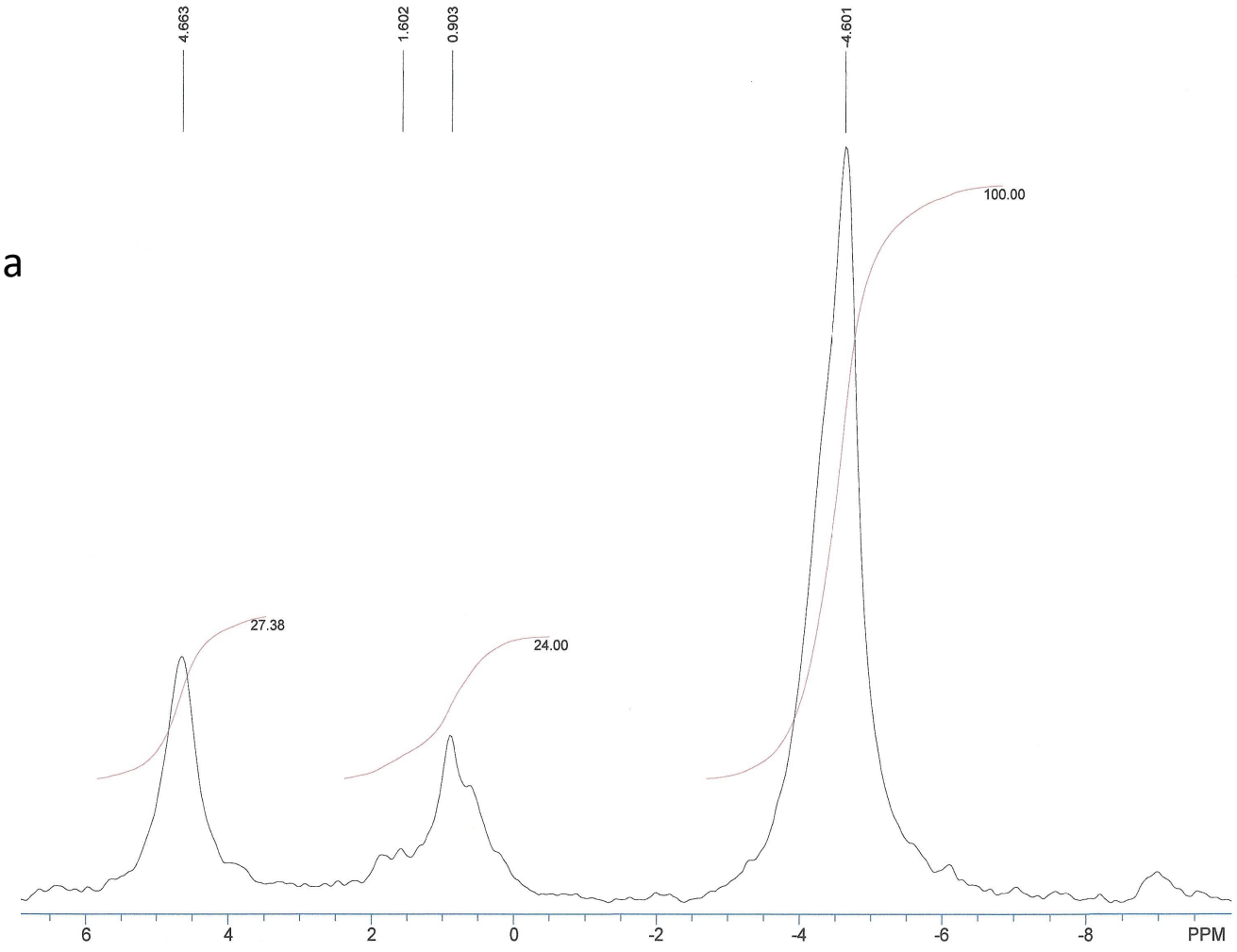

R. Mills, J. Lotoski, W. Good, J. He, "Solid Fuels that Form HOH Catalyst," Int'l J. Hydrogen Energy, Vol. 39 (2014), pp. 11930–11944 DOI: 10.1016/j.ijhydene.2014.05.170.

ToF-SIMS Spectrum of K_2CO_3-KCl (30:70 wt%) getter exposed to hydrino gas and having upfield shifted MAS NMR spectral peaks.

Multimer clusters of getter compounds with di-hydrogen as part of the structure, M:H_2 (M = KOH or K_2CO_3) such as $K^+(H_2{:}K_2CO_3)_n$ and $K^+(H_2{:}KOH)_n$ consistent with $H_2(1/p)$ as a complex in the structure were observed. These clusters were not observed in controls comprising the matrix exposed to H_2.

Positive ToF-SIMS, m/e = 90 to 100 region

Positive ToF-SIMS, m/e = 0 to 200 region.

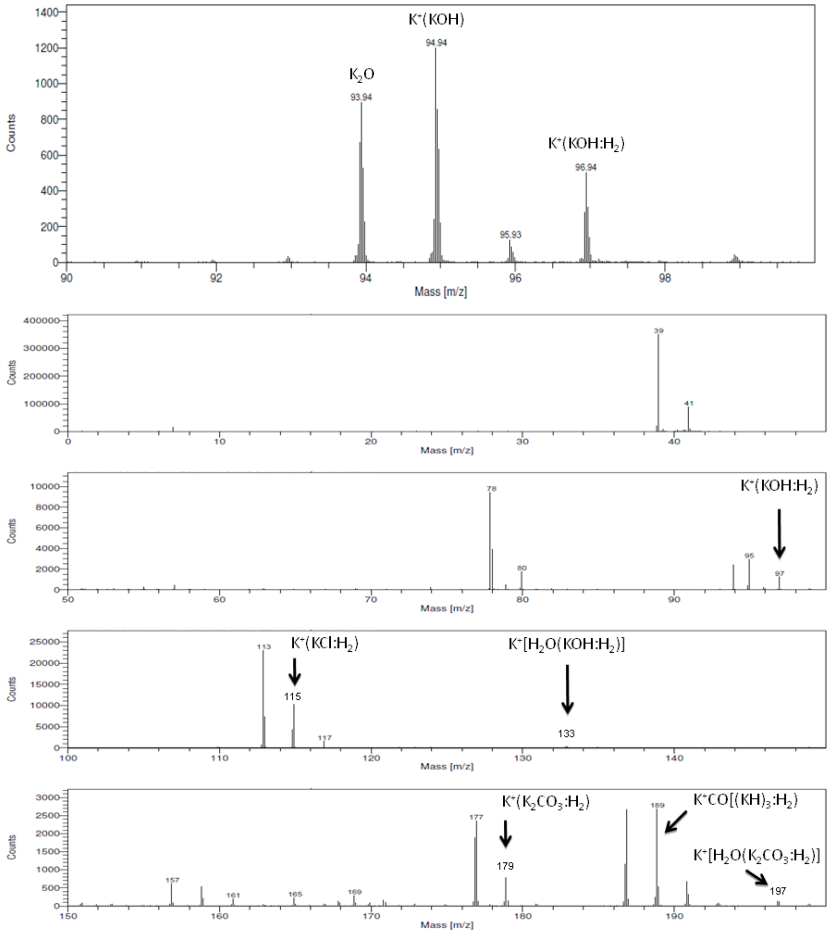

R. Mills, X Yu, Y. Lu, G Chu, J. He, J. Lotoski, "Catalyst induced hydrino transition (CIHT) electrochemical cell," (2012), Int. J. Energy Res., (2013), DOI: 10.1002/er.3142.

ToF-SIMS Spectrum of K_2CO_3-KCl (30:70 wt%) getter exposed to hydrino gas and having upfield shifted MAS NMR spectral peaks cont'd.

Positive ToF-SIMS, m/e = 200 to 1000 region.

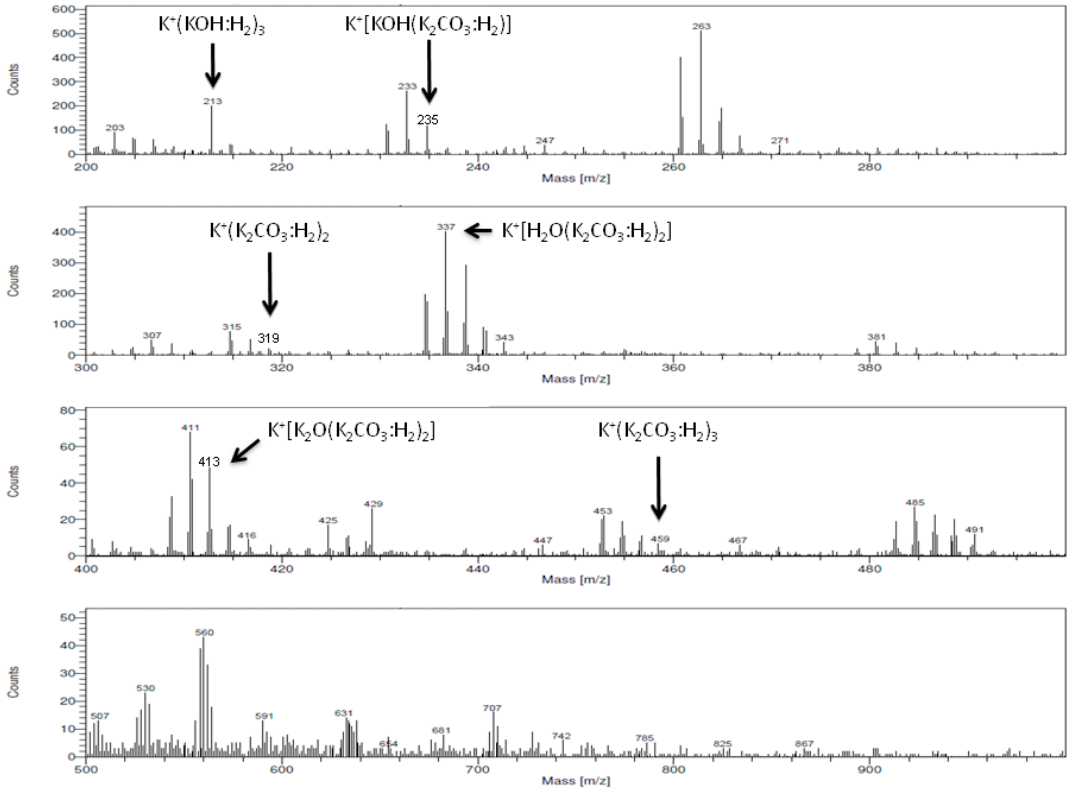

ESI-ToFMS Spectral Results

obtained on the same sample analyzed by ToF-SIMS comprising K_2CO_3-KCl (30:70 wt%) getter from the scale-up 5 W stack of 10 CIHT cells comprising [Mo/LiOH-LiBr-MgO/NiO] that output 1029 Wh at 137% gain having the upfield shifted MAS NMR spectral peaks. Multimer clusters of matrix compounds with di-hydrogen as part of the structure, $M:H_2$ (M = KCl, KOH, or K_2CO_3) consistent with $H_2(1/p)$ as a complex in the structure were observed. These clusters were not observed in controls comprising the matrix exposed to H_2.

Hydrino Compound or Fragment	Nominal Mass m/e	Observed m/e	Calculated m/e	Difference Between Observed and Calculated m/e
$K^+(KCl:H_2)$	115	114.9118	114.9114	0.0004
$K^+KHKOH:H_2$ or $K^+K_2O:(H_2)_2$	137	136.9583	136.9173	0.0410
$K^+[(KCl)_3:H_2]$	263	262.7772	262.7770	0.0002
$K^+[H_2O(K_2CO_3)_2:(H_2)]$	335	334.7661	334.8137	0.0476
$K^+[H_2O(K_2CO_3)_2:(H_2)_2]$	337	336.7324	336.8293	0.0969
$K^+[H_2O(K_2CO_3)_2:(H_2)_3]$	339	338.7099	338.8450	0.1351

R. Mills, X Yu, Y. Lu, G Chu, J. He, J. Lotoski, "Catalyst induced hydrino transition (CIHT) electrochemical cell," (2012), Int. J. Energy Res., (2013), DOI: 10.1002/er.3142.

Inorganic Hydrino Complex Behaves as an Organic Molecule in Chromatographic Analysis with an Aqueous Solution and an Organic Column Packing

- Using an Agilent Technologies 6230 TOFLC/MS and a C18 50 x 2mm 3µm (P/N 94641-12) column, liquid chromatography was performed on an energy dispersive X-ray spectroscopy (EDS) determined gallium (59 at%)/oxygen (38 at%)/carbon (2 at%) sample collected from a hydrino reaction run in the SunCell® and dissolved in 4M NaOH wherein the hydrino composition $H_2(1/4)$ was confirmed by XPS and EPR.
- Following the injection of 20 ul of the liquid sample, an inorganic hydrino complex was eluted with a water + acetonitrile-water gradient.
- When using an organic column, inorganic compounds such as sodium carbonate chromatographically elute with the void volume with no retention time.
- Remarkably, when molecular hydrino complexed with sodium carbonate organic molecular behavior was observed. The complex showed a chromatographic peak at 23 minutes.
- The peak fragmented into inorganic ions that identified the complex as comprising sodium carbonate.

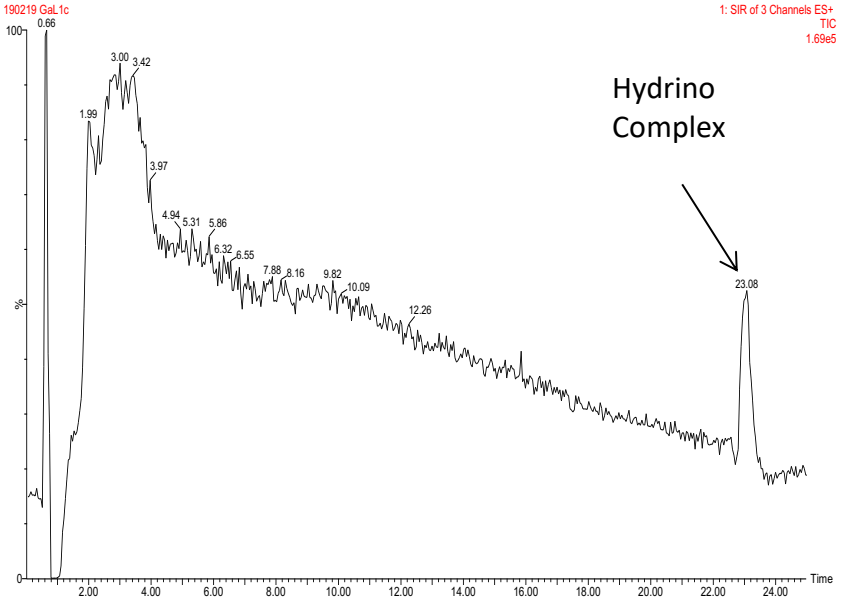

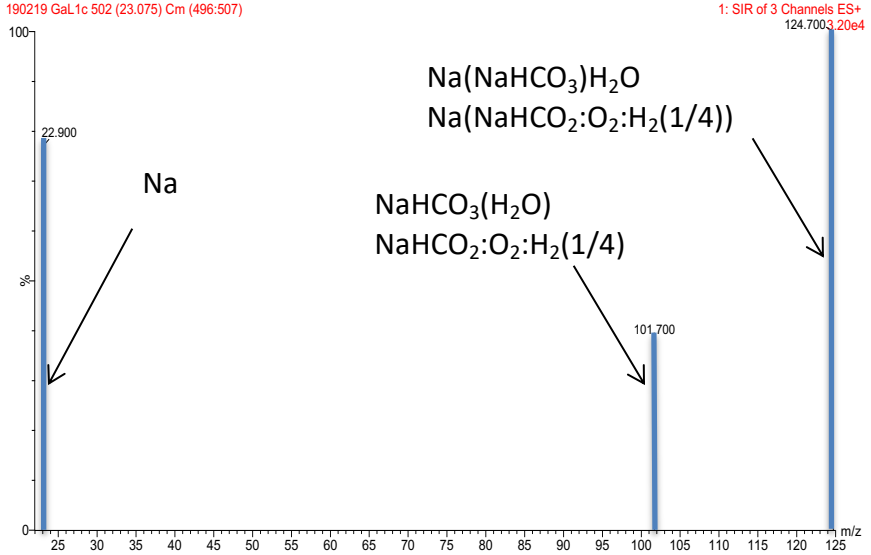

Isolation and Identification of Molecular Hydrino Gas Directly from SunCell® Gas Using a Cryopump

$H_2(1/4)$ gas was collected from a SunCell® operated at a cell pressure of 10-20 Torr over 100s using a valved microchamber connected to the vacuum line and cooled to 10.5 K by a cryopump system (Helix Corp., CTI-Cryogenics Model SC compressor; TRI-Research Model T-2000D-IEEE controller; Helix Corp., CTI-Cryogenics model 22 cryodyne). The SunCell® comprised a Type 347 stainless steel (SS) cylindrical tube measuring 7.3 cm ID, 19.7 cm in height, and 0.635 cm thick with 3.17 mm thick boron nitride (99%) liner and incorporating a 0.9 kg internal mass of liquid gallium wherein the gas flow rates were 2500 sccm H_2/50 sccm O_2, and the ignition current was 1500 A. Argon and trace oxygen were flowed before the reaction was initiated to serve as a solvent for hydrino gas $H_2(1/4)$.

The liquefied gas was warmed to room temperature to achieve 23 Torr chamber pressure and was injected into an HP 5890 Series II gas chromatograph with a capillary column (Agilent molecular sieve 5 Å, (50 m x 0.32, df = 30 µm) at 303 K (30 °C), argon carrier gas, and a thermal conductivity detector (TCD) at 60 °C.

- $H_2(1/4)$ was observed at 10.92 minutes, oxygen was observed at 18.05 minutes, and hydrogen that co-condensed with $H_2(1/4)$ gas was observed at 12.7 minutes.
- Hydrogen condensed under pressure and temperature conditions that violate the Clausius Clapeyron equation due to the raising of the H_2 liquefaction temperature by co-condensation with $H_2(1/4)$.

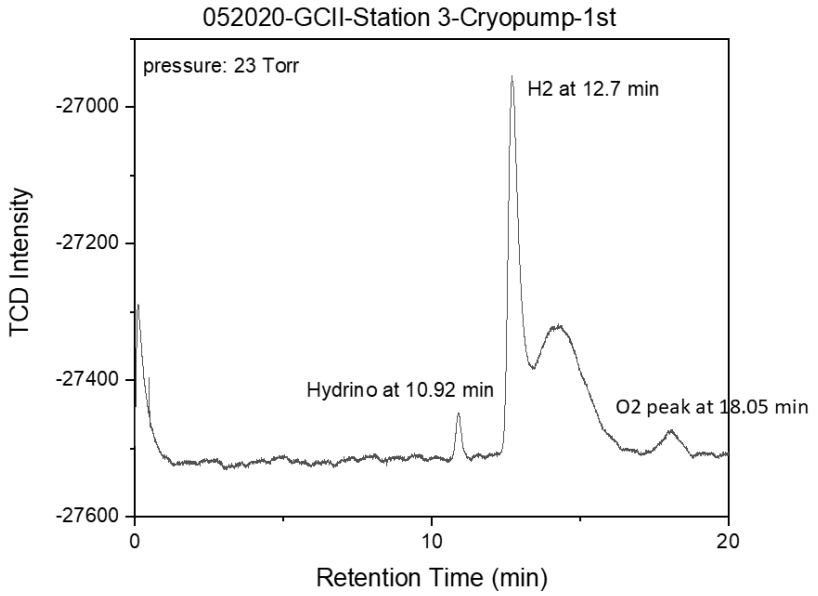

Isolation and Identification of Molecular Hydrino Gas Directly from SunCell® Gas Using Solid Carbon Dioxide Absorbent

The gas chromatograph of molecular hydrino gas flowed from the SunCell®, absorbed into solid CO_2, and then released by allowing the CO_2(s) to vaporize upon warming to 27 °C. The H_2(1/4) hydrino peak was observed at 9.3 minutes compared to hydrogen that was observed later at 11.1 minutes on the Agilent column (Agilent molecular sieve 5 Å, (50 m x 0.32, df = 30 µm) at 303 K (60 °C) using a second HP 5890 Series II gas chromatograph with a thermal conductivity detector at 60 °C and argon carrier gas at 19 PSI.

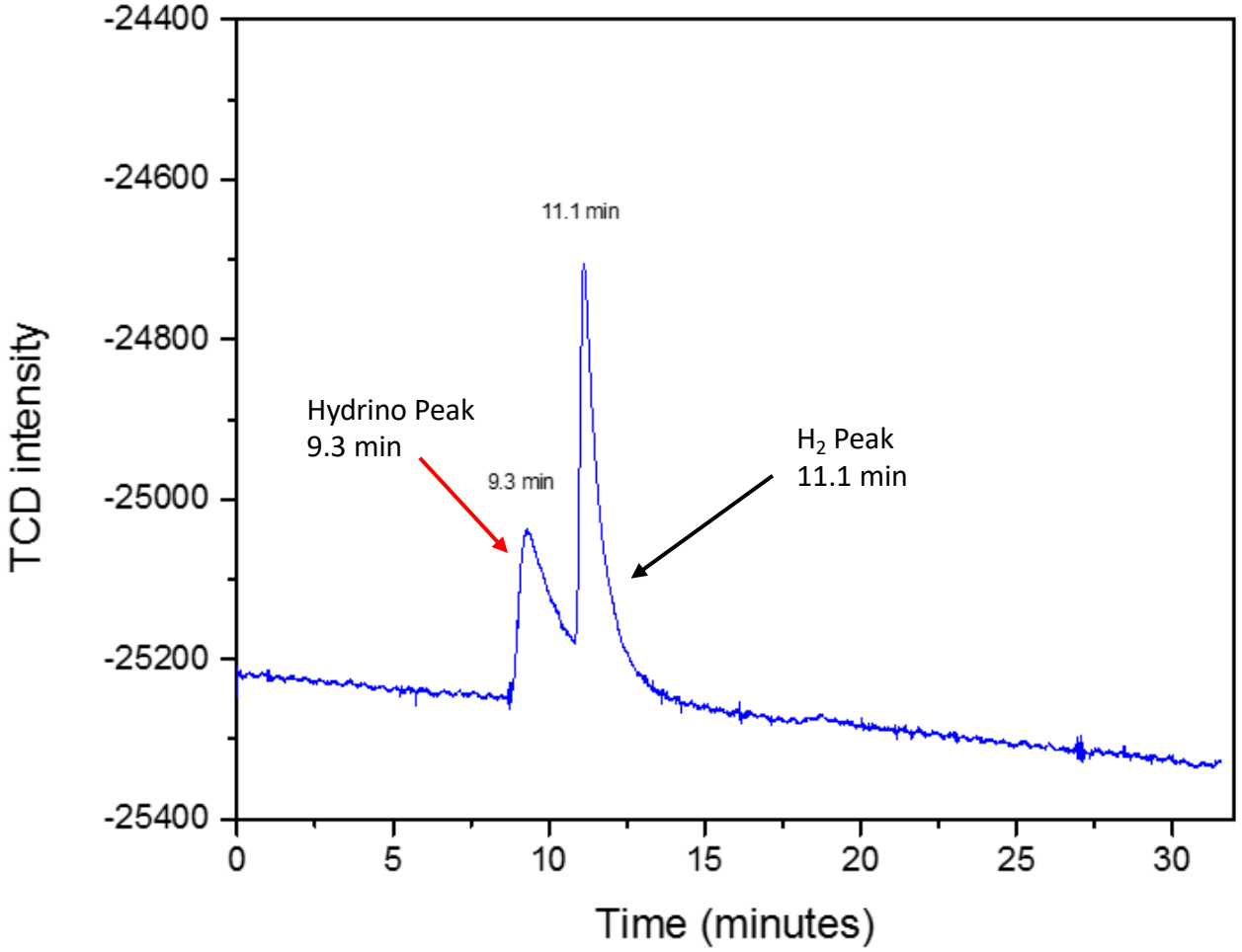

Isolation and Identification of Molecular Hydrino Gas Directly from SunCell® Gas Using a Cryopump Cont'd

- Hydrino atoms have a potential energy of an integer multiple of 27.2 eV matching the hydrino catalyst criterion.
- Thus, hydrino atoms serving as catalysts may react with H to form lower energy states than those of the catalysts.
- A favored reaction is the catalysis of H to H(1/17) by H(1/4) serving as the catalyst: H(1/4) + H to H(1/17).
- The SunCell was operated for one hour at excess power levels of over 100 kW with the intention of forming molecular hydrino states $H_2(1/p)$ with p=4 and p=17.
- The gas chromatograph of gas collected from the SunCell® by a cryopump showed a small reproducible peak at 1.95 minutes that is a candidate for $H_2(1/17)$ in addition to the $H_2(1/4)$ peak at 11 minutes.

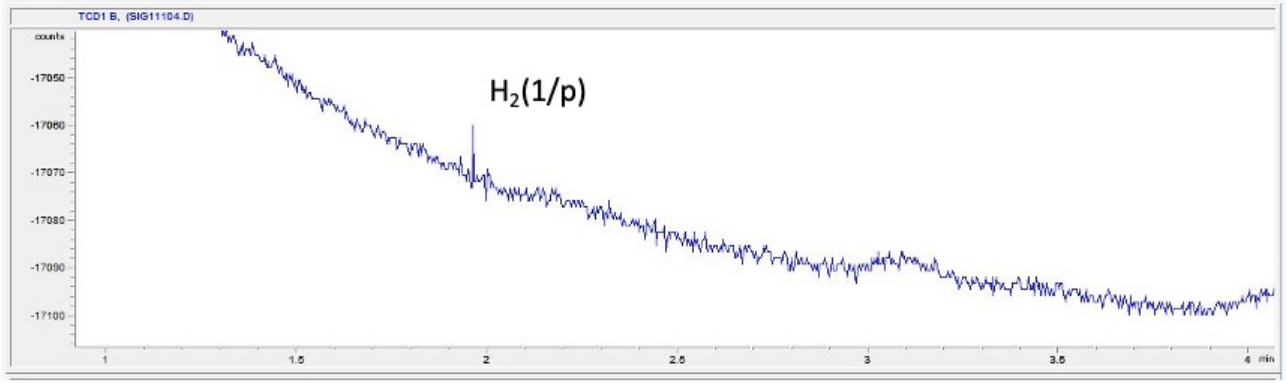

Isolation and Identification of Molecular Hydrino Gas Directly from SunCell® Gas Using Liquid Argon Solvent

To remove the high masking background from hydrogen that floods the gas chromatograph, liquid argon was used as a selective solvent.

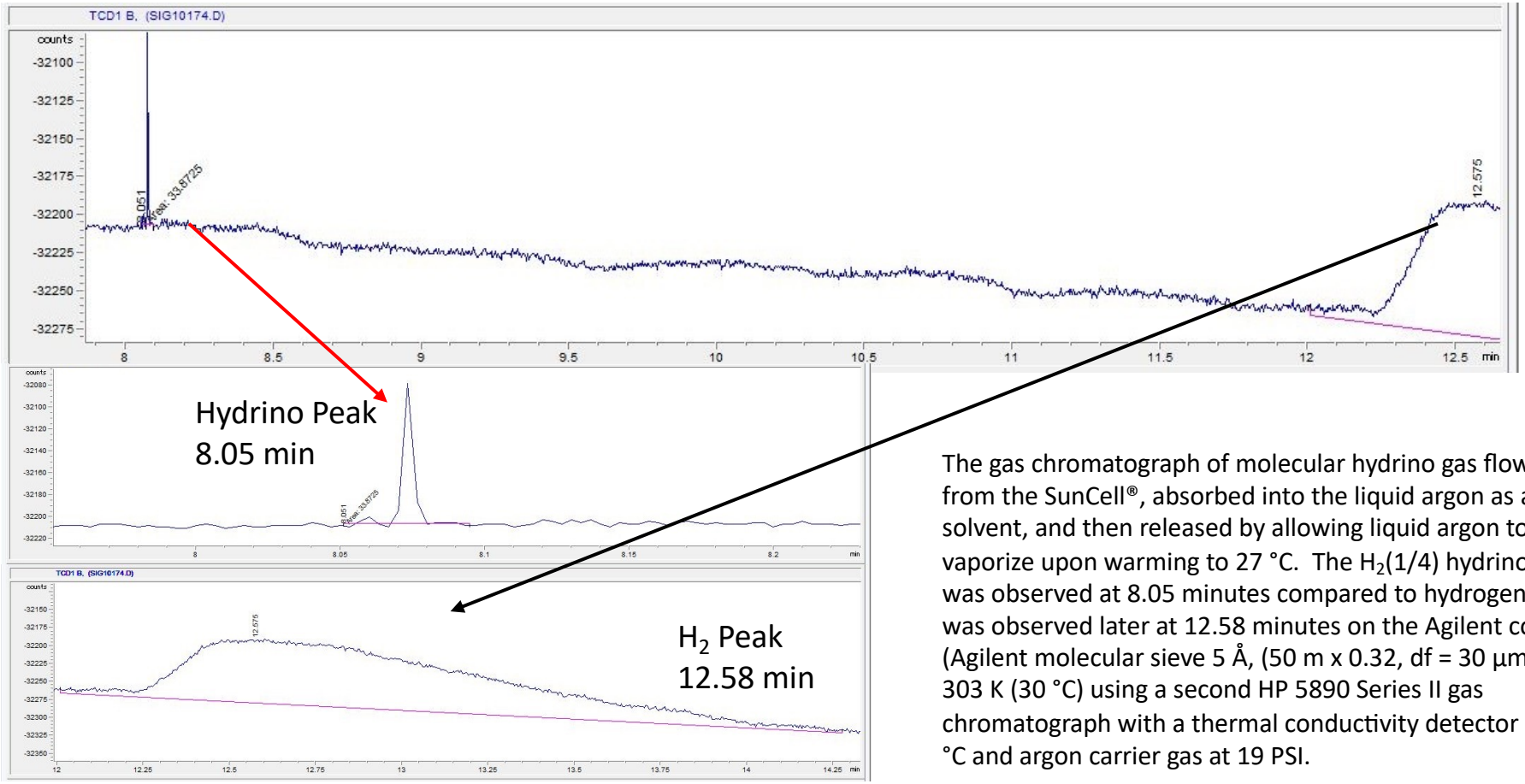

The gas chromatograph of molecular hydrino gas flowed from the SunCell®, absorbed into the liquid argon as a solvent, and then released by allowing liquid argon to vaporize upon warming to 27 °C. The $H_2(1/4)$ hydrino peak was observed at 8.05 minutes compared to hydrogen that was observed later at 12.58 minutes on the Agilent column (Agilent molecular sieve 5 Å, (50 m x 0.32, df = 30 µm) at 303 K (30 °C) using a second HP 5890 Series II gas chromatograph with a thermal conductivity detector at 85 °C and argon carrier gas at 19 PSI.

Hydrino $H_2(1/4)$ Observed by Gas Chromatography Following Isolation by Gas Purification Using Cryogenic Chromatography and Condensation at Cryogenic Temperature

- $H_2(1/4)$ gas of an argon/$H_2(1/4)$ mixture formed by recombination of hydrogen and oxygen on a supported noble metal catalyst in an argon atmosphere was enriched by flowing the mixture through a HayeSep® D chromatographic column cooled to a cryogenic temperature in a liquid argon.
- The argon was partially liquefied to permit the flowing molecular hydrino gas to be enriched as indicated by the dramatic increase in the ro-vibrational P branch of $H_2(1/4)$ observed by e-beam excitation emission spectroscopy.
- The molecular hydrino gas from the chromatographic column was also liquified with trace air as it was flowed into a valved microchamber cooled to 55 K by a cryopump system).
- The liquefied gas was warmed to room temperature to achieve 1000 Torr chamber pressure and was injected on to the Agilent column with argon carrier gas. Oxygen and nitrogen were observed at 19 and 35 minutes, respectively. $H_2(1/4)$ was observed at 6.9 minutes.

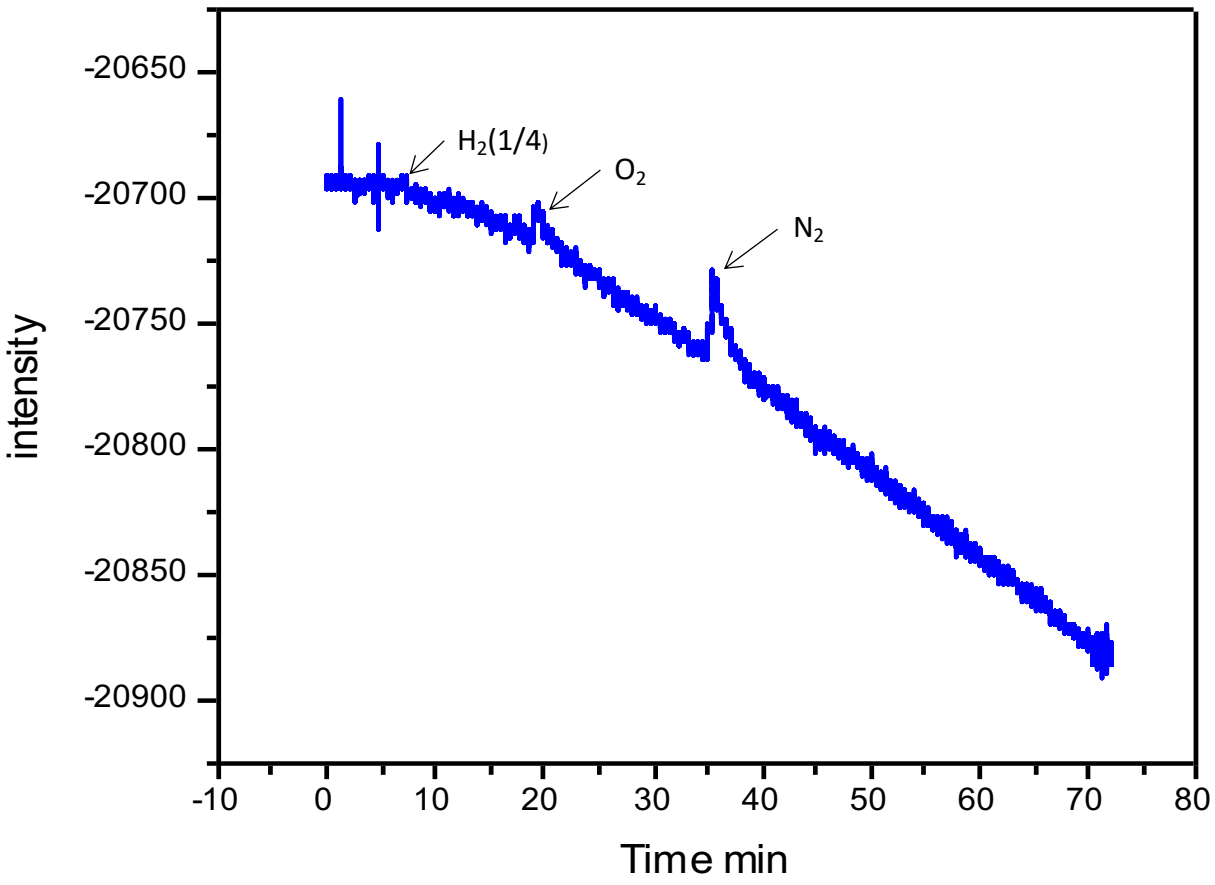

Identification of Molecular Hydrino Gas Released from Heating GaOOH and Stainless Alloys formed in the SunCell® that Had Absorbed $H_2(1/4)$ Gas

- The SunCell was operated for one hour at excess power levels of over 100 kW.
- The gallium temperature was elevated above the threshold for Ga_3Fe, Ga_3Ni, and Ga_3Cr to form while the oxygen of hydrino reaction mixture was maintained elevated to form Ga_2O_3.
- A mixture of alloys and gallium oxide was collected from the cell, dissolved in 4 M KOH, and filtered.
- Using an Agilent 8890 gas chromatograph system with a thermal conductivity detector (TCD), gas chromatograph was performed on hydrino gas evolved by heating the non-dissolved KOH-treated alloy/Ga_2O_3 material collected from the SunCell® to 800°C.
- The known hydrogen peak was observed at 8 minutes, a nitrogen peak was observed at 15 minutes, and a novel peak observed at 6 minutes was assigned to $H_2(1/4)$.

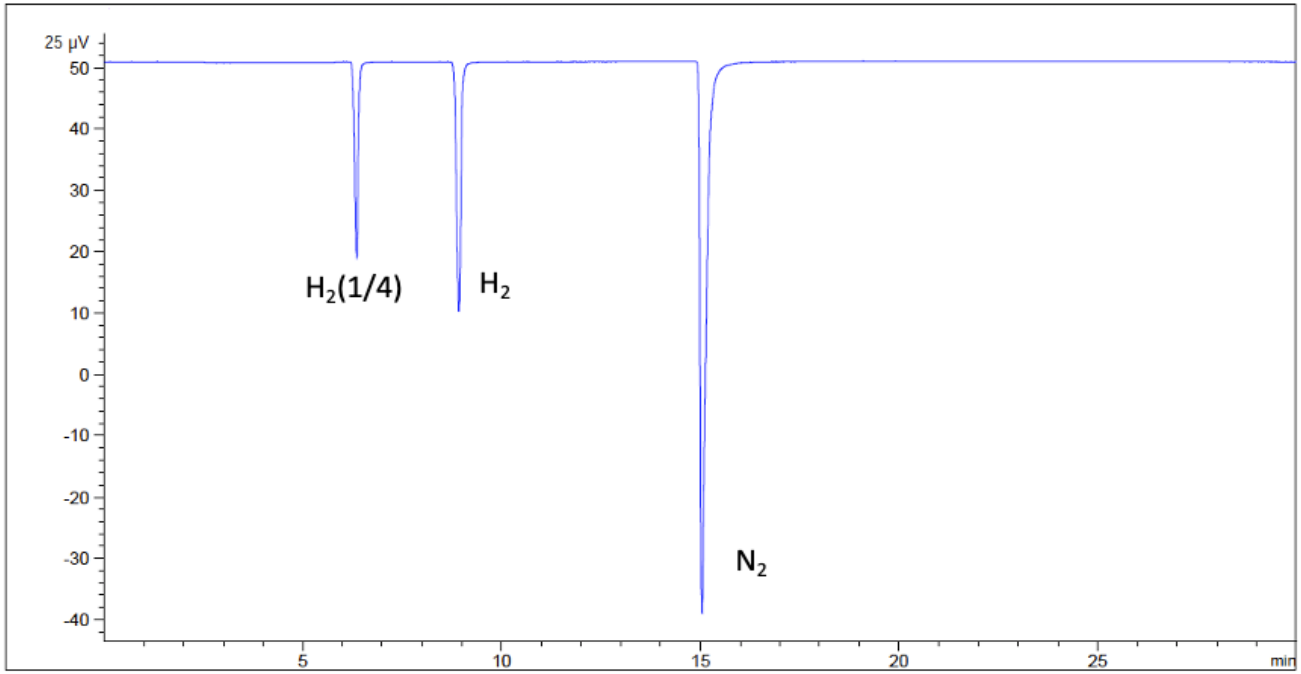

Identification of Molecular Hydrino Gas Released from Acid-Treatment of Ball Milled FeOOH Comprising Absorbed $H_2(1/4)$ Gas

- The gas chromatograph of hydrino gas evolved by acid reaction with ball milled FeOOH that was run within one hour of the acid addition.
- The two peaks observed at 4.049 minutes and 4.2 minutes before the H_2 peak at 4.597 minutes were assign to para-$H_2(1/4)$ and ortho-$H_2(1/4)$, respectively.

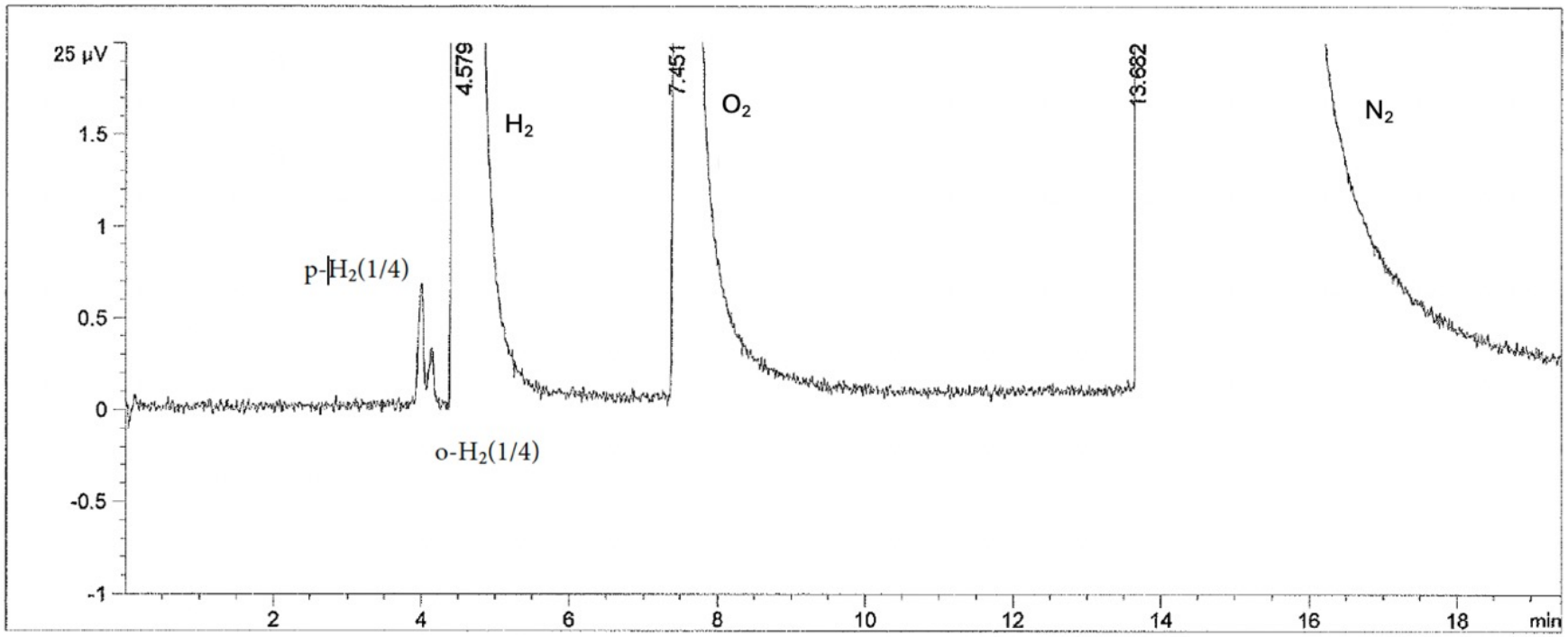

Randell L. Mills, Wilfred R. Hagen, "Spectral identical of Hydrino Compound Fe2O3:H2(1/4) by Five Complementary Spectroscopies, (2025), submitted, https://brilliantlightpower.com/pdf/FeOOH_Hydrino_Paper.pdf.

Identification of Molecular Hydrino Gas Released from Acid-Treatment of Ball Milled FeOOH Comprising Absorbed $H_2(1/4)$ Gas

- The gas chromatograph of hydrino gas evolved by acid reaction with ball milled FeOOH that was run after one week of the acid addition.
- Only one peak, the shorter-retention time peak, assign to p-$H_2(1/4)$,was observed at 4.049 minutes before the H_2 peak at 4.597 minutes.
- In addition to the fastest migration time ever observed on a molecular sieve column, the presence of ortho and para nuclear spin isomer peaks that interconverted on an Fe catalyst is characteristic of and identifies the peaks as hydrogen-type molecule $H_2(1/4)$.

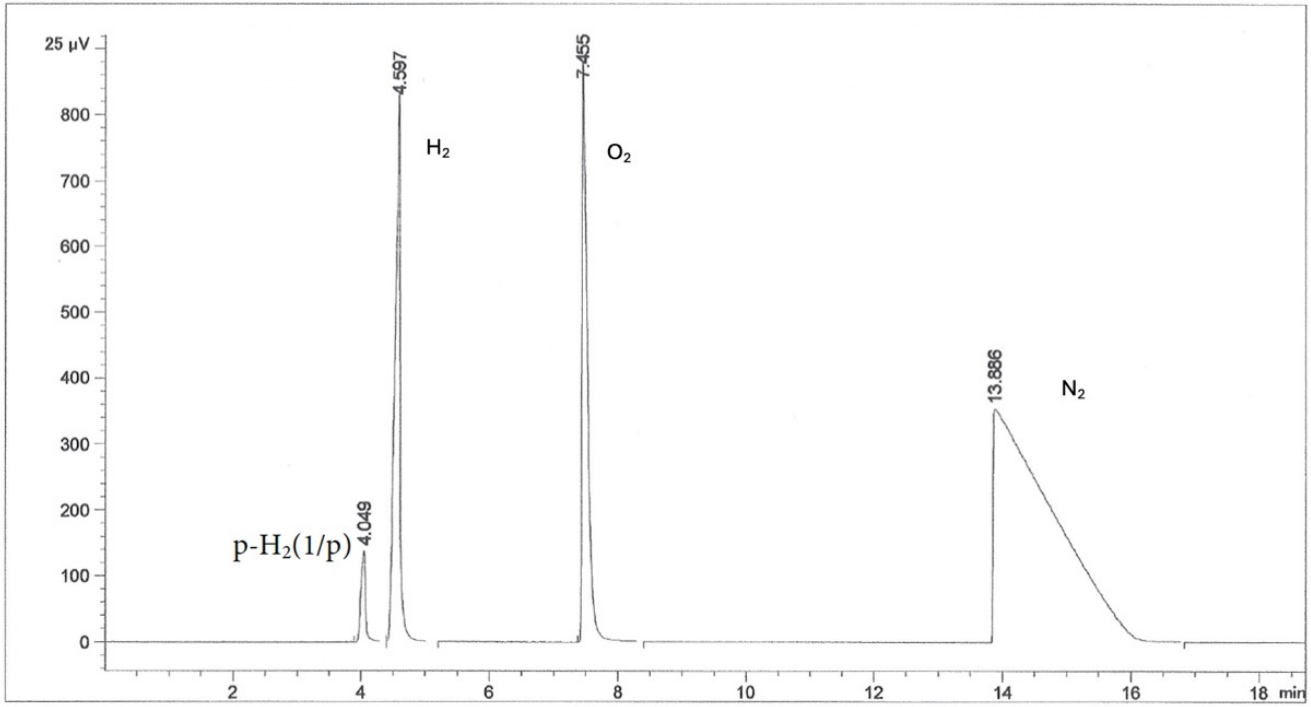

Thank you!

For more information please visit us at www.brilliantlightpower.com